**Università degli Studi di Genova**

SCUOLA POLITECNICA
Corso di Laurea Magistrale in Ingegneria Meccanica Energia & Aeronautica

TESI DI LAUREA:

# An experimental setup to investigate intermittency in pipe systems

Relatori:
**Prof. Ing. Alessandro Bottaro**
**Prof. Ing. R.I. Sujith**

Candidato:
**Diego Zangrillo**

**Luglio 2015**

# Abstract

This experimental thesis, was done in collaboration between Professor Alessandro Bottaro of the University of Genoa and Professor R.I. Sujith of the Indian Institute of Technology Madras located in Chennai (India) that they gave me the opportunity to be hosted at the IIT Madras for a period of six months from September 2014 to February 2015.

Prof. Sujith with the collaboration of the his researcher group, does both experiments and theory. He pursues both basic and applied research in the area of Combustion Instability and Laser Diagnostics of Flow and Combustion. Sujith's most important scientific contribution is the discovery of the non-normal nature of thermoacoustic interactions and its role in sub-critical transition to thermo-acoustic instabilities.

The work, make part and has been completely supported of TANGO project (Thermo-acoustic and Aero-acoustic Nonlinearities in Green combustors with Orifice structures). This project has like purpose the analyse and the study of instabilities of type Thermoacoustic and Aeroacoustic. These combustion instabilities represent a serious problem for combustion-driven devices, such as gas turbine engines and domestic burners. These instabilities can cause intense pressure oscillations, which in turn causes excessive structural oscillations, fatigue and even catastrophic damage to combustor hardware. In recent years, the development of clean combustion systems with reduced pollution of the environment has become a priority; however, such systems are particularly prone to combustion instabilities. There is an urgent need to understand the physical processes that are responsible so that methods to predict and prevent these instabilities can be developed. The research in the TANGO network is intended to address these issues.

In the thesis work, like already watched in literature, I showed that intermittent burst oscillations are a typical feature of turbulent flow-sound interaction, even in the absence of combustion. These pulsations are undesirable, not only because of the noise produced, but also because of the possibility of mechanical failures in the pipe network (and other parts of the application systems), like already explained. We had performed experiments on a cold-flow combustor with an in-duct orifice. Our control parameter was the air-flow rate. We measured the pressure time history for various air-flow rates. I then processed these time histories with some methods through the Matlab software. From the data processing, among which, I produced recurrence plots with the aim of investigate the intermittency phenomena and detection the intermittency type.

# Acknowledgements/Ringraziamenti

Firstly I would like to thank Prof. Alessandro Bottaro and Prof. R.I. Sujith for having proposed to me this interesting and prolific topic, and for the opportunity to work on it at IITM in Chennai. I am grateful to Prof. Sujith for the way he welcomed me in his group, for the time he dedicated to me and for his always enlightening advice, which has guided me through this research. I profoundly acknowledge Prof. Bottaro for his dedicated support, his careful oversight, his patience and especially for his trust, during all thesis work. I also want to express my gratitude to all the Sujith's Group. I thank Dileesh for his continuous help in the experimental lab, Nitin for his continuos help and for the his patience in the correction of my english both during the stay in Chennai and in the check of the thesis, Unni and Gopalakrishnan for their expertise in aeroacoustics and in all topics treated in this work, Samadhan for his lectures on the recurrence plot, Syam and Nalini for their friendship so like all people in the RGDLab. Each of you has given a fundamental professional and personal contribution to this work and to my stay in IIT. Besides I want thank luca for sharing with me this important experience. Another important acknowledgement to Prof. Maria Heckel in representing the TANGO project for gave to me the opportunity to make this experience thank her financial support.

I take this opportunity to also thank all the people that have been close to me in the last five and more years, of which this thesis and my graduation are somehow a conclusion. I hope nobody will feel offended if I switch from English to Italian to do that.

Non sapendo neanche da parte cominciare, parto da chi ha condiviso con me infinite giornate di studio all'Università, desidero ringraziare tutti da chi è partito con me fin dal principio come: Jig, Toma, Otto, Gio e Ken, a chi ho avuto la fortuna di incontrare e conoscere nel corso degli anni come Matte, la Vero e la Silvia che con Gio mi hanno supportato e soprattutto sopportato negli ultimi mesi, senza dimenticare tutti gli altri come Bruce "il Segugio", la Marti, la Laura, Fla, Api e il Naitans. Grazie per avermi reso migliori giornate dure in preparazione e durante gli esami stessi. Mi auguro che la fine della quotidianità all'università non cambi di una virgola il nostro rapporto.

Adesso passo agli amici di sempre, potrei citare solo "I Ravatti" che per me avrebbe rappresentato tutti perfettamente ma preferisco nominare tutti in "rigoroso" ordine... sparso: il Generale Rommel, Buns, Montini, Dibe, Massi, Ciccio, Compagno, Mere, Squalo, Curcia, Zaba e Vetto con i quali ho condiviso molto del poco tempo libero fin da prima gli anni universitari. Con loro è stato e sarà sempre piacevole festeggiare le vittorie e consolarsi nelle sconfitte. Inoltre mi fa piacere ringraziare anche chi non è ravatto ma ne fa indirettamente parte come la Ale, la Chiara, la Giulia, la Elena, la Clari, l'Arianna e la Mary.

Oltre a loro desidero citare anche Matte Baldo, con il quale sono partito dalla prima elementare. Nel corso degli anni le varie vicende ci hanno allontanato ma la nostra amicizia ha superato ogni distanza. Senza dimenticare altre amicizie intatte nonostante la mancanza della "Sacra" quotidianità come Fazza, Matte Volpi e Matte Martinato.

Grazie a tutti voi, ho potuto trovare la forza e l'energia di godermi i momenti belli e rialzarmi in quelli brutti!!

Infine anche se primi in ordine d'importanza desidero ringraziare i miei genitori e mia sorella Elisa, senza i quali mai avrei raggiunto questo tragurdo, probabilmente non avrei neanche iniziato questo percorso. Non sono e sicuramente mai sarò bravo con le parole ma se oggi sono qui molto è merito loro, mi hanno dato tutto ciò di cui potessi avere bisogno dall'educazione al sostegno morale affettivo a quello economico. In particolare durante gli anni universitari, mi hanno concesso sempre una fiducia incondizionata anche e soprattutto quando non ne avevo in me stesso, non mi hanno mai messo alcun tipo pressione concedendomi la libertà di sbagliare senza mai chiedere spiegazioni anche quando sarebbero state dovute. Per finire con il supporto e la sopportazione dei miei numerosi momenti difficili durante l'esperienza in India attraverso le interminabili chiamate su Skype.

Grazie nuovamente a tutti ed ora come mai prima ho capito quanto fosse (almeno per me) vera questa citazione a me cara: ....... *You'll Never Walk Alone..*

# Sommario

Questo lavoro di tesi di tipo sperimentale, è stato svolto grazie alla collaborazione tra il Professor Alessandro Bottaro per l'Università degli Studi di Genova e il Professor R.I. Sujith per l'Indian Institute of Technology Madras situato a Chennai (India) che mi hanno dato la possibilità di essere ospitato dall'IIT Madras per un periodo di 6 mesi a partire dal settembre del 2014 fino a Febbraio 2015. Il Professor Sujith con la collabolarazione del suo gruppo di ricerca, si occupa sia dal punto di vista teorico e sia da quello sperimentale di instabilità di combustione e sia di diagnostica del flusso con tecniche laser. Il suo principale contributo alla comunità scientifica internazionale è la scoperta della natura non-normale delle interazioni termoacustiche ed le loro regole nella transizione sub-critica alle instabilità di questa natura.

Questo lavoro fa parte ed è stato completamente finanziato dal progetto denominato TANGO (Thermo-acoustic and Aero-acoustic Nonlinearities in Green combustors with Orifice structures). Il progetto si occupa delle instabilità di combustione che rappresentano un problema di fondamentale importanza in molte applicazioni come ad esempio nei combustori per le turbine a gas ed in molti altri sistemi. Queste instabilità possono causare forti oscillazioni di pressione, che posso causare altrettanto forti sollecitazioni strutturali per fatica, con conseguente rischio di drammatiche rotture strutturali dei sistemi combustivi. Negli ultimi anni, lo sviluppo di combustori meno inquinanti è diventato fondamentale, ed il problema si è notevolmente evidenziato dato dalla notevole presenza di instabilità di combustione in questi sistemi. Perciò si è reso necessario capire la fisica di questi fenomeni per prevederli ed evitare che queste instabilità si possano verificare. Nel lavoro di tesi, come già visto in letteratura, ho osservato che queste fluttuazioni di pressione possono avvenire anche in assenza di fenomeni combustivi. Queste pulsazioni possono portare a conseguenze indesiderabili come la generazione di fastidiosi rumori e la possibilità di rotture strutturali per fatica, come già spiegato in precedenza. Queste sollecitazioni che si verificano, con il flusso "freddo" sono caratteristiche del fenomeno dell'*Intermittenza Aeroacustica*, oggetto principale di questa tesi. Come illustrerò nel dettaglio successivamente, durante il mio soggiorno a Chennai, abbiamo messo a punto un impianto sperimentale che simulava la forma di un combustore reale, e variando la portata d'aria siamo andati ad effettuare misure di pressione attraverso un microfono. Durante il lavoro sperimentale abbiamo effettuato delle prove variando alcuni fattori come ad esempio: la geometria dell'impianto o la posizione del microfono. Tuttociò al fine di riprodurre il fenomeno dell'intermittenza e studiarlo nelle migliori condizioni possibili. Per l'elaborazione dei dati ho utilizzato il software Matlab, con il quale tra gli altri ho utilizzato alcune metodi per identificare il tipo di intermittenza ottenuto sperimentalmente.

# Contents

# 1. Introduction

Low frequency acoustic pulsations in pipe networks have been observed in many technical applications. These pulsations are undesirable not only because of the noise produced but also because of the possibility of mechanical failures in the pipe network. The high amplitude of the acoustic pressure fluctuations results in mechanical stresses that can cause fatigue failure. Lower pulsation levels can already affect volume flow measurements or trigger vibration control equipment. Even when the vibration and pressure pulsation levels do not endanger the system safety and can be tolerated, they still cause additional pressure losses and reduce the efficiency. However small these losses might seem in percentage terms, they constitute, in absolute values, a significant amount of wasted energy. Forced pulsations, like the pulsations driven by compressors, can be predicted in the design phase by numerical models. A different kind of acoustic pulsations is the aeroacoustic oscillation caused by the instability of the flow in the pipe systems. This kind of pulsations is called self-sustained, or self-excited oscillations. Due to the nonlinearity of the governing equations it is very difficult to predict the sound production of fluid flows. This sound production occurs typically at high speed flows, for which nonlinear inertial terms in the equation of motion are much larger than the viscous terms (high Reynolds numbers). As sound production represents only a very minute fraction of the energy in the flow the direct prediction of sound generation is very difficult. This is particularly dramatic in free space and at low subsonic speeds. The fact that the sound field is in some sense a small perturbation of the flow, can, however, be used to obtain approximate solutions. Aeroacoustic provides such approximations and at the same time a definition of the acoustical field as an extrapolation of an ideal reference flow. The difference between the actual flow and the reference flow is identified as a source of sound. This idea was introduced by Lighthill who called this an analogy. A second key idea of Lighthill is the use of integral equations as a formal solution. The sound field is obtained as a convolution of the Green's function and the sound source. The Green's function is the linear response of the reference flow, used to define the acoustical field, to an impulsive point source. A great advantage of this formulation is that random errors in the sound source are averaged out by the integration. As the source also depends on the sound field this expression is not yet a solution of the problem. However, under free field conditions one can often neglect this feedback from the acoustical field to the flow. In that case the integral formulation provides a solution. When the flow is confined, the acoustical energy can accumulate into resonant modes. Since the acoustical particle displacement velocity can become of the same order of magnitude as the main flow velocity, the feedback from the acoustical field to the sound sources can be very significant. This leads to the occurrence of self-sustained oscillations which we call whistling. In spite of the back-reaction, the ideas of the analogy will appear to remain useful (Hirschberg & Rienstra et al. 2004). In the past, there have been many cases of birth of these phenomena, for examples: From 1940 to 1960, Oklahoma Gas and Electric Company had problems with the safety valves installed on its boilers. Unusual noise and vibration, coming from these valves were observed by operators. The problem arose with all the re-heater safety valves located on a horizontal portion of the re-heat steam inlet line just before it enters the steam generator, and just downstream of a pipe elbow. The vibration was so severe that within a few months several valves failed. These problems promoted a systematic investigation of the flow induced vibrations in safety valves. This investigation identified the standpipes of the valves, which form a row of closed side branches along a main pipe, as responsible for the occurrence of pulsations. Another case there was in 2002, the steam dryer in the boiling water reactor (BWR) of Quad Cities Unit 2 (QC2) experienced high cycle fatigue cracks after the reactor's maximum power was increased by approximately 17%. Repairing the dryer by using thicker plates and stronger welds did not resolve the problem, as the dryer exhibited new cracks upon continued operation. The pressure measurements on the steam dryer indicated that increasing the steam velocity in the main steam lines (MSLs), related to the increase in the reactor power, excited the acoustic modes in the standpipes of the safety valves, which are mounted on the MSLs. The resonance was so strong that it not only damaged some of the valves, but also propagated upstream in the MSLs and into the reactor dome and damaged the steam dryer. The problem was solved by changing the standpipe geometry to avoid the acoustic resonance at the increased rated power (Tonon, Hirschberg, Golliard & Ziada et al. 2010).

This thesis work has purpose to investigate the Intermittency in aeroacoustic systems: it is the appearance of irregularly spaced, alternating intervals of chaotic/burst state and steady/periodic behaviour. Such dynamical behaviour is commonly observed in physical systems and has been reported previously for biochemical systems (Lisa & Thomas 1993), binary fluid convection (Batiste et al. 2001), pH oscillators (Straube, Flockerzi & Hauser 2006) and coupled neural oscillators (Han & Postnov 2003). The phenomenon of intermittency occurs due to dynamics in the system and has been shown to conform to definite statistical characteristics of the laminar states occurring along with bursts. In an attempt to explain the occurrence of intermittency in physical systems, Pomeau & Manneville (1980) presented an analytical study of dynamical models of dissipative systems. They categorized the phenomenon of intermittency into three classes, type I, type II and type III, based on how transition occurred at the threshold of each of the models. The system dynamics corresponding to each of the three classes is also associated with a particular bifurcation scenario. Type I intermittency is associated with a saddle-node bifurcation. Type II occurs due to a Hopf bifurcation and is associated with the appearance of a quasi-periodic state. Finally, type III intermittency is associated with a reverse-period doubling bifurcation (Okamoto, Tanaka & Naito 1998). Intermittency was first studied in the Rayleigh–Bénard convection experiments and has been identified as a route to turbulence in hydrodynamic flows (Bérge et al. 1980; Gollub & Benson 1980; Swinney 1983). In most observations of intermittency, the intermittent state is followed by a chaotic regime. In the aeroacoustic system studied here, we find the appearance of limit cycle oscillations followed by a quasi-periodic state. The quasi-periodic oscillations then break down, leading to intermittency, indicating the presence of a type II intermittency. To investigate the bifurcation scenario and the associated system dynamics, we have conducted further investigations via nonlinear time series analysis. A major part of the analysis is based on studying the recurrence behaviour of reconstructed phase space trajectories, using recurrence plots.

The present experimental thesis work, make part of TANGO project (Thermoacoustic and Aero-acoustic Nonlinearities in Green combustors with Orifice structures). This project has like purpose the analyse and the study of instabilities of type Thermoacoustic and Aeroacoustic. In particular, the thesis is carried out at Indian Institute of Technology Madras (IITM) at Chennai (India), in the Aerospace department, under the supervision of the Professor Alessandro Bottaro for the University of Genova and Professor R. I. Sujith for IITM with the collaboration of the his researcher group. My work will be focused on the second type, in particular vortex shedding, which play an important role for example in combustion systems or like I already said prematurely in many other applications.

# 2. Background

## 2.1 Aeroacoustic

The sound / noise is a perturbation of pressure, density, temperature and velocity that propagates in space at a high distance from point of emission. In general we neglect the entropy changes, so the perturbation is isentropic. The choice of using the terms sound or noise depends on who perceives them (psychoacoustics) and in general is considered the noise less pleasant of sound. The aeroacoustic's problem, in engineering, is noise reduction without affecting performance of turbomachinery, propellers, nozzles and so on.

The subject of the present work is the flow of air through a square-edged circular orifice of finite thickness at the end of a circular duct. Audible, sharp tones, referred to as pipe tone, are excited under certain flow and geometric conditions in this case. Pipe tones are not produced outside a critical range of thickness of the orifice for a range of mean flow velocity in the duct. The excited tones also jump from one mode to the other as the flow velocity is varied over a wide range for a given geometry. The occurrence of these tones has been attributed to the formation and periodic shedding of vortices and their interaction with the duct resonance system. Anderson studied this problem extensively, and attributed the excitation of audible tones to periodic fluctuations in the jet cross-sectional area at the orifice. Audible tones are excited even in the absence of the duct; this phenomenon is referred to as jet tone. It is believed that the mechanism that causes the jet tone is basically the same as the one that causes the pipe tone. The difference lies in the fact that the resonance column of the pipe influences the jet tone to change its frequency. It is hypothesized that the vortex shedding is influenced by the duct acoustics in such a way that a rolled up vortex sheds at the time when the acoustic velocity changes direction against the mean flow, as shown in the studies on pipe side branch tone. In general, it is found that the pipe tone occurs more readily and over a larger range of flow conditions than the jet tone. The low frequency aeroacoustic response of orifices has recently been predicted theoretically with consideration of the Mach number dependence of the vena contract, in terms of the scattering matrix connecting the acoustic pressure amplitudes on either side of the orifice, which is treated as a discontinuity. However, the region of sound production lies across the thickness of the orifice. Howe points out that axisymmetric disturbances are generated at the upstream edge of the orifice, which produce sound by the diffraction of the near-field pressure distribution at the downstream edge. A number of other recent investigations related to sound production involving vortex shedding or vorticity fluctuations have been reported in the context of gas flows in pipe systems with closed side branches, vortex-nozzle interactions, and sharp edged open channel ends. In these works, the vortex shedding behaviour or vorticity variation has been simulated by means of point vortex method, a single panel method, or the vortex blob method in the two-dimensional potential flow framework in order to retain the simplicity in the analysis, and the Powell–Howe approach has been adopted to predict the acoustic power generated. This requires a good physical understanding of the nature of vorticity fluctuation under conditions that excite high amplitude sound. In the case of the problem considered here, the response of the shear layer originating from the separation point at the upstream edge of the orifice to the self-excited oscillations governs the sound production, and is being optically investigated at this laboratory. However, as a result of this behaviour, the near-field vortex roll-up in the free jet just downstream of the orifice is altered by the self-excitation of high amplitude acoustic oscillations in the duct. The vortex roll-up behaviour is almost symptomatic of the acoustic excitation inside the duct. The focus of the presentwork, specifically, is the phenomenon of jet forking into two trains of vortices at a certain flow Reynolds number coincident with transition of the excited acoustic oscillations from one mode to the other. This has indeed been reported by Anderson, but without any time-resolved visualization and correlation with the acoustic characteristics of the pipe tone. A similar behaviour is reported in the absence of duct acoustic resonance with a helium jet issuing out of a nozzle into air. This is accompanied by self-excitation of jet tone.

### 2.1.1 Acoustic

Acoustics is defined as the science of sound (Pierce, 1989). Sound is an oscillatory perturbation that moves away from a source and propagates through a medium. The pressure perturbations associated with sound are small compared to the atmospheric pressure ($p'/p_{atm} << 1$) and hence linear theory is good enough to study it under most circumstances. Aeroacoustics deals with the study of the production the sound by flows. The first normal definition of an aeroacoustic sound source was proposed by Lighthill (1952a, 1952b). The acoustical field is defined as an extrapolation of a linear perturbation of a reference flow in which a listener is submerged. The difference between this linear behaviour and the actual flow is defined as the source of sound.

The sound generation mechanisms or “sources” of sound in real life scenario is found to be highly complex. However, such complex sources can be built up from study of a few fundamental solutions of the wave equation (Pierce, 1989). The simplest source is the monopole which does not have any directional nature. The next type of source is the dipole source. This type of source occurs in the through the orifice. The third type of source is the quadrupole source which can be viewed as two dipoles placed near each other. A classic example of such a source is the noise generated due to turbulence in a free jet. In general, flow noise modelling involves all the three types of sources. An aeroacoustic source is considered to be compact if the source is small compared to the acoustical wavelength (Howe, 1998). For a compact source, Lighthill’s (1952a) sound source may be rewritten in terms of vorticity as shown by Powell (1964). Sound generated by vorticity is often referred to as “vortex sound”. Howe (1975) generalized Powell’s analogy for high Mach number flows. In a compact aeroacoustic source, the Coriolis force density $f_c = -\rho(\omega \times \nu)$, is a dominant source of sound (Howe, 1998). The time average of the acoustic source power generated by periodic oscillations for a cycle is given by the integral, $< P_{source} >=< -\rho \int_{\nu} (\omega \times U) u' d\nu \ldots$

### 2.1.2 Acoustic field in a fully developed turbulent pipe flow

High levels of noise radiation from piping systems occur when the internal turbulent pipe flow separates from the pipe wall due to disturbances caused by convex corners on the pipe surface. Flow separation in a pipe acts as an acoustic source and generates both non propagating near field is attenuated rapidly, but the far field disturbances (Agarwal, 1994a, 1994b). The pressure perturbation due to the near field is attenuated rapidly, but the far field disturbances results in a propagating internal acoustic field superposed on the fully developed turbulent wall pressure field. The presence of a surface like an orifice causes flow separation and hence an associated sound source. The sound thus generated could interact with the duct resonance system leading to amplification of the disturbances. Wall pressure spectra have a basic broad band character due to a turbulence in the flow. Narrow band peaks are found to be superposed over the broad band spectrum. These peaks are attributable to the duct acoustic mode with the frequencies matching the modal cut-off frequency.

### 2.1.3 Pure tones and their generation

Sharp acoustic tones get excited when air flows past certain geometries. Screech in jets with shock, cavity noise, edge tones, jet/collector interactions and howling of ejectors are some of the examples of flow induced resonance. Screech of high speed choked jets belong to the class of tones that do not involve an impingement surface (Blake, 1986). The disturbance convecting in the shear layer interacts with the shock waves and generates sound. The sound wave generated propagates upstream through the ambient and interacts with the shear layer completing a feedback loop (Howe, 1998). In most of these problems, the shear layer plays a very important role in the process of excitation. The frequencies of sound and the most preferred instability waves mach. Large amplitude tones are generated due to coupling between a shear flow and the resonant sound field that builds in the surrounding system.

The flow past two concentric circular orifices a spaced a short distance apart generates a sharp tone popularly referred to as the hole tone. The first orifice forms a jet, it passes through the second orifice to generate a discrete tone. Sondhauss reported about this phenomenon for the first time in 1854 (Chanaud and Powell, 1965). He found that the tone frequency increased with increasing jet velocity and decreased with increasing orifice spacing. The sound generated is maintained by a feedback loop. The pressure fluctuation generated at the second hole cause pulsations in the jet flow rate that excites axisymmetric instabilities in jet upstream. The planar version of the hole tone is the slot tone. When the second orifice is replaced by a wedge, the tone generated is referred to as the edge tone (Powell, 1961). The edge tone is caused by non-symmetric oscillation of the jet, and the secondary disturbances are generated by vortex formation at the apex of the edge alternately on either side of the wedge. Hole tone, slot tone and jet tone belong to the general class of discrete frequency tones typified by jet-edge systems. The jet-edge systems are hydrodynamic oscillators controlled by acoustic feedback. The feedback mechanism is generating self-sustained oscillations involves the following events in this mode:

1. A disturbance or instability wave is initiated at the nozzle lip.
2. The excited instability wave convects downstream growing in amplitude.

3. A feedback disturbance is produced by the flow surface interaction as the convecting instability (shear layer/organised vorticity fluctuations) impinges on downstream edge.

4. The feedback disturbance propagates upstream and excites the shear layer thereby completing the feedback loop.

Cavity tones (Rossiter, 1966) are again another class of tone generating system. A subsonic or supersonic flow past a rectangular cavity induces acoustic oscillations. The oscillations are caused due to an acoustic feedback. Concentrated vortices are shed periodically in the vicinity of the upstream lip of the cavity. These vortices travel downstream and interact with the downstream wall of the cavity and generate acoustic pulses. These acoustic disturbances propagate upstream inside the cavity and upon reaching the upstream end, cause the shear layer to separate and initiate the process of shedding of a new vortex. In the case of deep cavities, the acoustic disturbances generated gets amplified and results in standing waves in the cavity. In this case also, it is seen that strong acoustic field is created by the interactions of the vortices with the system resonance. It has been shown that for the ratio of acoustic velocity to mean flow very much less than 0.1, the acoustic field only triggers the shedding of vortices but does not affect the path of the vortex thereafter (Bruggman et al.,1991). For those values greater than 0.4, the acoustic field not only determines the vortex shedding but also non-linearly interacts with the vortices and affects the path of the vortex significantly. However, it should be noted that in this case, the vortex shedding and the path are perpendicular to the acoustic field.

Strong self-sustained oscillations occur in a whistler nozzle when acoustical energy accumulates in the standing wave of a resonator attached to the nozzle (Hirschberg et al., 1989). The acoustical resonator imposes the oscillation frequency and the pulsation amplitude reaches a peak value when he flow is adjusted to meet the critical Strouhal number condition. The coupling of two independent resonance mechanisms viz, shear layer tone resulting from the impingement of the pipe-exit shear layer on the collar lip and the organ pipe resonance of the duct causes acoustic excitation (Hussain and Hasan, 1983). Selamet et al. (2002) studied the suppression of whistle noise by the use of ramps. One of the most common example of self-sustained oscillations is the human whistling. Wilson et al. (1971) have shown that the human whistling is due to a coupling between vortex shedding at the lips and the Helmholtz resonance frequency of the mouth. The Strouhal condition for optimal whistling is easily observed by first fixing the geometrical configuration and then gradually increasing the volume flow. Above a certain velocity the whistling disappears again. This is due to the fact that at high flow rates the vortices are convected far outside the lips before they produce sound.

### 2.1.4 The technological applications

The interaction of acoustic waves with flow across an orifice is widely encountered in the present society. In compressor stations of natural gas transport system very complex manifolds of pipes of various cross-sections are used (Bruggeman et al., 1991). Due to an increasing demand for gas distribution, there is a tendency to transport gas at higher pressures. Thick orifices are used to generate pressure drop across the main distribution line and the destination (Durrieu et al., 2001). The flow past pipe side branches and orifices can cause self-sustained flow instabilities (Bruggeman et al. 1991; Hofmans et al., 2001a, 2001b; Dequand, 2001). Avoiding such flow instabilities is not an easy task. Orifices (diaphragms) are extensively used in car mufflers to suppress resonances in the exhaust pipe of automobiles (Hofmans et al., 2001a).

A similar flow scenario exists inside large segmented solid rocket motors (SRMs). Large SRM are assembled with segmented grains. The grains are terminated by a coating of inert material to inhibit the propellant from burning from the sides. The inhibitor burns substantially slowly when compared to the propellant. This causes an annular ring to protrude into the port flow perpendicular to the motor axis. The presence of a protrusion results in the establishment of shear layer instabilities, leading o the periodic shedding of vortices. The vortex shedding phenomenon can have a direct bearing on the SRM performance as well as affect indirectly through interaction with the acoustic environment in the motor cavity. It is seen that the acoustic pressure oscillations start occurring after a certain time and continue until the end of the burn time of the rocket motor. Abrupt jump in the frequency corresponding to one acoustic mode of the rocket chamber to the next higher mode is also observed in some cases. Such shifts in frequency and their amplitudes have not been amenable to theoretical predictions so far. Vortex shedding as a possible mechanism for the excitation of the longitudinal acoustic modes of the combustion chamber of the solid rocket motor was first suggested by Flandro and Jacobs (1975). A series of papers by Kourta (1996a, 1996b, 1997) has successfully computed and shown that the presence of surface discontinuities (inhibitors/cavities) to be the primary source of vortex shedding driven oscillations in solid rocket motors. The mechanism was found to be very complex and vortex pairing was detected. It was found that the amplitudes were higher with sharp inhibitors as compared to a smooth inhibitor. Most of the SRMs currently used are assembled with grain segments with a layer of inhibitor separating the segments. The flow instability generated in a rocket motor could be due to the interaction among flow, acoustics, structural (inhibitor flutter) and combustion (propellant) processes. However, the present knowledge indicates that the phenomenon is hydrodynamic in nature, and combustion is suspected to play a very limited role, provided the propellant does not amplify the excited oscillations further (Howe, 1998). The vortex shed at the inhibitor may interact with the chamber acoustic longitudinal modes to excite large amplitude acoustic pressure oscillations. The pressure oscillations by themselves may lead to an increase in propellant burning rate, resulting in an increase in mean pressure of the chamber. It could also manifest as thrust oscillations. The frequency could match the natural frequency of on board systems leading to failure of the system. The acoustic oscillations could reach a limit cycle when the amplitude of the oscillations stabilizes at a level at which the damping equals the driving. These persistent oscillations may result in structural failure. The occurrence of such oscillations has so far eluded prediction.

Dunlap and Brown (1981) performed exploratory cold flow experiments, with a simulated SRM with chocked nozzle. These experiments led to certain quantitative predictions. The possibility of generation of 5-10% pressure oscillation was demonstrated “under proper flow conditions”. The location of the inhibitors with the respect to the acoustic mode shapes was varied, and its effect on the acoustic amplification was studied. In a more elaborate study Brown at al. (1981) with a cold flow model of the Titan SRM, critically examined and confirmed periodic vortex shedding as a driving mechanism for acoustic oscillations. In this study, mass addition to the port flow due to solid propellant combustion was simulated by flow nitrogen through a chocked porous pipe. Hot wire anemometer measurements indicated the magnitude of the velocity fluctuations to be ten times more than that predicted from periodic oscillation measurements of acoustic velocity based on purely classical acoustic considerations. Vectorial resolution of the velocity oscillations was seen to be consistent with periodically shedding vortices. Further studies by Brown et al. (1985) focused on vortex shedding due to sudden flow area expansion at the dump plane applicable to grain transitions in boost/sustained type SRMs and co-axial inlet ramjet engines. These studies demonstrated that acoustic oscillations could be eliminated by insertion of a thin plate orifice in the inlet at the dump plane.

In recent times, extensive work has been done to understand the cause of the pressure oscillations in a solid rocket motor. Anthoine (2000) studied the aeroacoustics of Ariane P05 rocket motor experimentally as well as numerically and concluded that a coupling exists between the acoustic fluctuations induced by the nozzle cavity volume and the vortices in front of the nozzle cavity entrance. In the absence of nozzle cavity, the pressure fluctuations were much lower in magnitude.

## 2.2 Fast Fourier Transform

During data analysis for identify the principal frequencies, we used the Fast Fourier Transform through this method, can characterize the different tones that record with the microphone and watch clearly the switching mode during the increase and decreasing of the air flow rate.

A fast Fourier transform (FFT) is an algorithm to compute the discrete Fourier transform (DFT) and its inverse. Fourier analysis converts time (or space) to frequency (or wavenumber) and vice versa; an FFT rapidly computes such transformations by factorizing the DFT matrix into a product of sparse (mostly zero) factors. As a result, fast Fourier transforms are widely used for many applications in engineering, science, and mathematics. The basic ideas were popularized in 1965, but some FFTs had been previously known as early as 1805. In 1994 Gilbert Strang described the fast Fourier transform as "the most important numerical algorithm of our lifetime".

### 2.2.1 Overview

There are many different FFT algorithms involving a wide range of mathematics, from simple complex-number arithmetic to group theory and number theory; this article gives an overview of the available techniques and some of their general properties, while the specific algorithms are described in subsidiary articles linked below.

The DFT is obtained by decomposing a sequence of values into components of different frequencies. This operation is useful in many fields (see discrete Fourier transform for properties and applications of the transform) but computing it directly from the definition is often too slow to be practical. An FFT is a way to compute the same result more quickly: computing the DFT of N points in the naive way, using the definition, takes $O(N^2)$ arithmetical operations, while a FFT can compute the same DFT in only $O(N \log_2 N)$ operations. The difference in speed can be enormous, especially for long data sets where N may be in the thousands or millions. In practice, the computation time can be reduced by several orders of magnitude in such cases, and the improvement is roughly proportional to $N \log(N)$. This huge improvement made the calculation of the DFT practical; FFTs are of great importance to a wide variety of applications, from digital signal processing and solving partial differential equations to algorithms for quick multiplication of large integers.

The best-known FFT algorithms depend upon the factorization of N, but there are FFTs with $O(N \log N)$ complexity for all N, even for prime N. Many FFT algorithms only depend on the fact that $e^{-\frac{2\pi i}{N}}$ is an N-th primitive root of unity, and thus can be applied to analogous transforms over any finite field, such as number-theoretic transforms. Since the inverse DFT is the same as the DFT, but with the opposite sign in the exponent and a $1/N$ factor, any FFT algorithm can easily be adapted for it.

### 2.2.2 Definition and speed

An FFT computes the DFT and produces exactly the same result as evaluating the DFT definition directly; the most important difference is that an FFT is much faster. (In the presence of round-off error, many FFT algorithms are also much more accurate than evaluating the DFT definition directly, as discussed below).

Let $x_0, \ldots, x_{N-1}$ be complex numbers. The DFT is defined by the formula

$$X_k = \sum_{n=0}^{N-1} x_n e^{-i2\pi k \frac{n}{N}} \qquad k = 0, \ldots, N-1. \tag{2.1}$$

Evaluating this definition directly requires $O(N^2)$ operations: there are $N$ outputs $X_k$, and each output requires a sum of $N$ terms. An FFT is any method to compute the same results in $O(N \log N)$ operations. More precisely, all known FFT algorithms require $O(N \log N)$ operations (technically, O only denotes an upper bound), although there is no known proof that a lower complexity score is impossible.(Johnson & Frigo, 2007) To illustrate the savings of an FFT, consider the count of complex multiplications and additions. Evaluating the DFT's sums directly involves $N^2$ complex multiplications and $N(N-1)$ complex additions (of which $O(N)$ operations can be saved by eliminating trivial operations such as multiplications by 1). The well-known radix-2 Cooley–Tukey algorithm, for $N$ a power of 2, can compute the same result with only $(N2) \log_2(N)$ complex multiplications (again, ignoring simplifications of multiplications by 1 and similar) and $N \log_2(N)$ complex additions. In practice, actual performance on modern computers is usually dominated by factors other than the speed of arithmetic operations and the analysis is a complicated subject (see, e.g., Frigo & Johnson, 2005), but the overall improvement from $O(N^2)$ to $O(N \log N)$ remains.

### 2.2.3 Algorithms

#### Cooley–Tukey algorithm

By far the most commonly used FFT is the Cooley–Tukey algorithm. This is a divide and conquer algorithm that recursively breaks down a DFT of any composite size $N = N_1 N_2$ into many smaller DFTs of sizes $N_1$ and $N_2$, along with $O(N)$ multiplications by complex roots of unity traditionally called twiddle factors (after Gentleman and Sande, 1966). This method (and the general idea of an FFT) was popularized by a publication of J. W. Cooley and J. W. Tukey in 1965, but it was later discovered (Heideman, Johnson, & Burrus, 1984) that those two authors had independently re-invented an algorithm known to Carl Friedrich Gauss around 1805 (and subsequently rediscovered several times in limited forms). The best known use of the Cooley–Tukey algorithm is to divide the transform into two pieces of size N/2 at each step, and is therefore limited to power-of-two sizes, but any factorization can be used in general (as was known to both Gauss and Cooley/Tukey). These are called the radix-2 and mixed-radix cases, respectively (and other variants such as the split-radix FFT have their own names as well). Although the basic idea is recursive, most traditional implementations rearrange the algorithm to avoid explicit recursion. Also, because the Cooley–Tukey algorithm breaks the DFT into smaller DFTs, it can be combined arbitrarily with any other algorithm for the DFT, such as those described below.

#### Other FFT algorithms

There are other FFT algorithms distinct from Cooley–Tukey.

Cornelius Lanczos did pioneering work on the FFS and FFT with G.C. Danielson (1940).

For$N = N_1 N_2$ with coprime $N_1$ and $N_2$, one can use the Prime-Factor (Good-Thomas) algorithm (PFA), based on the Chinese Remainder Theorem, to factorize the DFT similarly to Cooley–Tukey but without the twiddle factors. The Rader-Brenner algorithm (1976) is a Cooley-Tukey-like factorization but with purely imaginary twiddle factors, reducing multiplications at the cost of increased additions and reduced numerical stability; it was later superseded by the split-radix variant of Cooley-Tukey (which achieves the same multiplication count but with fewer additions and without sacrificing accuracy). Algorithms that recursively factorize the DFT into smaller operations other than DFTs include the Bruun and QFT algorithms. (The Rader-Brenner and QFT algorithms were proposed for power-of-two sizes, but it is possible that they could be adapted to general composite n. Bruun's algorithm applies to arbitrary even composite sizes). Bruun's algorithm, in particular, is based on interpreting the FFT as a recursive factorization of the polynomial $z^N - 1$, here into real-coefficient polynomials of the form $z^M -$ and $z^{2M} + az^M + 1$.

Another polynomial viewpoint is exploited by the Winograd algorithm, which factorizes $z^N - 1$ into cyclotomic polynomials—these often have coefficients of 1, 0, or -1, and therefore require few (if any) multiplications, so Winograd can be used to obtain minimal-multiplication FFTs and is often used to find efficient algorithms for small factors. Indeed, Winograd showed that the DFT can be computed with only O(N) irrational multiplications, leading to a proven achievable lower bound on the number of multiplications for power-of-two sizes; unfortunately, this comes at the cost of many more additions, a tradeoff no longer favorable on modern processors with hardware multipliers. In particular, Winograd also makes use of the PFA as well as an algorithm by Rader for FFTs of prime sizes.

Rader's algorithm, exploiting the existence of a generator for the multiplicative group modulo prime N, expresses a DFT of prime size n as a cyclic convolution of (composite) size $N - 1$, which can then be computed by a pair of ordinary FFTs via the convolution theorem (although Winograd uses other convolution methods). Another prime-size FFT is due to L. I. Bluestein, and is sometimes called the chirp-z algorithm; it also re-expresses a DFT as a convolution, but this time of the same size (which can be zero-padded to a power of two and evaluated by radix-2 Cooley–Tukey FFTs, for example), via the identity $nk = -(k-n)^2/2 + n^2/2 + k^2/2$.

### 2.2.4 FFT algorithms specialized for real and/or symmetric data

In many applications, the input data for the DFT are purely real, in which case the outputs satisfy the symmetry

$$X_{N-k} = X_k^* \tag{2.2}$$

and efficient FFT algorithms have been designed for this situation (see e.g. Sorensen, 1987). One approach consists of taking an ordinary algorithm (e.g. Cooley–Tukey) and removing the redundant parts of the computation, saving roughly a factor of two in time and memory. Alternatively, it is possible to express an even-length real-input DFT as a complex DFT of half the length (whose real and imaginary parts are the even/odd elements of the original real data), followed by $O(N)$ post-processing operations.

It was once believed that real-input DFTs could be more efficiently computed by means of the discrete Hartley transform (DHT), but it was subsequently argued that a specialized real-input DFT algorithm (FFT) can typically be found that requires fewer operations than the corresponding DHT algorithm (FHT) for the same number of inputs. Bruun's algorithm (above) is another method that was initially proposed to take advantage of real inputs, but it has not proved popular.

There are further FFT specializations for the cases of real data that have even/odd symmetry, in which case one can gain another factor of (roughly) two in time and memory and the DFT becomes the discrete cosine/sine transform(s) (DCT/DST). Instead of directly modifying an FFT algorithm for these cases, DCTs/DSTs can also be computed via FFTs of real data combined with $O(N)$ pre/post processing.

### 2.2.5 Computational issues

#### Bounds on complexity and operation counts

A fundamental question of longstanding theoretical interest is to prove lower bounds on the complexity and exact operation counts of fast Fourier transforms, and many open problems remain. It is not even rigorously proved whether DFTs truly require $\Omega(N\log(N))$ (i.e., order $N\log(N)$ or greater) operations, even for the simple case of power of two sizes, although no algorithms with lower complexity are known. In particular, the count of arithmetic operations is usually the focus of such questions, although actual performance on modern-day computers is determined by many other factors such as cache or CPU pipeline optimization.

Following pioneering work by Winograd (1978), a tight $O(N)$ lower bound is known for the number of real multiplications required by an FFT. It can be shown that only $4N - 2\log_2^2 N - 2\log_2 N - 4$ irrational real multiplications are required to compute a DFT of power of two length$N = 2^m$. Moreover, explicit algorithms that achieve this count are known (Heideman & Burrus, 1986; Duhamel, 1990). Unfortunately, these algorithms require too many additions to be practical, at least on modern computers with hardware multipliers.

A tight lower bound is not known on the number of required additions, although lower bounds have been proved under some restrictive assumptions on the algorithms. In 1973, Morgenstern proved an $\Omega(N\log(N))$ lower bound on the addition count for algorithms where the multiplicative constants have bounded magnitudes (which is true for most but not all FFT algorithms). It should be noted, however, that Morgenstern's result applies only to the unnormalized transform of determinant $N^{N/2}$, while the normalized transform (which is a complex unitary transformation) does not lend itself to these arguments. Incidentally, Morgenstern's result also implies that the identity transformation scaled by $\sqrt{N}$ also requires $\Omega(N\log(N))$ operations, which is not satisfactory. In 2014, Ailon showed that any scaling of the Fourier transform requires at least $\Omega(N\log(N))$ operations, assuming the computation is well-conditioned. The argument uses a notion of quasi-entropy of matrices, introduced in the same work. Well-conditioned computation is important for numerical stability and is hence a reasonable computational requirement.

Pan (1986) proved an $\Omega(N\log(N))$ lower bound assuming a bound on a measure of the FFT algorithm's "asynchronicity", but the generality of this assumption is unclear. For the case of power of two N, Papadimitriou (1979) argued that the number $N\log_2 N$ of complex-number additions achieved by Cooley–Tukey algorithms is optimal under certain assumptions on the graph of the algorithm (his assumptions imply, among other things, that no additive identities in the roots of unity are exploited). (This argument would imply that at least $2N\log_2 N$ real additions are required, although this is not a tight bound because extra additions are required as part of complex-number multiplications.) Thus far, no published FFT algorithm has achieved fewer than $N\log_2 N$ complex-number additions (or their equivalent) for power-of-two N.

A third problem is to minimize the total number of real multiplications and additions, sometimes called the "arithmetic complexity" (although in this context it is the exact count and not the asymptotic complexity that is being considered). Again, no tight lower bound has been proven. Since 1968, however, the lowest published count for power of two N was long achieved by the split-radix FFT algorithm, which requires $4N\log_2 N - 6N + 8$ real multiplications and additions for $N > 1$. This was recently reduced to $\sim \frac{34}{9}N\log_2 N$ (Johnson and Frigo, 2007; Lundy and Van Buskirk, 2007). A slightly larger count (but still better than split radix for $N \geq 256$) was shown to be provably optimal for $N \leq 512$ under additional restrictions on the possible algorithms (split-radix-like flowgraphs with unit-modulus multiplicative factors), by reduction to a Satisfiability Modulo Theories problem solvable by brute force (Haynal & Haynal, 2011). Most of the attempts to lower or prove the complexity of FFT algorithms have focused on the ordinary complex-data case, because it is the simplest. However, complex-data FFTs are so closely related to algorithms for related problems such as real-data FFTs, discrete cosine transforms, discrete Hartley transforms, and so on, that any improvement in one of these would immediately lead to improvements in the others (Duhamel & Vetterli, 1990).

### Accuracy and approximations

All of the FFT algorithms discussed above compute the DFT exactly (in exact arithmetic, i.e. neglecting floating-point errors). A few "FFT" algorithms have been proposed, however, that compute the DFT approximately, with an error that can be made arbitrarily small at the expense of increased computations. Such algorithms trade the approximation error for increased speed or other properties. For example, an approximate FFT algorithm by Edelman et al. (1999) achieves lower communication requirements for parallel computing with the help of a fast multipole method. A wavelet-based approximate FFT by Guo and Burrus (1996) takes sparse inputs/outputs (time/frequency localization) into account more efficiently than is possible[citation needed] with an exact FFT. Another algorithm for approximate computation of a subset of the DFT outputs is due to Shentov et al. (1995). The Edelman algorithm works equally well for sparse and non-sparse data, since it is based on the compressibility (rank deficiency) of the Fourier matrix itself rather than the compressibility (sparsity) of the data. Conversely, if the data are sparse—that is, if only $K$ out of $N$ Fourier coefficients are nonzero—then the complexity can be reduced to$O(K \log(N) \log(N/K))$, and this has been demonstrated to lead to practical speedups compared to an ordinary FFT for $N/K > 32$ in a large-N example ($N = 222$) using a probabilistic approximate algorithm (which estimates the largest K coefficients to several decimal places).

Even the "exact" FFT algorithms have errors when finite-precision floating-point arithmetic is used, but these errors are typically quite small; most FFT algorithms, e.g. Cooley–Tukey, have excellent numerical properties as a consequence of the pairwise summation structure of the algorithms. The upper bound on the relative error for the Cooley–Tukey algorithm is $O(\varepsilon \log N)$, compared to $O(\varepsilon N^{3/2})$ for the naïve DFT formula (Gentleman and Sande, 1966), where $\varepsilon$ is the machine floating-point relative precision. In fact, the root mean square (rms) errors are much better than these upper bounds, being only $O(\varepsilon\sqrt{\log N})$ for Cooley–Tukey and $O(\varepsilon\sqrt{N})$ for the naïve DFT (Schatzman, 1996). These results, however, are very sensitive to the accuracy of the twiddle factors used in the FFT (i.e. the trigonometric function values), and it is not unusual for incautious FFT implementations to have much worse accuracy, e.g. if they use inaccurate trigonometric recurrence formulas. Some FFTs other than Cooley–Tukey, such as the Rader-Brenner algorithm, are intrinsically less stable.

In fixed-point arithmetic, the finite-precision errors accumulated by FFT algorithms are worse, with rms errors growing as $O(\sqrt{N})$ for the Cooley–Tukey algorithm (Welch, 1969). Moreover, even achieving this accuracy requires careful attention to scaling in order to minimize the loss of precision, and fixed-point FFT algorithms involve rescaling at each intermediate stage of decompositions like Cooley–Tukey.

To verify the correctness of an FFT implementation, rigorous guarantees can be obtained in $O(N\log(N))$ time by a simple procedure checking the linearity, impulse-response, and time-shift properties of the transform on random inputs (Ergün, 1995).

## 2.3 Dynamical Systems

### 2.3.1 What is dynamical system?

A dynamical system is a function with an attitude. A dynamical system is doing the same thing over and over again. A dynamical system is always knowing what you are going to do next. The difficulty is that virtually anything that evolves over time can be thought of as a dynamical system. So let us begin by describing mathematical dynamical systems and then see how many physical situations are nicely modeled by mathematical dynamical systems. A dynamical system has two parts: a state vector which describes exactly the state of some real or hypothetical system, and a function (i.e., a rule) which tells us, given the current state, what the state of the system will be in the next instant of time.

#### State vectors

Physical systems can be described by numbers. This amazing fact accounts for the The state vector is a numerical description of the current configuration of a system. successful marriage between mathematics and the sciences. For example, a ball tossed straight up can be described using two numbers: its height $h$ above the ground and its (upward) velocity $v$. Once we know these two numbers, $h$ and $v$, the fate of the ball is completely determined. The pair of numbers $(h,\ v)$ is a vector which completely describes the state of the ball and hence is called the state vector of the system. Typically, we write vectors as columns of numbers, so more properly, the state of this system is $\left[\begin{smallmatrix} h \\ v \end{smallmatrix}\right]$

It may be possible to describe the state of a system by a single number. For example, consider a bank account opened with \$100 at 6% interest compounded annually. The state of this system at any instant in time can be described by a single number: the balance in the account. In this case, the state vector has just one component. On the other hand, some dynamical systems require a great many numbers to describe. For example, a dynamical system modeling global weather might have millions of variables accounting for temperature, pressure, wind speed, and so on at points all around the world. Although extremely complex, the state of the system is simply a list of numbers a vector. Whether simple or complicated, the state of the system is a vector; typically we denote vectors by bold, lowercase letters, such as x. (Exception: When the state can be described by a single number, we may write $x$ instead of x).

#### The next instant: discrete time

The second part of a dynamical system is a rule which tells us how the system changes over time. In other words, if we are given the current state of the system, the rule tells us the state of the system in the next instant. In the case of the bank account described above, the next instant will be one year later, since interest is paid only annually; time is discrete. That is to say, time is a sequence of separate chunks each following the next like beads on a string.

**The next instant: continuous time**

Bank accounts which change only annually or computer chips which change only during clock cycles are examples of systems for which time is best viewed as progressing in discrete packets. Many systems, however, are better described with time progressing smoothly. Consider our earlier example of a ball thrown straight up. Its instantaneous status is given by its state vector $x = \left[\begin{smallmatrix} h \\ v \end{smallmatrix}\right]$ However, it doesn't make sense to ask what its state will be in the "next" instant of time—there is no "next" instant since time advances continuously. We reflect this different perspective on time by using the letter t (rather than Continuous time is denoted k) to denote time. Typically t is a nonnegative real number and we start time at by $t = 0$. Since we cannot write down a rule for the "next" instant of time, we instead describe how the system is changing at any given instant.

### 2.3.2 Non Linear Systems

During the thesis work, we face a problems Nonlinear systems and for this reason, the next chapter will focus on them.
The general forms for dynamical systems are:

$$x_0 = f(x) \quad \text{continuous time, and}$$
$$x(k+1) = f(x(k)) \quad \text{discrete time.}$$

We have closely examined the case when f is linear. In that case, we can answer nearly any question we might consider. We can work out exact formulas for the behavior of $x(t)$ (or $x(k)$) and deduce from them the long-term behavior of the system. There are two main behaviors: (1) the system gravitates toward a fixed point, or (2) the system blows up. There are some marginal behaviors as well.

**What is a fixed point?**

The vector $x$ is the state of the dynamical system, and the function $f$ tells us how A state vector that doesn't change. the system moves. In special circumstances, however, the system does not move. The system can be stuck (we will say fixed) in a special state; we call these states fixed points of the dynamical system.

For example, consider the nonlinear discrete time system

$$x(k+1) = [x(k)]^2 - 6.$$

Suppose the system is in the state $x(k) = 3$; where will it be in the next instant? This is easy to compute:

$$x(k+1) = x(k)^2 - 6 = 3^2 - 6 = 3.$$

The system is again at state $x = 3$. Where will it be in the next time period? Of course, still in state 3. The value $x = 3$ is a fixed point of the system $x(k+1) = x(k)^2 - 6$, since if we are ever in state 3 we remain there for all time. (This system has another fixed point; try to find it.)

Let's consider a continuous time example:

$$x' = x^3 - 8$$

What happens if $x(t) = 2$? We compute that dx/dt equals $x^3 - 8 = 23 - 8 = 0$. Thus $x(t)$ is neither increasing nor decreasing; in other words, it's stuck at 2. Thus $\tilde{x} = 2$ is a fixed point of this system. (This system has no other fixed points; try to figure out why.) Thus a fixed point of a dynamical system is a state vector $\tilde{x}$ with the property that if the system is ever in the state $\tilde{x}$, it will remain in that state for all time.

### Stability

Not all fixed points are the same. We call some stable and others unstable. We begin by illustrating these concepts with an example.

Let $f(x) = x^2$ and consider the discrete time dynamical system

$$x(k+1) = f(x(k)) = [x(k)]^2.$$

In other words, we are interested in seeing what happens when we iterate the square function. The system has two fixed points: 0 and 1 (these are the solutions to $f(x) = x$, i.e., $x^2 = x$). If you enter either 0 or 1 into your calculator and start pressing the x2 button, you will notice something very boring: nothing happens. Both 0 and 1 are fixed points, and the x2 function just leaves them alone. Now, let's put other numbers into our calculator and see what happens. First, let us start with a number which is close to (but not equal) 0, say 0.1. If we iterate $x^2$, we see

$$0.1 \to 0.01 \to 0.0001 \to 0.0000001 \to \dots.$$

Clearly $x(k) \to 0$ as $k \to 1$. It's not hard to see why this works. If we begin with any number $x_0$, our iterations go

$$x_0 \to x_0^2 \to x_0^4 \to x_0^8 \to \cdots \to x_0^{2^k} \to \dots$$

Thus if $x_0$ is near 0, then, clearly, $x(k) \to 0$ as $k \to \infty$. (How near zero must we be? All we need is $\mid x_0 \mid < 1$). We say that $x_0$ is a stable or an attractive fixed point of the system $x(k+1) = f(x(k))$ because if we start the system near $x_0$, then the system gravitates toward $x_0$.

Now let's examine the other fixed point, 1. What happens if we put a number near (but not equal to) 1 in our calculator and start iterating the $x^2$ function. If $x_0 = 1.1$, we see

$$1.1 \to 1.21 \to 1.4641 \to 2.1436 \to 4.5950 \to 21.1138 \to 445.7916 \to \dots.$$

Clearly, $x(k) \to 1$. If we take $x_0 = 0.9$, we see

$$0.9 \to 0.81 \to 0.6561 \to 0.4305 \to 0.1853 \to 0.0343 \to 0.0012 \to \dots$$

Clearly $x(k) \to 0$. In any case, starting points near (but not equal to) 1 tend to iterate away from 1. We call 1 an *unstable* fixed point of the system.

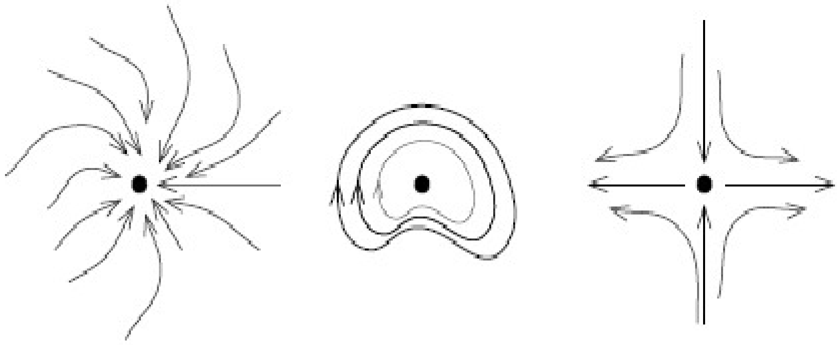

Figure 2.1: Fixed points with three different types of stability. The fixed point on the left is stable. The fixed point in the center is marginally stable. The fixed point on the right is unstable.

Let us now describe three types of fixed points a system may possess.

First, a fixed point $\tilde{x}$ is called *Stable* fixed point. stable provided the following is true: For all starting values $x_0$ near $\tilde{x}$, the system not only stays near $\tilde{x}$ but also $x(t) \to \tilde{x}$ as $t \to \infty$ [or $x(k) \to \tilde{x}$ as $k \to \infty$ in discrete time]. Marginally stable (or Second, a fixed point $\tilde{x}$ is called marginally stable or neutral provided the folneutral) fixed point. lowing: For all starting values $x_0$ near $\tilde{x}$, the system stays near $\tilde{x}$ but does not converge to $\tilde{x}$. Unstable fixed point. Third, a fixed point $\tilde{x}$ is called unstable if it is neither stable nor marginally stable. In other words, there are starting values $x_0$ very near $\tilde{x}$ so that the system moves far away from $\tilde{x}$.
Figure 2.1 illustrates each of these possibilities. The fixed point on the left of the figure is stable; all trajectories which begin near $\tilde{x}$ remain near, and converge to, $\tilde{x}$. The fixed point in the center of the figure is marginally stable (neutral). Trajectories which begin near $\tilde{x}$ stay nearby but never converge to $\tilde{x}$. Finally, the fixed point on the right of the figure is unstable. There are trajectories which start near $\tilde{x}$ and move far away from $\tilde{x}$.

### 2.3.3 Non Linear Systems: Periodicity and Chaos

The dissipative nonlinear systems such as fluid flows reach a random or chaotic state when the parameter measuring nonlinearity, where Rayleigh number is large. The change to the chaotic stage generally takes place through a sequence of transitions, with the exact route depending on the system. It has been realized that chaotic behaviour not only occurs in continuous systems having an infinite number of degrees of freedom, but also in discrete nonlinear systems having only a small number of degrees of freedom, governed by ordinary nonlinear differential equations. In this context, a chaotic system is defined as one in which the solution is extremely sensitive to initial conditions. That is, solutions with arbitrarily close initial conditions evolve into quite different states. Other symptoms of a chaotic system are that the solutions are aperiodic, and that the spectrum is broadband instead of being composed of a few discrete lines. Numerical integrations have recently demonstrated that nonlinear systems governed by a finite set of deterministic ordinary differential equations allow chaotic solutions in response to a steady forcing. This fact is interesting because in a dissipative linear system a constant forcing ultimately (after the decay of the transients) leads to constant response, a periodic forcing leads to periodic response, and a random forcing leads to random response. In the presence of nonlinearity, however, a constant forcing can lead to a variable response, both periodic and aperiodic. It has been found that transition to chaos in the solution of ordinary nonlinear differential equations displays a certain universal behaviour and proceeds in one of a few different ways. At the moment it is unclear whether the transition in fluid flows is closely related to the development of chaos in the solutions of these simple systems; this is under intense study.

Returning to dynamical systems, they do not live by fixed points alone. Exist three possible behaviors for dynamical systems: attraction to a fixed point, divergence to infinity, and (in continuous time) "cyclic" behavior. In this paragraph we see that periodic behavior can also occur in discrete time and that another type of behavior—chaos—is a possibility as well. What is "*periodicbehavior*"? A dynamical system exhibits periodic behavior when it returns to a previously visited state. We can write this as $x(t_1) = x(t_1 + T)$ for some $T > 0$. Notice that whatever trajectory the system took from time $t_1$ to time $t_1+T$, the system is destined to repeat that same path again and again because the state at time $t_1+T$ is exactly the same as the state at time $t_1$. Thus we realize that $x(t_1) = x(t_1 + T) = x(t_1 + 2T) = x(t_1 + 3T) = \ldots$. The system retakes the same steps over and over again, visiting the same states infinitely often. A fixed point is an extreme example of periodic behavior. What is "chaos"? We discuss this concept later, but for now we want to point out that a system can behave in a nonperiodic and nonexplosive manner which, although completely determined, is utterly unpredictable!

**Phase Space**

Very few nonlinear equations have analytical solutions. For nonlinear systems, a typical procedure is to find a numerical solution and display its properties in a space whose axes are the dependent variables. For example: Consider the equation governing the motion of a simple pendulum of length l:

$$\ddot{X} + \frac{g}{l}\sin x = 0$$

where $X$ is the angular displacement and $\ddot{X}(= d^2X/dt^2)$ is the angular acceleration. (The component of gravity parallel to the trajectory is $-g\sin X$, which is balanced by the linear acceleration $l\ddot{X}$ ). The equation is nonlinear because of the $\sin X$ term. The second-order equation can be split into two coupled first-order equations:

$$\dot{X} = Y$$
$$\dot{Y} = -\frac{g}{l}\sin X$$

Starting with some initial conditions on $X$ and $Y$ , one can integrate set $(n \circ 2eq)$. The behaviour of the system can be studied by describing how the variables $Y(= \dot{X})$ and $X$ vary as a function of time. For the pendulum problem, the space whose axes are $\dot{X}$ and $X$ is called a *phasespace*, and the evolution of the system is

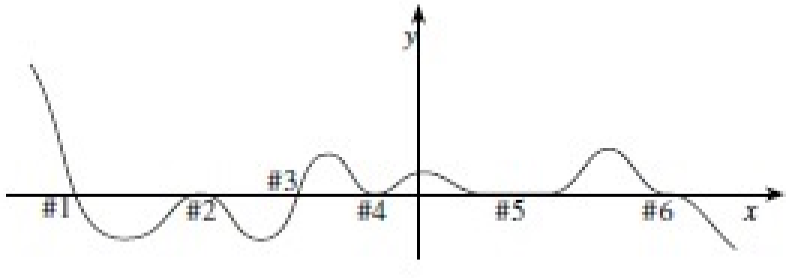


Figure 2.2: Graph of a function $f$ for a one-dimensional dynamical system. Various fixed points are marked.

described by a *trajectory* in this space. The dimension of the phase space is called the *degree of freedom* of the system; it equals the number of independent initial conditions necessary to specify the system. For example, the degree of freedom for the set previous is two.

### Continuos time

### One dimension: no periodicity

We begin by discussing the long-term fate of the simplest systems: continuous time One-dimensional continuous time systems either explode or tend to fixed points. dynamical systems in one variable, $x' = f(x)$. Pick an $x$, any $x$. There are three possibilities: $f(x)$ is zero, positive, or negative. If $f(x)$ is zero, we know that x is a fixed point. If $f(x)$ is positive, then $x(t)$ must be increasing, and if $f(x)$ is negative, $x(t)$ is decreasing. Our first observation is that periodic behavior is not possible (except for fixed Periodic behavior is not possible for one-dimensional continuous time systems. points). Consider a state $x_1$ which we allegedly visit at times $s$ and $t$, with $s < t$. This is possible if $x_1$ is a fixed point, but otherwise we have $f(x_1)$ either positive or negative. If $f(x_1)$ is positive, then, in the short run, the system moves to a state $x_2$ greater than $x_1$. Since $f$ is continuous, we may assume that $f$ is positive over the entire interval $[x_1, x_2]$. So we're at $x_2$ and still increasing. Now, how can we ever return to $x_1$? To get there, we must decrease through the interval $[x_1, x_2]$, but the equation $x' = f(x)$ says that $x$ must increase throughout the same interval. Thus it's impossible to ever revisit the state $x_1$. By a similar analysis, we can never revisit a state with $f(x_1) < 0$.

Thus the only type of recurrent behavior one-dimensional continuous systems can exhibit is that of fixed points. Figure 2.2 shows the graph of a function $f$ for a one-dimensional continuous time dynamical system $x' = f(x)$. Several fixed points are marked, with each somewhat different from the others.

- Fixed point #1. This is a stable fixed point; to its left the system is increasing and to its right, decreasing.
- Fixed point #2. This is a "semistable" fixed point. To its left the system is

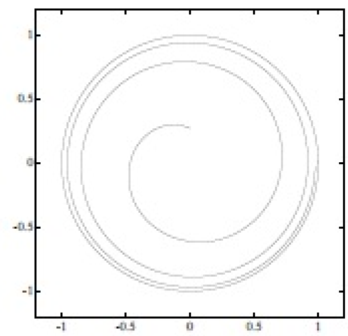


Figure 2.3: An orbit approaching a periodic orbit. The trajectory starts near the middle of the figure and spirals outward, becoming more and more like a circle.

decreasing, and so starting values less than $\tilde{x}$ move away from $\tilde{x}$. To the right the system is also decreasing, and so the fixed point behaves like an attractor on this side.

- Fixed point #3. This is an unstable fixed point. To its left, the system is decreasing and to its right, increasing.
- Fixed point #4. This is another semistable fixed point, but its action is opposite that of #2. This fixed point is an attractor on its left and a repellor on its right.
- Fixed points #5. This is an entire interval where $f(x) = 0$. These fixed points are marginally stable. Perturbing the system slightly away from one of these fixed points neither causes the system to return to the fixed points nor to fly away.
- Fixed point #6. This is another stable fixed point, but one where $f'(x) = 0$. Thus the linearization test of the previous chapter would fail at this fixed point.

In conclusion, the behaviors of one-dimensional continuous dynamical systems are rather limited. Ultimately, such a system must either gravitate toward a fixed point or explode to infinity.

### Two dimensions: the Poincaré-Bendixson theorem

One-dimensional continuous systems either converge to a fixed point or diverge to infinity. These behaviors are exhibited by two-dimensional continuous systems as well. However, two-dimensional systems also exhibit another behavior: periodicity. Let $x' = f(x)$ be a two-dimensional continuous time dynamical system. Each state of this system, $x$, is a point in the plane (the phase space) of the system. If $x_0$ is a fixed point of the system, then the trajectory starting at $x_0$ is not very exciting: The system is "stuck" at $x_0$ and remains there for all time. Otherwise ($x_0$ is not a fixed point) the trajectory is a proper curve. In principle (and often in actuality) this curve can return to $x_0$. Suppose the first return is at time $T$. Now, at time $T$ it

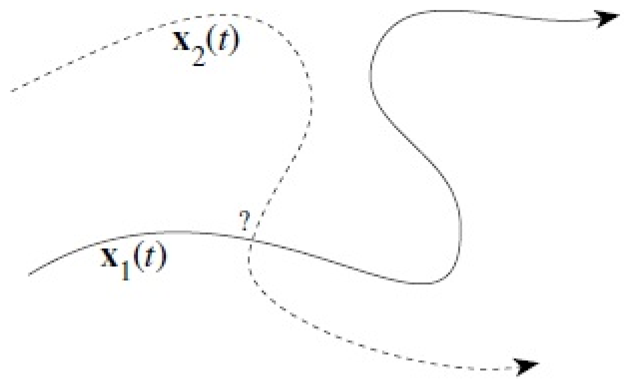


Figure 2.4: Two orbits of a dynamical system cannot cross.

is as if we have started all over. Thus at time $t+T$ we are exactly in the same state as at time $t$. In other words, for any time t we have $x(t+T) = x(t)$. Such a curve is called periodic, and the smallest positive number $T$ for which $x(t+T) = x(t)$ is called the period of the curve. For example, for the system

$$\begin{bmatrix} x_1' \\ x_2' \end{bmatrix} = \begin{bmatrix} 0 & 1 \\ -1 & 0 \end{bmatrix} \begin{bmatrix} x_1 \\ x_2 \end{bmatrix}$$

we find that (for any $x_0$ other than 0) the trajectories are periodic with period $2\pi$. If a dynamical system starts near, but not at, an stable fixed point $\tilde{x}$, we expect the system to gravitate to $\tilde{x}$. Note that we expect $x(t)$ to approach $\tilde{x}$; it need not be the case that $x(t) = \tilde{x}$ for any $t$. Similarly, it is possible that a trajectory will never exhibit periodic behavior but will approach a periodic orbit; see Figure 2.3. A trajectory of this system begins at $x_0 = \left[\begin{smallmatrix} 0 \\ 0.27 \end{smallmatrix}\right]$ and spirals outward approaching, but never quite reaching, the unit circle. Thus, as time progresses, the trajectory becomes more and more like the periodic orbit. To be more specific, let $x_1(t)$ and $x_2(t)$ be two different trajectories of a system $x' = f(x)$. We say that trajectory $x_1$ approaches trajectory $x_2$ provided $\mid x_1(t) - x_2(t+c) \mid \rightarrow 0$ (where $c$ is a constant) as $t \rightarrow \infty$. Two trajectories of a dynamical system, however, cannot cross; see Figure 2.4. Trajectories cannot cross. Consider the point of intersection if two trajectories actually did intersect. The trajectory of the system starting at that point of intersection is completely determined and therefore must proceed along a unique path. The situation in Figure 2.4 is therefore impossible. Now imagine all the possible trajectories of a two-dimensional dynamical system drawn in a plane. You should see a situation akin to the one depicted in Figure 2.5. Since the curves cannot cross one another (or themselves), their behavior is greatly limited.

Essentially they can (1) bunch together toward a point, (2) zoom off toward infinity, or (3) wrap more and more tightly around a simple closed curve. These intuitive ideas are the heart The three behaviors open to of the Poincarè-Bendixson theorem, which continuous time two-dimensional systems. states that a two-dimensional continuous time dynamical system $x' = f(x)$ will have one of three possible behaviors as $t \rightarrow \infty$: It may (1) converge to a fixed point, (2) diverge to infinity, or (3) approach a periodic orbit.

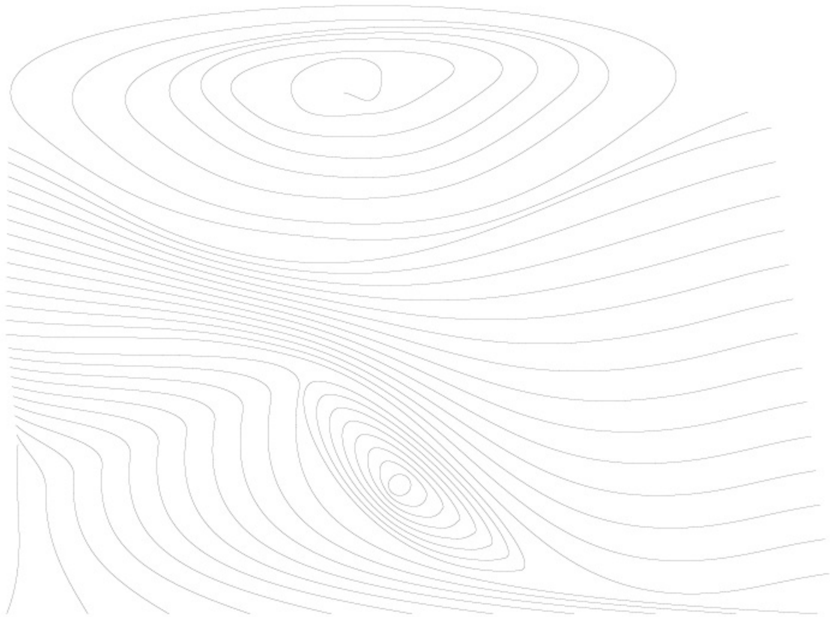

Figure 2.5: Many different orbits of a two-dimensional dynamical system.

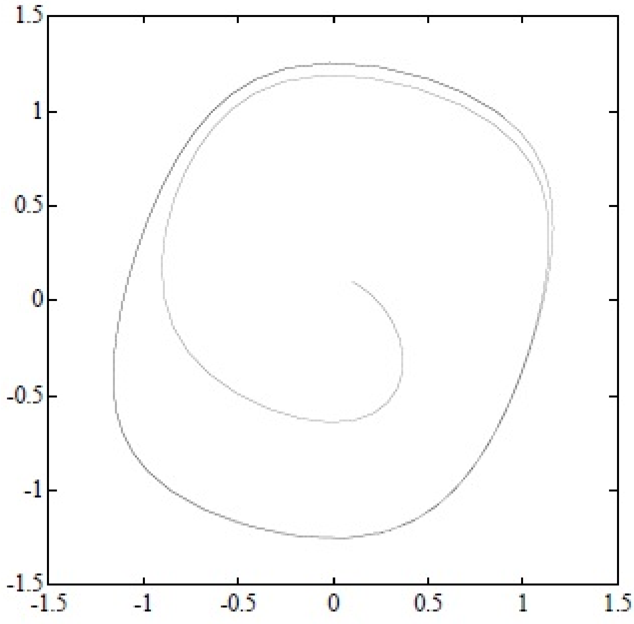


Figure 2.6: Starting near the unstable fixed point and approaching a stable cycle. (The trajectory starts near the origin and spirals outward.)

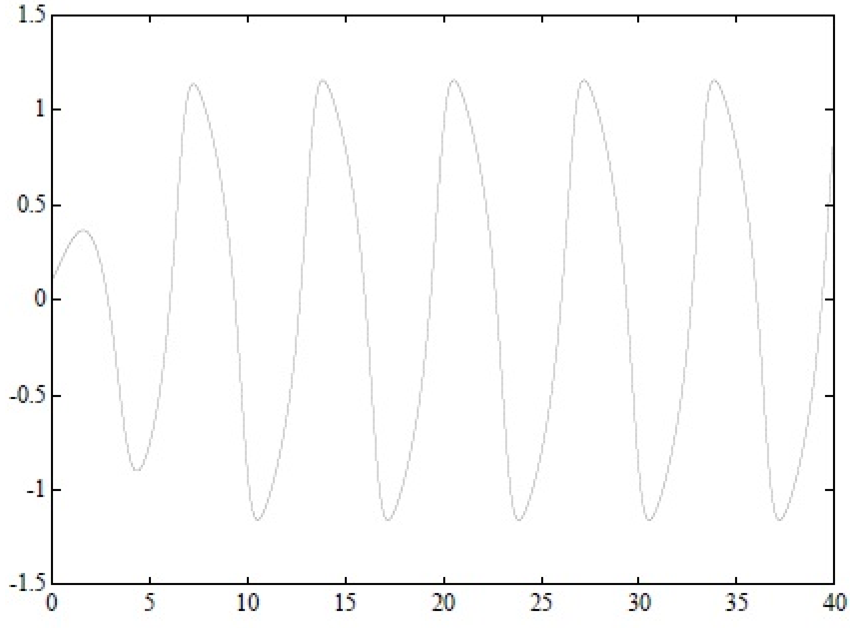


Figure 2.7: Example: Like the system quickly becomes periodic.

### Bifurcation

Bifurcation theory is the mathematical study of changes in the qualitative or topological structure of a given family, such as the integral curves of a family of vector fields, and the solutions of a family of differential equations. Most commonly applied to the mathematical study of dynamical systems, a bifurcation occurs when a small smooth change made to the parameter values (the bifurcation parameters) of a system causes a sudden 'qualitative' or topological change in its behaviour. Bifurcations occur in both continuous systems (described by ODEs, DDEs or PDEs), and discrete systems (described by maps). The name "bifurcation" was first introduced by Henri Poincaré in 1885 in the first paper in mathematics showing such a behavior. Henri Poincaré also later named various types of stationary points and classified them.

Exist differents Bifurcation Types:

- Local bifurcations, which can be analysed entirely through changes in the local stability properties of equilibria, periodic orbits or other invariant sets as parameters cross through critical thresholds; and
- Global bifurcations, which often occur when larger invariant sets of the system 'collide' with each other, or with equilibria of the system. They cannot be detected purely by a stability analysis of the equilibria (fixed points).

### Local bifurcations

Period-halving bifurcations (L) leading to order, followed by period doubling bifurcations (R) leading to chaos.

A local bifurcation occurs when a parameter change causes the stability of an equilibrium (or fixed point) to change. In continuous systems, this corresponds to the real part of an eigenvalue of an equilibrium passing through zero. In discrete systems (those described by maps rather than ODEs), this corresponds to a fixed point having a Floquet multiplier with modulus equal to one. In both cases, the equilibrium is non-hyperbolic at the bifurcation point. The topological changes in the phase portrait of the system can be confined to arbitrarily small neighbourhoods of the bifurcating fixed points by moving the bifurcation parameter close to the bifurcation point (hence 'local').

More technically, consider the continuous dynamical system described by the ODE

$$\dot{x} = f(x, \lambda) \quad f \colon \mathbb{R}^n \times \mathbb{R} \to \mathbb{R}^n.$$

A local bifurcation occurs at $(x_0, \lambda_0)$ if the Jacobian matrix $\mathrm{d}f_{x_0,\lambda_0}$ has an eigenvalue with zero real part. If the eigenvalue is equal to zero, the bifurcation is a steady state bifurcation, but if the eigenvalue is non-zero but purely imaginary, this is a Hopf bifurcation.

For discrete dynamical systems, consider the system

$$x_{n+1} = f(x_n, \lambda) .$$

Then a local bifurcation occurs at $(x_0, \lambda_0)$ if the matrix $\mathrm{d}f_{x_0,\lambda_0}$ has an eigenvalue with modulus equal to one. If the eigenvalue is equal to one, the bifurcation is either a saddle-node (often called fold bifurcation in maps), transcritical or pitchfork bifurcation. If the eigenvalue is equal to -1, it is a period-doubling (or flip) bifurcation, and otherwise, it is a Hopf bifurcation.

Examples of local bifurcations include:

- Saddle-node (fold) bifurcation
- Transcritical bifurcation
- Pitchfork bifurcation
- Period-doubling (flip) bifurcation
- Hopf bifurcation
- Neimark (secondary Hopf) bifurcation

### Global bifurcations

Global bifurcations occur when "larger" invariant sets, such as periodic orbits, collide with equilibria. This causes changes in the topology of the trajectories in the phase space which cannot be confined to a small neighbourhood, as is the case with local bifurcations. In fact, the changes in topology extend out to an arbitrarily large distance (hence "global").

Examples of global bifurcations include:

- Homoclinic bifurcation in which a limit cycle collides with a saddle point.
- Heteroclinic bifurcation in which a limit cycle collides with two or more saddle points.

- Infinite-period bifurcation in which a stable node and saddle point simultaneously occur on a limit cycle.

- Blue sky catastrophe in which a limit cycle collides with a nonhyperbolic cycle.

Global bifurcations can also involve more complicated sets such as chaotic attractors (e.g. crises).

After We will see that the bifurcation type is fundamental to detection the Intermittency type. Also, if it is very complex.

## 2.4 Instability as a loss multifractality

As we have seen so far, the dynamic processes happening inside a pipe with an orifice involve the coupled nonlinear processes which cannot be described by simple linear techniques. In this chapter, we shall introduce the framework of fractals and multifractals in order to tackle this complexity. Using a technique known as multifractal detrended fluctuation analysis, the deviations of the central moments of measured fluctuations with time are computed, which can directly be related to the fractal dimension of the time signal. It is shown that noise generated from the aeroacoustic phenomennons are multifractal and that the onset of hydrodynamic instability results in a loss of this multifractality. The rate of variation of central moments decrease gradually towards zero as instability is approached, which can be used as yet another early warning signal to impending hydrodynamic instability.

### 2.4.1 Fractal and Fractality

The term "fractal" is used to describe objects that have a fractional dimension (Mandelbrot 1982). Whereas classical Euclidean geometry deals with smooth objects that have integer dimensions, structures in nature often tend to be fractals because they are wrinkly at all levels of magnification. Measures such as length, area or volume cannot be defined for such objects since they depend on the scale of measurement. For instance, the length of a fractal curve increases when the ruler is made smaller because additional details are now revealed. A logarithmic plot of the measured length of the curve against the length of the ruler for such a curve would then show an inverse powerlaw; i.e., a straight line with a negative slope. This slope, which is a number between one and two, is referred to as the "fractal dimension" of the curve. Thus, we see that such curves occupy more space than a straight line which scales as the length of the ruler, but less space than a square which scales as the square of the length of the ruler. The concept of fractals can also be used to describe complex dynamics that results in fluctuations spread over multiple orders of temporal magnitude. A fractal process is characterized by a broad-band power spectrum with an inverse power-law, known more popularly as the $1/f$ spectrum (Montroll and Schlesinger, 1982; Schlesinger, 1987) since there is here an inverse relationship between frequency and power. Similar to a fractal curve, a fractal time signal also has a dimension between one and two. A fractal time series also displays a property known as "scale invariance", which means that features of the signal look the same on many different scales of observation (seconds, minutes etc ...). Mathematically, for a fractal time signal, $p(ct) = p(t)/cH$ for some scaling $c$ and a constant $H$. Scale invariance thus relates the time series across multiple time scales.

Such a dependence on multiple time scales results in a broad profile of responses in the amplitude spectrum representative of details that are present at these time scales. On the contrary, if the process can adequately be represented in terms of one or a few discrete time scales, then the signal would have an amplitude spectrum with discrete, narrow peaks. In the next subsection, we will show how the presence of fractality is related to the memory of a time signal.

### Statistical description of a time signal

Statistical analysis of time signals involve obtaining the distribution of their fluctuations (Gaussian, Poisson, Levy etc ...) or representing this distribution in terms of representative measures computed around the most likely measurement value (central moments). Fluctuations that are fractals, but appear noise-like, differ from noise in that they do not satisfy the statistics of classical random variables. Whereas the central moments of a random variable are bounded in time, the central moments of a fractal signal diverge with time at least over a short range (Mandelbrot 1974). This can happen for instance when the measurement values represent variations both in time and space, which makes the signal non-stationary. A signal is non-stationary, if the central moments vary with time, or in other words, there is a variation in the underlying distribution of data values. In the description of non-stationary time signals, classical measures such as mean or variance are not very useful since they vary with time Instead, they are characterized by examining how the moments depend on the time interval over which they are evaluated. For instance, the dependency of the standard deviation of the time signal on time interval is encapsulated in a parameter called the Hurst exponent $H$ (H. E. Hurst, 1951). It measures the amount of correlation or the memory in a time series and is related to the fractal dimension $D$ of the time series as $D = 2 - H$ (Basingthwaighte et al., 1994). The concept of structure functions introduced by Kolmogorov (Kolmogorov, 1941; Frisch, 1995) is a generalized version of this idea, which explores scaling relationships between the variations in the moments of measured fluctuations and the time interval of measurement. A time series is called persistent (anti-correlated) if a large value is typically (i.e., with high statistical preference) followed by a large value and a small value is followed by a small value (Kantelhardt, 2011). In other words, the signal retains a memory of what happened in the previous time step and has an increased probability of the next step being in the same direction—such signals have a trend. For a persistent signal, the Hurst exponent $H$ lies between 0.5 and 1 and the strength of the trend increases as $H$ approaches one. An anti-persistent (correlated) time series, on the other hand, is one in which a large value is typically followed by a small value, and a small value is followed by a large value. Such signals have a tendency to revert to its mean value. For antipersistent signals, values of $H$ lie between 0 and 0.5. The strength of mean reversion increases as $H$ approaches zero. For time signals that are persistent or anti-persistent, fractal scaling law holds in at least a limited range of scales (Kantelhardt, 2011). For an uncorrelated time series, the Hurst exponent is 0.5. This is expected, since the variance of fluctuations in a memory-less diffusion process should scale linearly with time. The Hurst exponent also determines the scaling properties of the fractal time series. If $p(t)$ is a fractal time signal with Hurst exponent $H$, then $p(ct) = p(t)/cH$ is another fractal signal with the same statistics (West et al., 2003). Algorithms that compute the Hurst exponent are mostly based on this scaling property. This scaling behaviour typically has an upper and a lower cut-off that is dependent on the system dynamics. Detrended fluctuation analysis (DFA) (Peng et al., 1994) provides an easy approach to characterize fractality in a given time series data. Through an evaluation of the structure functions, correlations in the data are sought for by computing the Hurst exponent which can then be related to the fractal dimension of the time series.

### When fractality is not more enough

Many time signals exhibit a complex scaling behaviour that cannot be accounted for by a single fractal dimension. A full description of the scaling in such signals involves multiple generalized Hurst exponents, resulting in interwoven subsets of varying fractal dimension (varying Hurst exponents) producing what is termed a 'multifractal' behaviour (Frisch and Parisi, 1985). In other words, fluctuations in a time signal that have different amplitudes follow different scaling rules. The method of DFA can be expanded to explore multifractality in a time signal and the technique is called multifractal detrended fluctuation analysis (Kantelhardt et al., 2001, 2002). The procedure involves computing generalized Hurst exponents that describe the scaling of central moments for various negative as well as positive orders of the moments ($q$) that have been appropriately scaled. For instance, standard deviation has an order of two and its scaling with time interval gives the Hurst exponent. For a multifractal signal, the generalized Hurst exponents would have different values for different orders of the moments. Through a Legendre transform, this variation in generalized Hurst exponents at different orders can alternately be represented as a spectrum of singularities $f(\alpha)$, in terms of the new variable $\alpha$ which is conjugate to$q$. A plot of $f(\alpha)$ for various values of $\alpha$ is termed the multifractal spectrum, the width of which provides a measure of the multifractality in the signal. An excellent description of multifractal processes may be found in Paladin and Vulpiani (1987).

The presence of multifractality is an indication that there are multiplicative processes involved in the transfer of energy across various time scales (Sreenivasan, 1991). Provided one accepts Taylor's frozen flow hypothesis (Taylor, 1938), the argument can be extended to hold for energy transfer across various spatial scales as well. The energy transfer at turbulent flow conditions involve a multiplicative Richardson's cascade (Richardson, 1922) in the inertial subrange from the integral scale down to Kolmogorov scale. The onset of instability transforms the dynamics from one characterized by a multiplicity of scales to one dominated by a few discrete time scales associated with the formation of large-scale coherent structures in the flow field. It remains an interesting problem to identify how the interaction of turbulence with the acoustic field of a confinement transforms such an energy transfer across multiple time-scales to transfers that are dominated by a few time-scales. This can happen—for instance—through an inverse cascade (Kraichnan, 1967), wherein the energy of the smaller scales gets transferred to progressively larger scales. The formation of large-scale coherent structures during instability possibly hints at the presence of such an inverse cascade co-existing simultaneously with the usual direct cascade that dissipates energy at Kolmogorov scales.

### 2.4.2 Evaluation of Hurst exponents and the multifractal spectrum

In recent years the detrended fluctuation analysis (DFA) method has become a widely used technique for the determination of (mono-) fractal scaling properties and the detection of long-range correlations in noisy, nonstationary time series. It has successfully been applied to diverse Lelds such as DNA sequences, heart rate dynamics, neuron spiking, human gait, long-time weather records, cloud structure, geology, ethnology, economics time series, and solid state physics. One reason to employ the DFA method is to avoid spurious detection of correlations that are artifacts of nonstationarities in the time series. Many records do not exhibit a simple monofractal scaling behavior, which can be accounted for by a single scaling exponent. In some cases, there exist crossover (time-) scales $s_x$ separating regimes with different scaling exponents, e.g. long-range correlations on small scales $s \ll s_x$ and another type of correlations or uncorrelated behavior on larger scales $s \gg s_x$. In other cases, the scaling behavior is more complicated, and different scaling exponents are required for different parts of the series. This occurs, e.g., when the scaling behavior in the Lrst half of the series differs from the scaling behavior in the second half. In even more complicated cases, such different scaling behavior can be observed for many interwoven fractal subsets of the time series. In this case a multitude of scaling exponents is required for a full description of the scaling behavior, and a multifractal analysis must be applied. In general, two different types of multifractality in time series can be distinguished: (*i*) Multifractality due to a broad probability density function for the values of the time series. In this case the multifractality cannot be removed by shuffing the series. (*ii*) Multifractality due to different long-range (time-) correlations of the small and large fluctuations. In this case the probability density function of the values can be a regular distribution with finite moments, e.g. a Gaussian distribution. The corresponding shuffled series will exhibit nonmultifractal scaling, since all long-range correlations are destroyed by the shuffling procedure. If both kinds of multifractality are present, the shuffled series will show weaker multifractality than the original series. The simplest type of multifractal analysis is based upon the standard partition function multifractal formalism, which has been developed for the multifractal characterization of normalized, stationary measures. Unfortunately, this standard formalism does not give correct results for nonstationary time series that are affected by trends or that cannot be normalized. Thus, in the early 1990s an improved multifractal formalism has been developed, the wavelet transform modulus maxima (WTMM) method, which is based on wavelet analysis and involves tracing the maxima lines in the continuous wavelet transform over all scales. Here, we propose an alternative approach based on a generalization of the DFA method. This multifractal DFA (MF-DFA) does not require the modulus maxima procedure, and hence does not involve more effort in programming than the conventional DFA (Kantelhardt, Zschiegner, Koscielny-Bunde, Havlin, Bunde, Stanley et. al. 2002).

To estimate the Hurst exponent using detrended fluctuation analysis (DFA), the time signal $p(t)$ of length $N$ is first mean-adjusted and then a cumulative deviate series $y_k$ is obtained as:

$$y_k = \sum_{t=1}^{k} (p(t) - m) \tag{2.3}$$

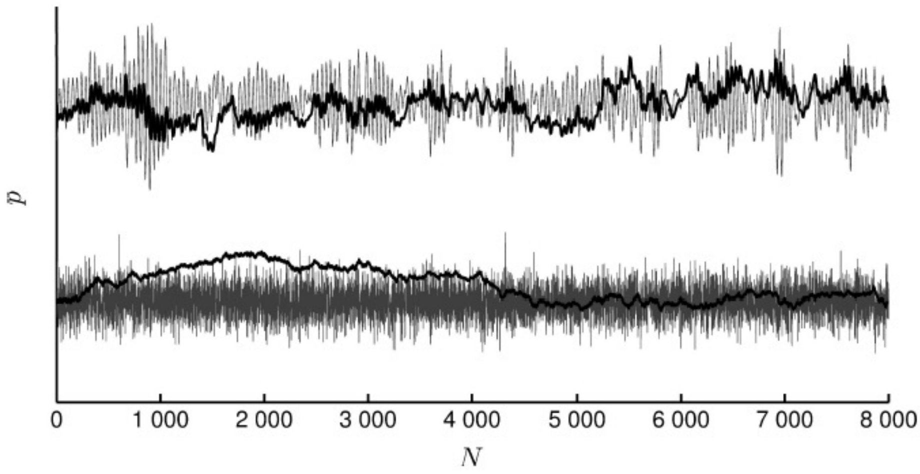


Figure 2.8: Example: A portion of the time signal (gray) and its cumulate deviate series (black) for (a) combustion noise and (b) Gaussian white noise.

$$m = \frac{1}{N}\sum_{t=1}^{N} p(t) \tag{2.4}$$

The deviate series is then divided into a number nw of non-overlapping segments ($y_i(t), i = 1, \dots, n_w$) of equal span $w$. The signal (2.9) which has been split into non-overlapping bins. In order to remove the trends in these segments, a local linear fit yi is made separately to each of the sections of the deviate series $y_i$. These linear fits are shown as dashed lines in Fig. (2.9). The detrended fluctuations are then obtained by subtracting the polynomial fit from the deviate series. The structure function of order $q$ and span $w$, $F_q^w$ can be obtained from the detrended fluctuations as:

$$F_w^q = \left(\frac{1}{n_w}\sum_{t=1}^{n_w}\left(\sqrt{\frac{1}{w}\sum_{t=1}^{w}(y_i(t) - \vec{y_i})^2}\right)^q\right)^{\frac{1}{q}} \tag{2.5}$$

The generalized Hurst exponents $H_q$ are the slopes of the straight lines in a log-log plot of the structure functions for various order exponents $q$ for variations in the segment width (time interval), $w$. The information contained in $H_q$ for different $q$ can alternatively be represented as a spectrum of singularities $f(\alpha)$ that are related to the slopes of the generalized Hurst exponents via a Legendre transform (Zia et al., 2009) as follows:

$$\tau_q = qH^q - 1 \tag{2.6}$$

$$\alpha = \frac{\partial \tau_q}{\partial q} \tag{2.7}$$

$$f(\alpha) = q\alpha - \tau_q \tag{2.8}$$

This spectrum, represented as a plot of $f(\alpha)$ against $\alpha$, is known as the multifractal spectrum (also called the Hölder spectrum) and provides information on varying nature of the fractal dimension in the data.

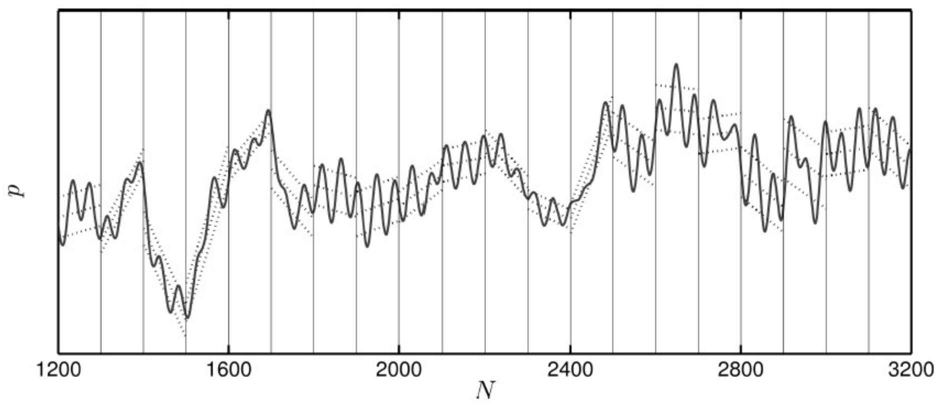


Figure 2.9: Example: The cumulative deviate series and its linear fit in 20 segments from a portion of the noise signal. The deviate series yi(t) is shown in gray and the linear fit yi and its local standard deviation are shown as black dashed lines.

## 2.5 Recurrence Quantification

### 2.5.1 Recurrence Plot

Recurrence is a fundamental property of dynamical systems, which can be exploited to characterise the system's behaviour in phase space .A powerful tool for their visualisation and analysis called recurrence plot was introduced in the late 1980's. The recurrence plots theory, like the recurrence quantification analysis, which is highly effective to detect, e. g., transitions in the dynamics of systems from time series.A main point is how to link recurrences to dynamical invariants and unstable periodic orbits. This and further evidence suggest that recurrences contain all relevant information about a system's behaviour. As the respective phase spaces of two systems change due to coupling, recurrence plots allow studying and quantifying their interaction. This fact also provides us with a sensitive tool for the study of synchronisation of complex systems. This theory has applications in economy, physiology, neuroscience, earth sciences, astrophysics and engineering are shown (Marwan et al., 2007). The technique requires reconstruction of the mathematical phase space of evolution of the pressure fluctuations. In reconstructing an appropriate phase space, a knowledge of the appropriate embedding dimension $d_0$ and the optimum time lag $\tau_{opt}$ that is used to generate the delay vectors from the measured pressure time series (of length $N_0$) is necessary. A recurrence plot is constructed by computing the pairwise distances between points in the phase space. Then, a matrix of recurrences may be obtained as:

$$R_{ij} = \theta(\epsilon - \parallel p'_i - p'_j \parallel) \qquad i, j = 1, 2, \ldots, N_0 - d_0\tau_{opt} \tag{2.9}$$

where $\theta$ is the Heaviside step function and $\epsilon$ is a threshold or the upper limit of the distance between a pair of points in the phase space to consider them as close or recurrent. The indices represent the various time instances when the distances are computed and the boldface represents the vector of coordinates in the phase space. The recurrence matrix is a symmetric matrix composed of zeros and ones and a recurrence plot is the 2D representation of this matrix as the trajectories evolve in time. The ones in the recurrence plot are marked with black points and represent

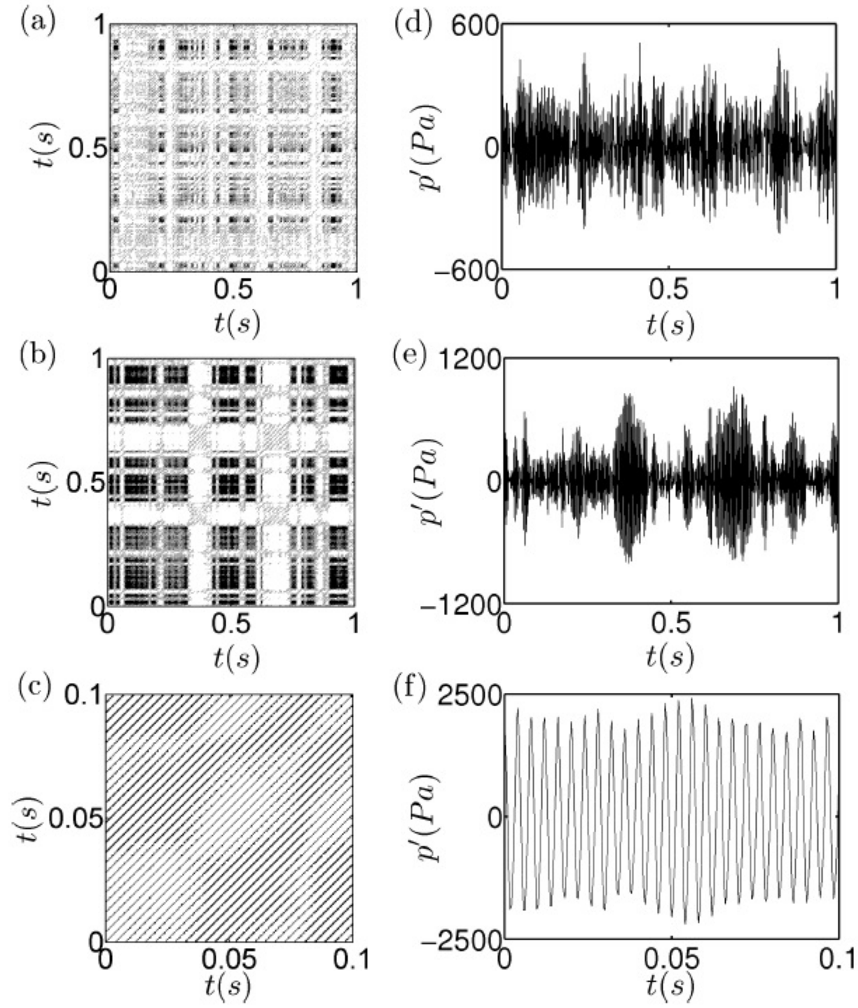


Figure 2.10: Example di Recurrence plots and the corresponding unsteady pressure signals acquired during combustion noise (top row, intermediate intermittent regime (middle row) and combustion instability (bottom row) from the bluff-body stabilized combustor.

those time instants when the pairwise distances are less than the threshold $\epsilon$. White points in the recurrence plot correspond to the zeros in the recurrence plot and correspond to those instants when the pairwise distances exceed the threshold.

Figure 2.10 shows an example of the recurrence plots drawn, in Thermoacoustic for the pressure signals acquired during (i) combustion noise, (ii) intermittent regime and (iii) combustion instability. In example, the time duration of the signal was chosen to be 0.1s to highlight the diagonal lines in the recurrence plot which would otherwise not be visible. The separation between the diagonal lines gives the fundamental time period of oscillation during combustion instability. The black patches represent the times when the system exhibits low amplitude chaotic oscillations and white patches represent the higher amplitude periodic bursts. This is a pattern typical of intermittent burst oscillations. The recurrence plots thus help visually identify the route to instability in turbulent combustors. The transition proceeds from chaos (combustion noise) to order (combustion instability) through an intermediate intermittent regime.

The RP is obtained by plotting the recurrence matrix, Eq. (2.9), and using different colours for its binary entries, e.g., plotting a black dot at the coordinates $(i, j)$, if $R_{i,j} \equiv 1$, and a white dot, if $R_{i,j} \equiv 0$. Both axes of the RP are time axes and show rightwards and upwards (convention). Since $R_{i,i} \equiv 1 \,|_{i=1}^{N}$ by definition, the RP has always a black main diagonal line, the line of identity (LOI). Furthermore, the RP is symmetric by definition with respect to the main diagonal, i.e. $R_{i,j} \equiv R_{j,i}$. In order to compute an RP, an appropriate norm has to be chosen. The most frequently used norms are the $L_{1-norm}$, the $L_{2-norm}$ (Euclidean norm) and the$L_{\infty-norm}$ (Maximum or Supremum norm). Note that the neighbourhoods of these norms have different shapes. Considering a fixed $\epsilon$, the $L_{\infty-norm}$ finds the most, the $L_{1-norm}$ the least and the$L_{2-norm}$ an intermediate amount of neighbours. To compute RPs, the $L_{\infty-norm}$ is often applied, because it is computationally faster and allows to study some features in RPs analytically.

### Selection of the threshold $\epsilon$

A crucial parameter of an RP is the threshold $\epsilon$. Therefore, special attention has to be required for its choice. If $\epsilon$ is chosen too small, there may be almost no recurrence points and we cannot learn anything about the recurrence structure of the underlying system. On the other hand, if $\epsilon$ is chosen too large, almost every point is a neighbour of every other point, which leads to a lot of artefacts. A too large $\epsilon$ includes also points into the neighbourhood which are simple consecutive points on the trajectory. This effect is called tangential motion and causes thicker and longer diagonal structures in the RP as they actually are. Hence, we have to find a compromise for the value of $\epsilon$. Moreover, the influence of noise can entail choosing a larger threshold, because noise would distort any existing structure in the RP. At a higher threshold, this structure may be preserved. Several "rules of thumb" for the choice of the threshold $\epsilon$ have been advocated in the literature, e.g., a few per cent of the maximum phase space diameter has been suggested. Furthermore, it should not exceed 10% of the mean or the maximum phase space diameter. A further possibility is to choose $\epsilon$ according to the recurrence point density of the RP by seeking a scaling region in the recurrence point density. However, this may not be suitable for non-stationary data. For this case it was proposed to choose $\epsilon$ such that the recurrence point density is approximately 1%. Another criterion for the choice of $\epsilon$ takes into account that a measurement of a process is a composition of the real signal and some observational noise with standard deviation $\sigma$. In order to get similar results as for the noise-free situation, $\epsilon$ has to be chosen such that it is five times larger than the standard deviation of the observational noise, i.e. $\epsilon > 5\sigma$. This criterion holds for a wide class of processes. For (quasi-)periodic processes, the diagonal structures within the RP can be used in order to determine an optimal threshold. For this purpose, the density distribution of recurrence points along the diagonals parallel to the LOI is considered (which corresponds to the diagonal-wise defined -recurrence rate RR , Eq. ((2.14))). From such a density plot, the number of significant peaks $N_p$ is counted. Next, the average number of neighbours $N_n$ (2.11), that each point has, is computed. The threshold $\epsilon$ should be chosen in such a way that $N_p$ is maximal and $N_n$ approaches $N_p$. Therefore, a good choice of $\epsilon$ would be to minimise the quantity

$$\beta(\epsilon) = \frac{\mid N_n(\epsilon) - N_p(\epsilon) \mid}{N_n(\epsilon)} \tag{2.10}$$

Where:

$$N_n(\epsilon) = \frac{1}{N} \sum_{i,j=1}^{N} R_{i,j}(\epsilon) \tag{2.11}$$

This criterion minimises the fragmentation and thickness of the diagonal lines with respect to the threshold, which can be useful for de-noising, e.g., of acoustic signals. However, this choice of $\epsilon$ may not preserve the important distribution of the diagonal lines in the RP if observational noise is present (the estimated threshold can be underestimated). Other approaches use a fixed recurrence point density. In order to find an $\epsilon$ which corresponds to a fixed recurrence point density RR (or recurrence rate, Eq.(2.14), the cumulative distribution of the $N^2$ distances between each pair of vectors $P_c(D)$ can be used. The RRth percentile is then the requested $\epsilon$. An alternative is to fix the number of neighbours for every point of the trajectory. In this case, the threshold is actually different for each point of the trajectory, i.e. $\epsilon = \epsilon(-\vec{x_i}) = \epsilon_i$. The advantage of the latter two methods is that both of them preserve the recurrence point density and allow to compare RPs of different systems without the necessity of normalising the time series beforehand. Nevertheless, the choice of $\epsilon$ depends strongly on the considered system under study.

### 2.5.2 Recurrence Quantification Analysis

Simply put, recurrence plots, especially colored versions expressing recurrence distances as contour maps, are beautiful to look. With little debate, global recurrence plots of time series and signals extant in nature captivate one's attention. Admittedly, such curious and intriguing graphical displays tend more to evoke artistic than scientific appreciation, and rightfully so. Recalling the brief history of recurrence analysis, recurrence plots were originally posited as qualitative tools to detect hidden rhythms graphically (Eckmann et al., 1987). From the outset, color was not the key; rather the specific patterns of multi-dimensional recurrences gave hints regarding the underlying dynamic. Early on it was understood how important it was to hold the radius parameter to small values so as to keep the recurrence matrix sparse. In so doing, emphasis was placed on local recurrences that formed delicate, lacy patterns. All of this is well and good, but the next logical step was to promote recurrence analysis to quantitative status (Zbilut & Webber, 1992; Webber and Zbilut, 1994). Instead of trusting one's eye to "see" recurrence patterns, specific rules had to be devised whereby certain recurrence features could be automatically extracted from recurrence plots. In so doing, problems relating to individual biases of multiple observers and subjective interpretations of recurrence plots were categorically precluded. We will highlight the fundamental rules of recurrence quantification analysis (RQA) by employing the classic strange attractor of Hénon (1976). This chaotic attractor is a geometrical structure (system) that derives its form (dynamic) from the nonlinear coupling of two variables. Note in Equation (2.12) that the next data point, $X_{i+1}$, is a nonlinear function of the previous $X_i$ and $Y_i$ terms (the $X_i^2$ term provides the nonlinear interaction), whereas in Equation (2.13) the next $Y_{i+1}$

is a linear function of the previous Xi term.

$$X_{i+1} = Y_i + 1.0 - (1.4X_i^2) \tag{2.12}$$

$$Y_{i+1} = 0.3X_i \tag{2.13}$$

We seeded the coupled Hènon variables with initial zero values (e.g.,$X_0 = Y_0 = 0.0$) and iterated the system 2000 times to create a sample time series. To make sure the dynamic settled down on its attractor, the first 1000 iterations were rejected as transients. The next 200 iterations of the system shows the complex dynamics of the coupled variables. Plotting $Y_i$ as a function of $X_i$ generates the Hènon strange attractor. It is called an attractor because dynamical points are "attracted" to certain positions on the map and "repelled" from other positions (the white space). The dimension of the Hénon attractor is estimated to be around 1.26 (Girault, 1991), which is a fractal or non-integer dimension. Fractal dimensions relate more to the mathematical concept of scaling than real-world dimensions, which must be integers (see Liebovitch & Shehadeh, Chapter 5). During the analysis of the Recurrence Plot, We will focus on the diagonal and vertical structures since from those stem the seven recurrence (dependent) variables or quantifications. Because the recurrence plot is symmetrical across the central diagonal, all quantitative feature extractions take place within the upper triangle, excluding the long diagonal (which provides no unique information) and lower triangle (which provides only redundant information).

The first recurrence parameter is number of suitable markers that foretell an impending instability may be constructed by counting the number of black points in the recurrence plot. The density of black points in a recurrence plot measures the recurrence rate in the dynamics of the system and can be obtained as:

$$\%RR = 100(\frac{1}{N_i^2}\sum_{i,j=1}^{N_1} R_{ij}) \tag{2.14}$$

where $N_1 = N_0 - d_0\tau_{opt}FsR_{ij}$ is one for a black point and zero for a white point. The signal was sampled at a frequency Fs of 10kHz for 30s to give a value of N0 of 100,000 and was embedded in a phase space of $d_0 = 10$ with an embedding delay $\tau_{opt} = 1ms$. This density of points in the recurrence plot is seen to decrease on the approach of instability. This is expected since the number of black points in the recurrence plot would come down as instability is reached because the pairwise distances now exceed the threshold more often.

The second recurrence variable is %determinism (%DET). %DET measures the proportion of recurrent points forming diagonal line structures. Diagonal line segments must have a minimum length defined by the line parameter, lest they be excluded. The name determinism comes from repeating or deterministic patterns in the dynamic. Periodic signals (e.g. sine waves) will give very long diagonal lines, chaotic signals (e.g. Hénon attractor) will give very short diagonal lines, and stochastic signals (e.g. random numbers) will Recurrence Quantification Analysis give no diagonal lines at all (unless parameter RADIUS is set too high).

$$\%DET = 100\frac{number\ points\ in\ diagonal\ lines}{number\ recurrent\ points} \tag{2.15}$$

The third recurrence variable is linemax ($L_{MAX}$), which is simply the length of the longest diagonal line segment in the plot, excluding the main diagonal line of identity ($i = j$). This is a very important recurrence variable because it inversely scales with the most positive Lyapunov exponent (Eckmann et al., 1987; Trulla et al., 1996). Positive Lyapunov exponents gauge the rate at which trajectories diverge, and are the hallmark for dynamic chaos. Thus, the shorter the linemax, the more chaotic (less stable) the signal.

$$L_{MAX} = length\ of\ longest\ diagonal\ line\ in\ recurrence\ plot \tag{2.16}$$

The fourth recurrence variable is entropy (ENT), which is the Shannon information entropy (Shannon, 1948) of all diagonal line lengths distributed over integer bins in a histogram. ENT is a measure of signal complexity and is calibrated in units of bits/bin. Individual histogram bin probabilities ($P_{bin}$) are computed for each non-zero bin and then summed.

$$ENT = -\sum (P_{bin}) \log_2(P_{bin}) \tag{2.17}$$

The fifth and sixth recurrence variables, $\%laminarity$ ($\%LAM$) and trapping time ($TT$), were introduced by Marwan, Wessel, Meyerfeldt, Schirdewan, and Kurths (2002). $\%LAM$ is analogous to $\%DET$ except that it measures the percentage of recurrent points comprising vertical line structures rather than diagonal line structures. The line parameter still governs the minimum length of vertical lines to be included. $TT$, on the other hand, is simply the average length of vertical line structures.

$$\%LAM = 100\ \frac{number\ points\ in\ vertical\ lines}{numbers\ recurrent\ points} \tag{2.18}$$

$$TT = average\ length\ of\ vertical\ lines\ \geq\ parameter\ line \tag{2.19}$$

Recurrence plots and recurrence quantifications are strongly dependent on the sequential organization of the time series or data string. By contrast, standard statistical measures such as mean and standard deviation are sequence independent. Random shuffling of the original sequence destroys the small-scale structuring of line segments (diagonal as well as vertical) and alters the computed recurrence variables, but does not change the mean and standard deviation. A good analogy would be that of Morse code. Random shuffling of the dots and dashes would not change the percentage of dots and dashes in the code, but it would certainly alter/destroy the encoded message!

## 2.6 Intermittency

In this thesis work, we will see that intermittent burst oscillations are also observed in the combustion chamber with only cold flow. Intermittent dynamics is thus a typical feature in the dynamics of turbulent combustors—even more so than limit cycle oscillations. The section aims to establish that such intermittent bursts arise naturally in systems composed of two attractors through the formation of homoclinic orbits in the phase space of the global system dynamics. It also aims, through analyzing the recurrence properties of these intermittent states, to provide a systematic way to inspect the presence of such homoclinic orbits from a measured time signal.

The phenomenon of intermittency has received a lot of attention in the description of deterministic dynamics arising from pattern forming complex systems. Through a study of simple dissipative dynamical systems, Pomeau and Manneville (1980) presented three models of intermittency classified as type I-III to describe the routes of transition from a stable periodic behaviour to chaos. Even more varieties of intermittency were discovered later on such as chaos-chaos intermittency (Richardson, 1993) (eg: on-off intermittency (Ott and Sommerer, 1994) and in-out intermittency (Covas et al., 2001), crisis-induced intermittency (Grebogi et al., 1987), type-X intermittency (Price and Mullin, 1991) or type-V intermittency (Bauer et al., 1992). There has also been a number of experimental observations (Hammer et al., 1994; Argoul et al., 1993) of intermittent dynamics in the literature. As we have seen so far, interaction of sound with a reacting turbulent flow provides us with yet another dynamical system where intermittency is observed-seen as intermittent bursts of pressure oscillations that emerge from a chaotic background.

### 2.6.1 Intermittency and homoclinic horbit

A homoclinic orbit is one in which the unstable manifold of a hyperbolic equilibrium state of the system merges with its own stable manifold. Although a close association between homoclinicity and intermittency has been shown experimentally in the literature (Richetti et al., 1986; Herzel et al., 1991; Parthimos et al.), identification of homoclinic orbits from a measured time series has proved a difficult task. In Fig. (2.11), the evolution in phase space of an intermittent burst is shown for the pressure signal acquired prior to lean blowout. The trajectory is seen to spiral out of the center to the unstable orbit and then spirals back in through the plane of oscillations, which could possibly represent a homoclinic orbit. However, the existence of such orbits cannot be concluded by a mere visual inspection of the phase space. Therefore, we propose a new technique to infer the presence of homoclinic orbits in the phase space of the global attractor.

The circulation time of trajectories in phase space for homoclinic orbits are dominated by their passage time near the saddle fixed point. This time is highly sensitive to external perturbations and the distribution of passage times for a given initial distribution of points near the saddle point is given by the expression (Holmes, 1990):

$$P(T) = \frac{2\lambda\Delta(T)e^{\Delta^2(T)}}{\sqrt{\pi}(1 - e^{-2\lambda T})} \tag{2.20}$$

where $\Delta(T) = \delta[(\frac{\alpha^2}{\lambda})(e^{2\lambda T} - 1)]^{-1/2}$, $\lambda$ is the unstable eigenvalue of the saddle point, $\alpha$ is the noise level rms, $\delta$ is the size of the neighbourhood influenced by noise. $P(T)$ is a skewed distribution with its peak value different from the mean and has an exponential tail (Holmes, 1990) as $T \to \infty (P(T) \approx \frac{2\delta}{\sqrt{2\pi}}\lambda^{3/2}e^{-\lambda T})$. This behaviour is independent of the details of the initial distribution (Stone and Holmes, 1991). It is known that the distribution of the laminar phases (quiet, aperiodic regimes) for both type-II and type-III intermittencies have an exponential tail (Klimaszewska and Zebrowski, 2009). Inspection of the recurrence plots of the combustor pressure signal acquired during intermittency is inconclusive; however, the detected features correspond to type-II or type-III intermittency. As the analysis described above

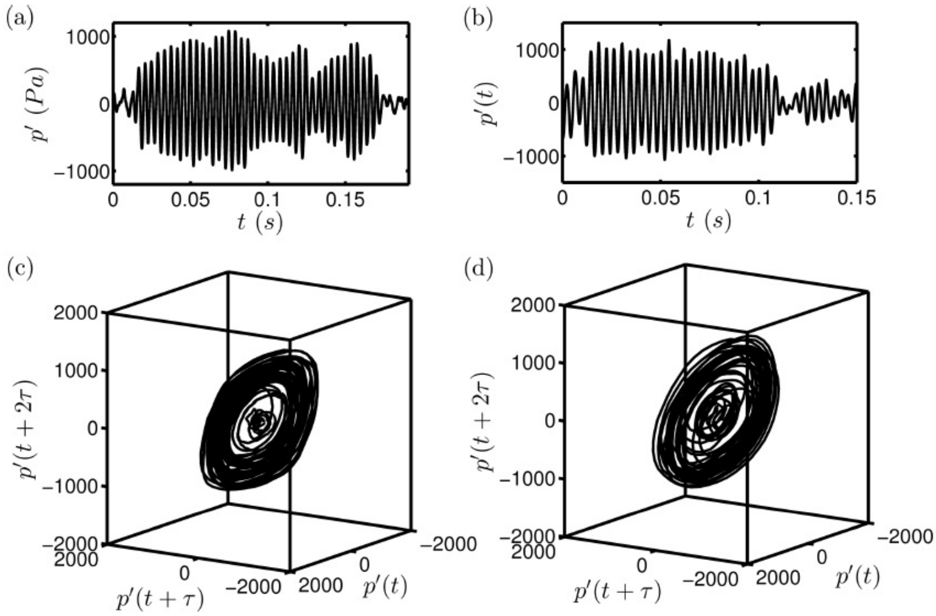


Figure 2.11: Example: the intermittent signals (a) - (b) and the corresponding phase portraits (in 3D) are shown in (c) - (d) respectively. The evolution of burst oscillations in phase space results in the aperiodic oscillations spiraling out into high amplitude oscillations and then again spirals back into the low amplitude aperiodic dynamics.

illustrates, systems exhibiting type-II or type-III intermittency are characterized by homoclinic orbits in the underlying phase space.

The distribution of the passage time of the dynamics in low amplitude regimes can be estimated from a recurrence plot as the frequency distribution of the vertical lines (or horizontal lines since the matrix is symmetric) in the recurrence plot. Histograms of this vertical length frequency distribution for example the two signals were plotted in Fig. 2.11 to understand the variation of the frequency of visits as a function of the trapping time. The histogram reveals a skewed distribution with its peak off the mean and has an exponentially decaying tail. The presence of such an exponential tail is thus indicative of homoclinic orbits in the system (Stone et al., 1996). The trajectory of such a homoclinic orbit is repeatedly injected near the stable manifold of a saddle node as a result of the perturbations in the turbulent base flow. Thus, recurrence quantification serves as an efficient tool for the inspection of homoclinic orbits in the phase space of the system dynamics.

### 2.6.2 Detection of the type of intermittency with recurrence plots

Like we have already saw, one of the common routes to chaos is intermittency. In such a state, the dynamical system switches between two different kinds of behavior (called *phases*). The residence time in each of them is different and varies with the time, so that it is impossible to foresee the moment for the next switching. There exist several different types of intermittency (three types of intermittencies investigated by Pomeau and Manneville, type X, V, and a group of chaos-chaos intermittencies among them the on-off and the in-out intermittencies). Each type

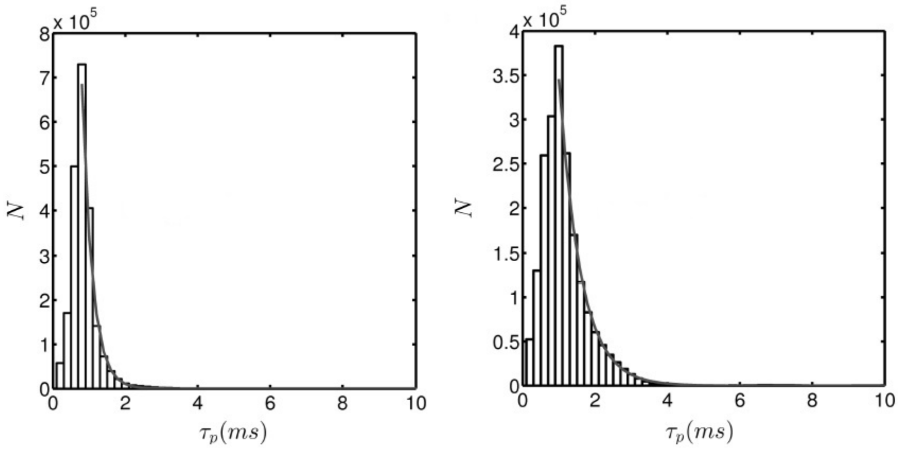


Figure 2.12: Example: Histograms of the number of visits and the duration of time spent trapped in the low amplitude aperiodic regimes for the intermittent signals. A skewed distribution with an exponential fall-off is visible in both the histograms which is a distinctive feature of systems that have homoclinic orbits in the phase space of dynamics. An exponential fit to the tail is shown as gray lines over the histogram.

of the phenomenon is related to a different kind of bifurcation. For example, type I intermittency occurs when the system is close to a saddle-node bifurcation, type II is due to the Hopf bifurcation, and type III the reverse period doubling bifurcation. One kind of chaos-chaos intermittency is due to crisis phenomena occurring in the system. Thus, the recognition of the type of the intermittency observed in the dynamical system is equivalent to determining the type of the bifurcation characteristic for the dynamics of that system in the particular part of parameter space investigated. The identification of the intermittency type is usually based on the probability distribution of the length $l$ of the laminar phases $P(l)$ and the properties of the average length of the laminar phases $l$. Both properties have a statistical character. Thus, to obtain them a long time series has to be examined. In practice, often, the length of the time series is limited, so it is important to find a method capable to recognize the type of the intermittency using short time series. In 2002 Marwan showed that it is possible to distinguish between time series with intermittency and with other kinds of chaos using recurrence plots (RP) and recurrence quantification analysis (RQA). They showed that the laminar phases of intermittency correspond to horizontal (and vertical) lines on the RP and that such lines form squares and rectangles. Occurrences of such patterns on the RP are a sign that intermittency is present in the data. However, Marwan did not define which kind of intermittency they had observed. It is the aim of this paper to examine the possibility to distinguish the kind of intermittency occurring in the system given the pattern obtained in a recurrence plot and using RQA. We examined four kinds of intermittency: the three types of intermittency defined by Pomeau and Manneville and the chaos-chaos intermittency induced by an interior crisis. To distinguish between the different kinds of intermittency, we extended the RQA by introducing two parameters. With our method, we were able to determine the type of inter-

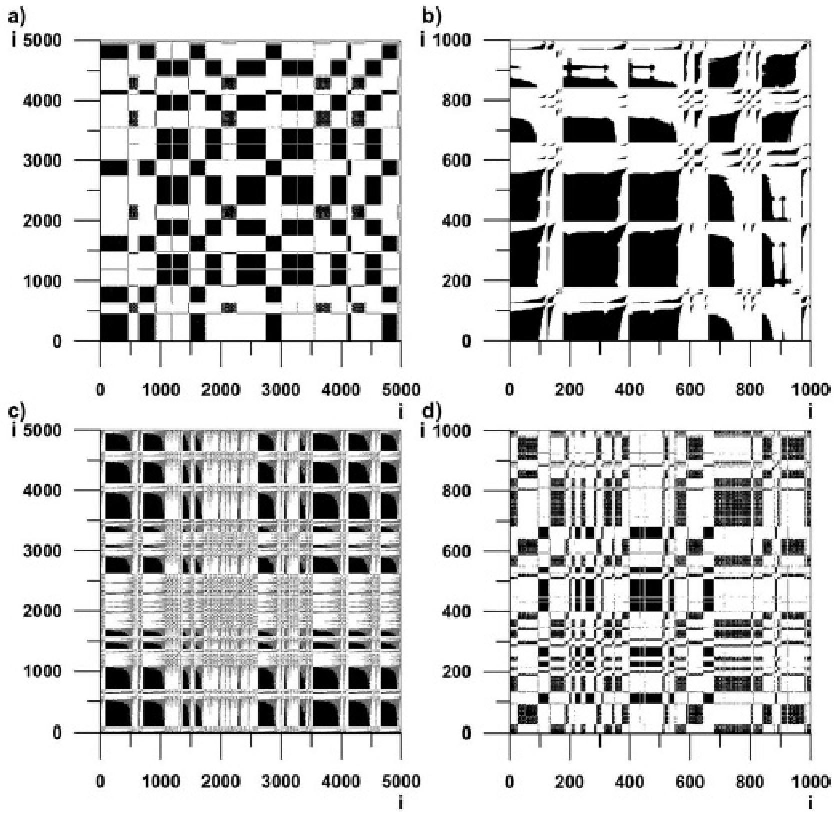


Figure 2.13: Example: The recurrence plots of four different types of intermittencies with measurement noise added to the time series. The noise level was 10 %. (a) Type I intermittency; (b) type II intermittency; (c) type III intermittency; (d) chaos-chaos intermittency

mittency even in the presence of a moderately high level of measurement noise (K. Klimaszewska and J. J. Żebrowski et. al. 2009).

In the my work thesis has not been possible, detention with security the intermittency type because with my data it is not very clear but securely in future will be possible determine it, with a bit more work.

# 3. Experimental Setup and Acquiring System

We show that intermittent burst oscillations are a typical feature of turbulent flow-sound interaction, even in the absence of combustion. The onset of self-sustained oscillations in a turbulent pipe flow across an orifice is investigated in a whistling apparatus. Analysis of measured pressure fluctuations reveals that this emergence of order from turbulence happens through an intermediate intermittent regime characterized by bursts of periodic oscillations that appear in a near-random fashion amidst the background chaotic fluctuations. The interesting feature is that these intermittent bursts correspond to a frequency distinct from the final oscillatory state as the boundary condition at the orifice exit undergoes a transition at the onset of whistling.

### Introduction

Pressure fluctuations in unsteady flows are classified as sound or pseudo-sound depending on whether the underlying pressure field is propagating or non-propagating (Williams, 1969). The pressure variations $p'$ in a sound field (acoustic waves) are dependent on the local speed of sound $c_0$ via $p' \sim \theta(a_0 c_0 u)$, where $\rho_0$ is the mean flow density and u refers to the typical magnitude of the local flow velocity. On the other hand, the local variations in pressure due to a pseudo-sound field vary as $p' \sim \theta(\rho_0 u^2)$, thus independent of the sound speed. When an unsteady flow passes through a confinement, both forms of pressure fluctuations are induced and these fluctuations are characterized by a multiplicity of time scales associated with local unsteadiness and acoustic wave propagation. When one of the local hydrodynamic time scales matches an acoustic time scale, self-sustained periodic oscillations, which are difficult to control in practice, are established. Screech in jets with shocks, edge tones, howling of ejectors, cavity noise, whistling in pipes (pipe tones) are some such examples of flow-induced oscillations (Dequand, 2001). In this chapter, the mechanism underlying the transition from a turbulence-dominated state to a state dominated by periodic dynamics in a system without combustion will be illustrated through experiments and theoretical arguments. This emergence of order (periodic dynamics) from turbulence is contrary to the transitions often encountered in hydrodynamic flow-fields where an increase in the Reynolds number results in a transition from periodic oscillations to turbulence (Swinney and Gollub, 1981).

## 3.1 Experimental Setup

Motivated by the pioneering work on pipe tones by Anderson (Anderson, 1952, 1955), we investigate the multi-scale temporal dynamics of turbulent flow-sound interaction in an experimental setup. In Indian Institute of Technology, at the RGDL lab of the Aerospace Department, we have installed the our setup (Fig. 3.1). To first experiment, it is consisting of a pipe of length $L = 600mm$ and diameter $D = 50mm$ terminated by a circular orifice of diameter $d_o = 10mm$ and thickness $t = 5mm$ (Fig. 3.2), connect at another pipe of $600mm$ with open end.

Such a configuration is present, for instance, in automobile exhaust pipes (Hoffman et al., 2001), segmented solid rocket motors (SRMs) (Flandro and Jacobs,

Figure 3.1: The setup complete installed in RGDLab at IIT Madras

Figure 3.2: Orifice of 10mm installed in the our setup

1975) and gas transport systems (Durrieu et al., 2001; Bruggeman et al., 1991). The pressure-driven flow, after passing through a moisture separator and a mass flow controller (used to measure the incoming flow rates), enters the pipe through an upstream cylindrical chamber of length $L_c = 300mm$ and diameter $d_c = 300mm$. A region of strong velocity gradients (shear layer) forms at the leading edge of the orifice and rolls up into a vortex sheet that convects downstream. It has previosuly been conjectured that the separated shear flow produces fluctuations in the effective aerodynamic orifice area due to the growth and periodic shedding of vortices from the orifice side walls (Anderson, 1952). These area fluctuations in turn produce variations in the pressure drop across the orifice (Anderson, 1955). When the frequency of these variations matches one of the acoustic modes of the pipe-orifice combination, self-sustained pipe tones or whistling is established. Later studies have further proposed that whistling is established when the separation streamline from the leading edge of the orifice impinges on the trailing edge (Karthik et al., 2008). Experimental measurements were performed by systematically increasing $\dot{m}$ from $0.42g/s$ to $2.12g/s$ in steps of $0.02g/s$ and then decreasing back to $0.42g/s$, after the measurements were performed, focused on the first two transitions: the first from $0.58g/s$ to $0.78g/s$ and the second from $1.17g/s$ to $1.42g/s$ in step of $0.01g/s$, where $\dot{m}$ is the mass flow rate of air through the duct-orifice system. The Reynolds number, which serves as the non-dimensional control parameter, is defined as $Re = 4\dot{m}/(\pi d_o \mu)$, where $\mu = 1.85 \times 10^{-5} Pa \cdot s$ is the dynamic viscosity of air at the ambient condition of $26^oC$ and $1atm$. The variation in Re was in the range $2.87 \times 10^3 \div 14.57 \times 10^3$ with a measurement uncertainty of 2.7%. The pressure fluctuations generated by turbulence (pseudo-sound) decays much faster than the radiated sound field downstream of the orifice (Lighthill, 1952, 1954). Hence, pressure measurements were acquired with a transducer located $2mm$ to the right of the trailing edge of the orifice, a location where the levels of the turbulent pressure field were above the noise threshold of the transducer. A total of 316 pressure measurements were performed; each pressure measurement corresponds to an acquisition for a duration of $30s$ at a sampling frequency $Fs$ of $10kHz$ using a free-field microphone. Though the microphone has a resolution of $200\mu Pa$, measuring the electrical noise prior to the experiments revealed that pressure fluctuations below $\sim 0.09Pa$ are not well resolved. To obtain the amplitude of pressure $P$ at various frequencies $f$, a Fast Fourier Transform (FFT) was performed on the pressure time series with a spectral bin size of $f = 0.08Hz$.

## 3.2 Acquiring System

During the experiments, we have used some instruments to data capture:

**Hardware:**

- 2 Mass Flow Controllers (MCR Series - Mass Gas Flow Controllers Alicat Scientific)
- Microphone Preamplifier Power Supply (Model 2221 - Larson Davis)
- Signal Conditioner
- Personal Computer installed in the experimental lab

**Software:**

- Flow Vision 1.1.39.0 - Alicat Scientific
- SignalExpress - National Instruments LabVIEW
- Matlab to the data processing

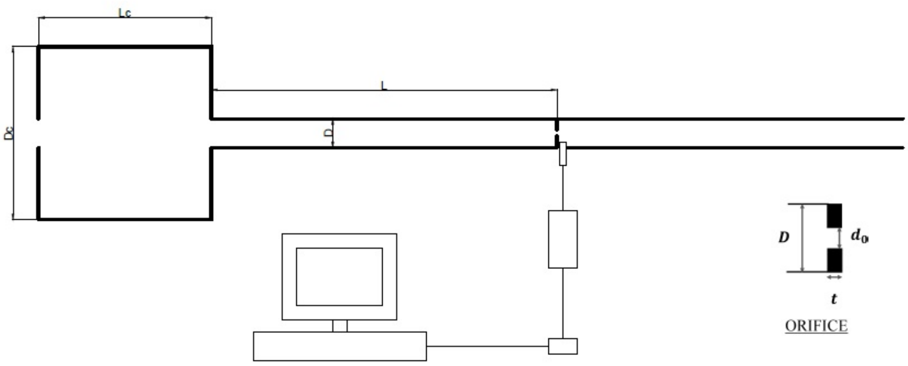


Figure 3.3: Schematic of the experimental setup used in the present study. The two pipes have a length $L = 600mm$ and diameter $D = 50mm$ terminated by a circular orifice of diameter $d_o = 10mm$ and thickness $t = 5mm$. Air enters the upstream cylindrical chamber, of length Lc = 300mm and diameter dc = 300mm, through the opening in the left.

Before bringing the air flow rate in the setup, it passes through the mass flow controller that we set by software Flow Vision. This instrument calibrate the flow rate so we can check it in the real time, furtheremore show also temperature, parameter very important in the our experiment. We used the model MCR-Series with 100 slpm like maximum value measurable (Fig. 3.4a)and it has been installed between the compressor and the inlet of the setup. For the air flow rate superior at 100 slpm, we installed two mass flow controllers in parallel.

After that, we used to data capture one microphone: Microphone Preamplifier Power Supply Model 2221 of the Larson Davis (Fig. 3.4b). Through it, we have obtained the measures of pressure. The Model 2221 provides the highly stable DC polarization voltage required by precision microphones along with low noise amplification enabling it to drive input and output cables as long as 500 feet. It is rugged, lightweight and will provide up to forty hours of continuous operation (with PRM902 Microphone Preamplifier) using six AA internal batteries. It can also provide sufficient current to power the PRM903 Microphone Preamplifier, which has an internal heater.


(a) *Mass Flow controller (Technical Data in appendix)*


(b) *Microphone Preamplifier Power Supply Model 2221 (Technical Data in appendix)*

Figure 3.4: Instruments used in the data capture

Furthermore, we have utilized a signal conditioner. It is a device that converts one type of electronic signal into a another type of signal. Its primary use is to convert a signal that may be difficult to read by conventional instrumentation into a more easily read format. In performing this conversion a number of functions may take place.

From PC, we could set the air flow rate through the software Flow Vision, visualized the signal with Signal Express by Labview and at the end with Matlab, we made the data processing.

# 4. Results

During the data collection, we have done some initial experiments, to find the best configuration to generate of Intermittency phenomena.
But not only the aero-acoustic intermittency, also more generally, we wanted investigate the multi-scale temporal dynamics of the turbulent flow-sound interaction in the experimental setup which was previously described. In this work, we measured (using one microphone), the pressure fluctuations that generate the change of the sound tone through small geometry variation. Furthermore, another parameter which was varied was the air flow rate. Sound changes were also measured due to variation of air flow rate.

For the geometry, we have changed some characteristics of the setup:

- The number of the pipes: Initially we had the setup just with the settling chamber and one pipe with orifice at the end. We added the second pipe because we had an increase of the phenomena.
- The position of the orifice: Initially we had put it at the end of the second pipe, but later, we moved it to the middle of the pipes because the results were better.
- The orifice diameter: we had tried with different diameters, in particular, we focused on 10 and 15 millimeters, but we selected the smaller one because it required a lesser air flow rate to obtain a clear signal. In experimental laboratory obtain low flow rate is easier because it requires less power at compressor.
- The position of the microphone: we have tried to take data with it at different positions, from inside and outside the pipe (in each case 50 millimeters from the end of the pipe), upstream and downstream at the orifice (always 50 millimeters from orifice).

For these reasons we have selected the layout, precedently described. Throughout the experimental work, we have improved the setup and took data in the best situation possible. During the experiment we need to bear in mind that there are also some boundary conditions that have very influence in the measures. For example in the our case: the atmospheric conditions (pressure and temperature) and the noise present in experimental lab. For these reasons we have taken data with a pressure and temperature steady (thanks to air conditioner present in the lab) and in the night to have less noise possible. For the data processing, I used the software MATLAB R2013a, and re-elaborate a code in MATLAB currently in use in RGDLab write from a PhD Student of IIT Madras, Vishnu R. Unni. Furthermore, I used two different Toolboxes:

- Espen A. F. Ihlen, "*Introduction to multifractal detrended fluctuation analysis in Matlab*", John G. Holden, University of Cincinnati, USA.
- Norbert Marwan, "*Cross Recurrence Plot Toolbox for Matlab*", Potsdam Institute for Climate Impact Research (PIK), Potsdam, Germany.

## 4.1 Time Series and Fast Fourier Transform

During the data collection through the equipment (hardware and software), we have obtained a lot of measurements of the pressure fluctuations in the sampling time for varied air flow rates. Looking at the time series, often, it is very difficult to understand the signal evolution in the time. Therefore, we use the Fast Fourier Transform (2.2). Through this algorithm, we can watch the signal in frequency field and locate the peaks that indicate the principal frequencies. From here, we can see, very clear, the different tones present in our signal. Here, I show the time series and the FFT of a random noise (Fig. 4.1). This corresponds to the first signal sampled at the air flow rate of 25 slpm:

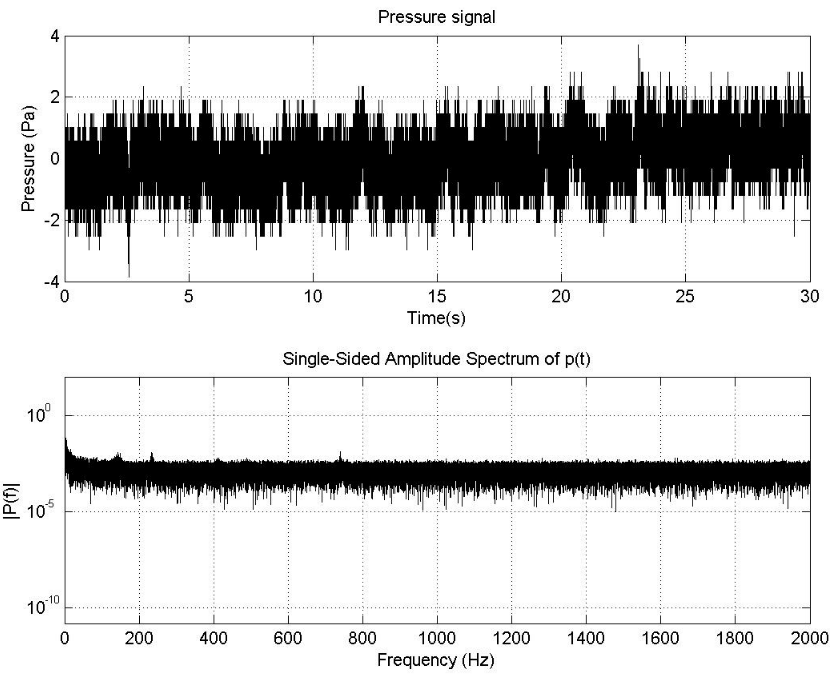


Figure 4.1: Random noise signal: there are not principal frequency

After that, we have started to increase the air flow rate and the tonal sound appears. Fig. 4.2)shows the signal at 34 slpm. The FFT shows the different tones. In this case, the dominant frequency is about 240 Hz.

Increasing again the air flow rate, we have arrived at 40 slpm and an intermittent sound is observed (Fig. 4.3)). We can observe the dominant frequency start to move towards the higher frequencies, more exactly to about 480 Hz. Furthermore, many bursts are seen in the time series.

After that, we have an unusual phenomenon: for three different flow rate, we have found a signal with very high frequency and very low amplitude (Fig. 4.4). We have tried to understand this behavior, but in literature also, this problem has not been solved. We assumed that it was mistake of measure but this hypothesis is not possible because we have found the same behavior, always, for all experiments.

After this strange behavior, the signal starts to have bursts again but with the main frequency higher (about 480Hz) (Fig. 4.5). On further increase of the air flow

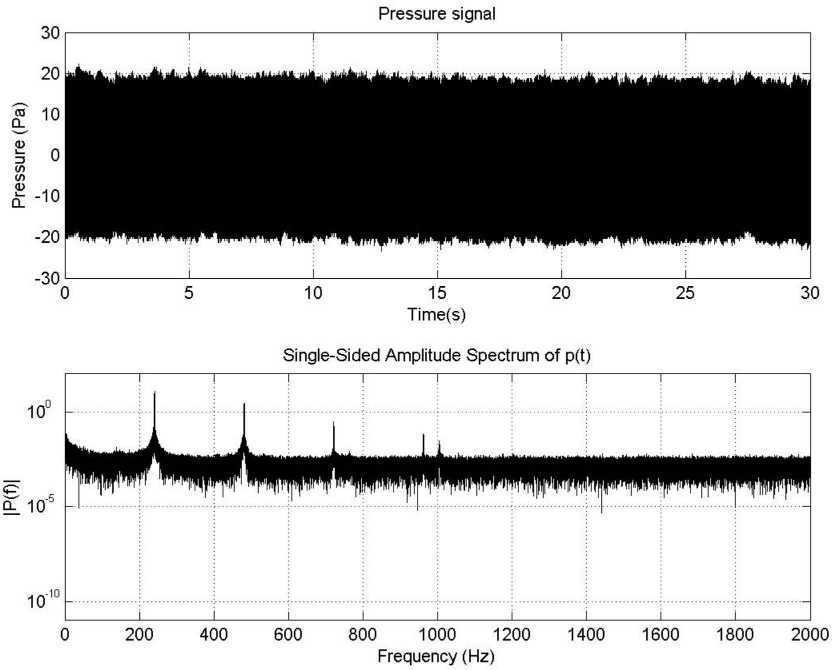


Figure 4.2: Time series and FFT at 34 slpm

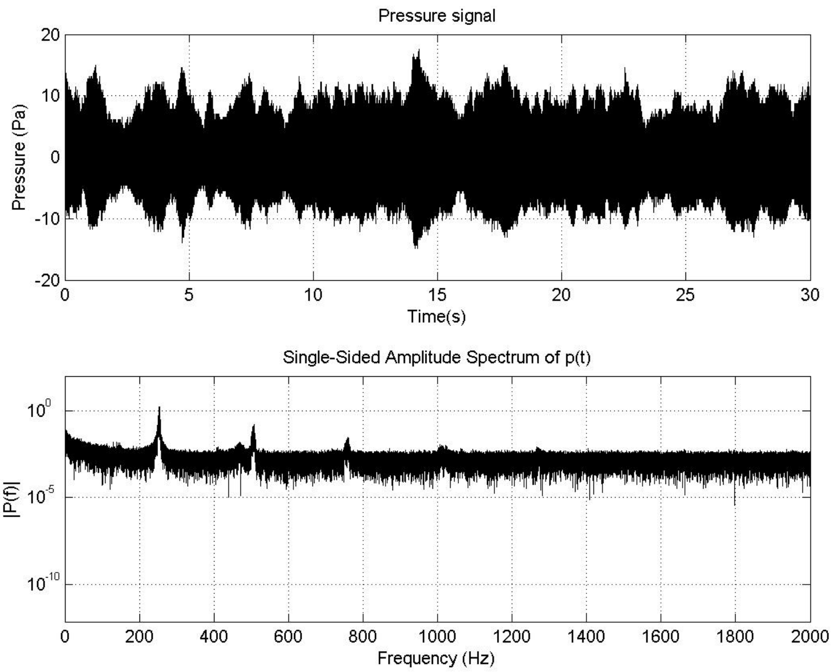


Figure 4.3: Time series and FFT at 40 slpm where the intermittent phenomena starts.

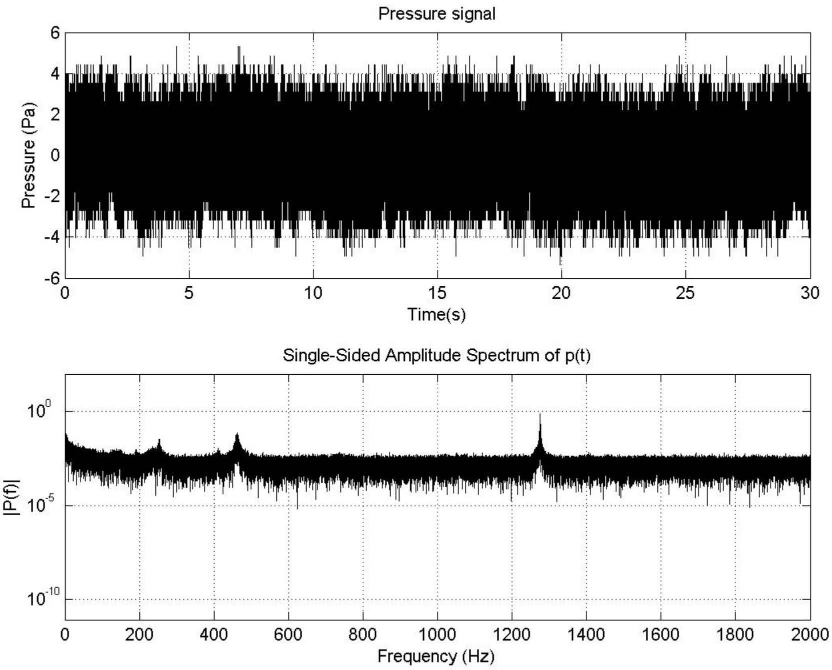


Figure 4.4: Time series and FFT at 42 slpm after start the intermittent sound. We found signal with very high frequency and very low amplitude

rate, we observe again only one characteristic tone (Fig. 4.6):

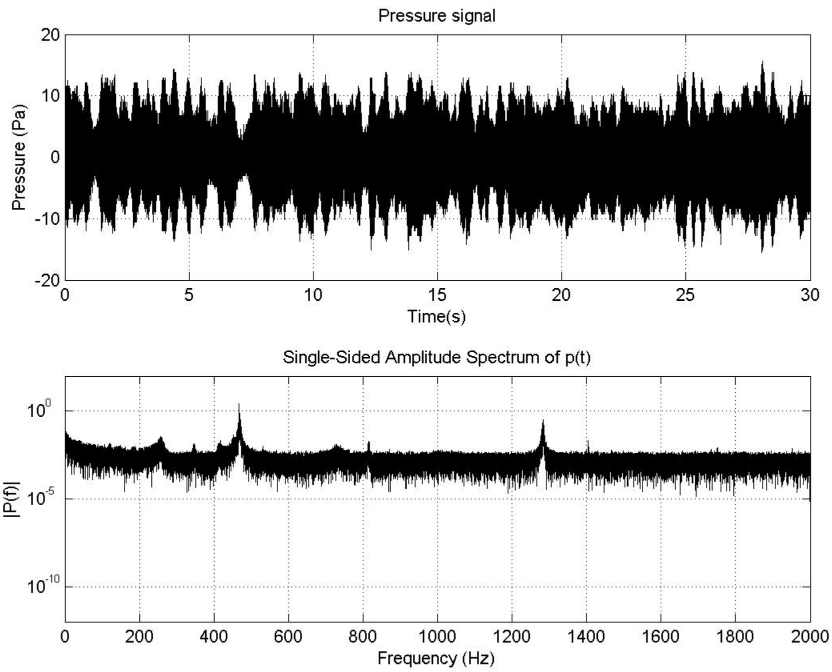


Figure 4.5: Time series and FFT at 44 slpm - bursts appear again

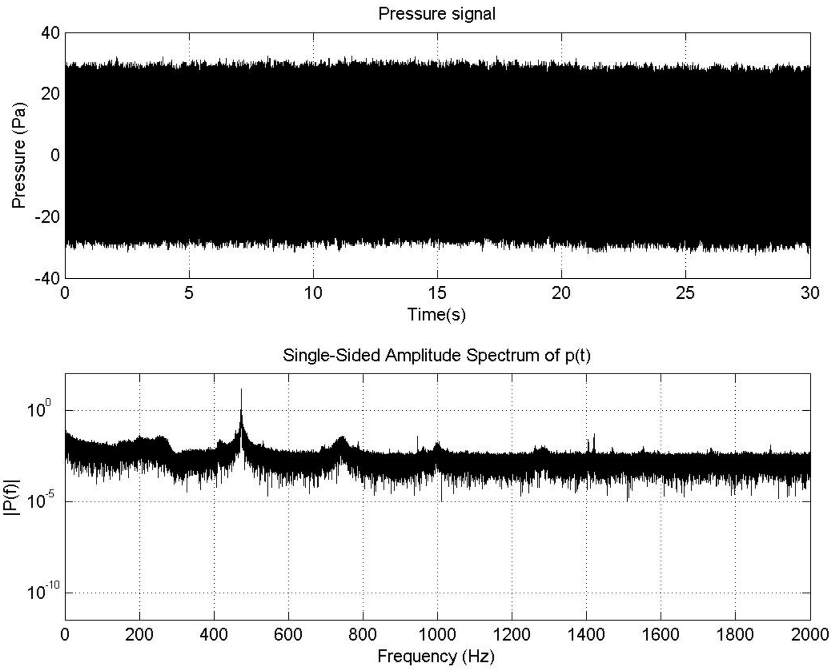


Figure 4.6: Time series and FFT at 51 slpm

In (Fig. 4.7), we observe the comparison of the time series and the FFT of 4 different signals during the first transition: the first before instability (27 slpm), second where intermittency starts to appear with the typical bursts (40 slpm), third when we had the unusual behavior which was explained earlier (42 slpm) and the last one where we have again the bursts but with the dominant frequency about 480Hz (44 slpm).

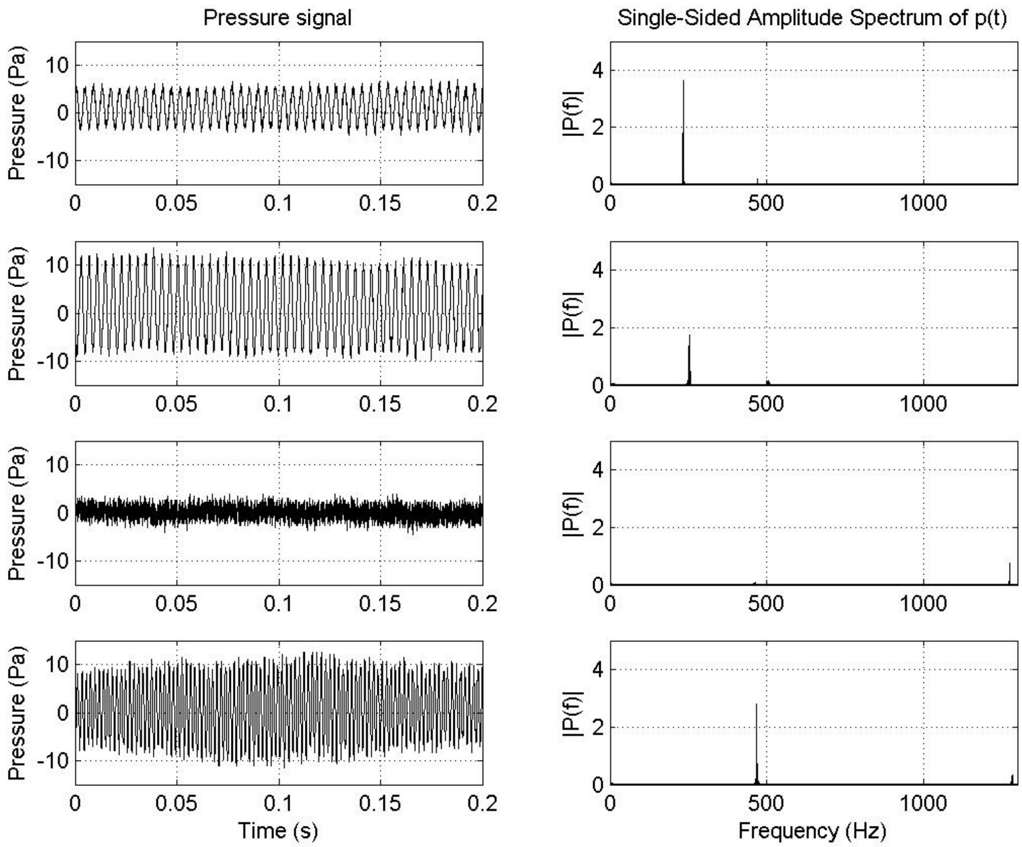


Figure 4.7: Compare four different signals before, during and after the first transition

Next we compare four different signals for the second transition (Fig. 4.8):the first signal before the transition occurs (69 slpm), the second (77 slpm) and third (78 slpm) during the transition phase and the fourth signal (93 slpm) when instability is reached.

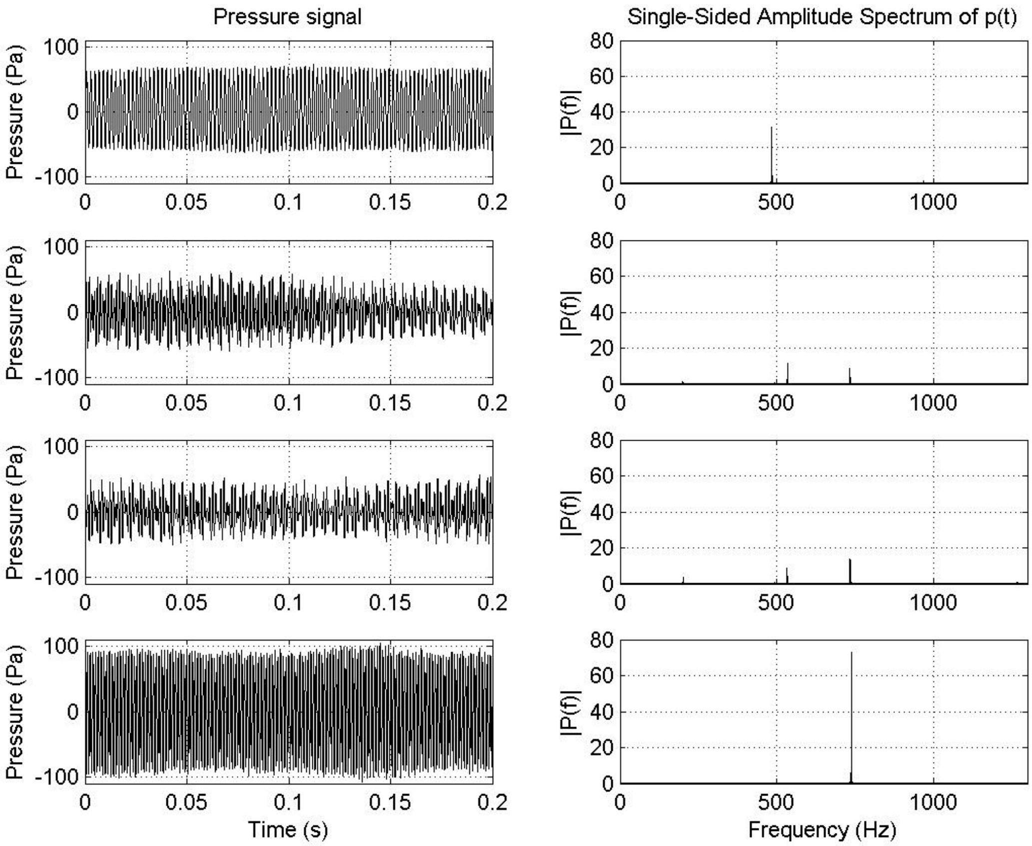


Figure 4.8: Compare four different signals before, during and after the second transition

Returning back to explanation of signals singularly with gradually increase of the flow rate, we have found the same behaviour (also after the first transition) with a periodic signal interrupted from a range with the bursts, but in this case like another cases, where there is the transition from one frequency to another, we did not find unusual case with very high frequency and very low amplitude (Like in Fig. 4.4). Like I will show in the next section, in the range of air flow rate that we used, there are three transitions, after the third, the signal does not come back periodic but remain almost random, even if this could be limit of our setup or acquiring system.

## 4.2 Frequency Transitions and Acoustics Amplitude

In the last section, we have seen evaluation of the pressure fluctuations on varying of air flow rate. After that, through the software for data acquisition and processing, we have obtained the frequency spectrum and amplitude of the acoustic pressure oscillations. We have plotted all in Fig. 4.9:

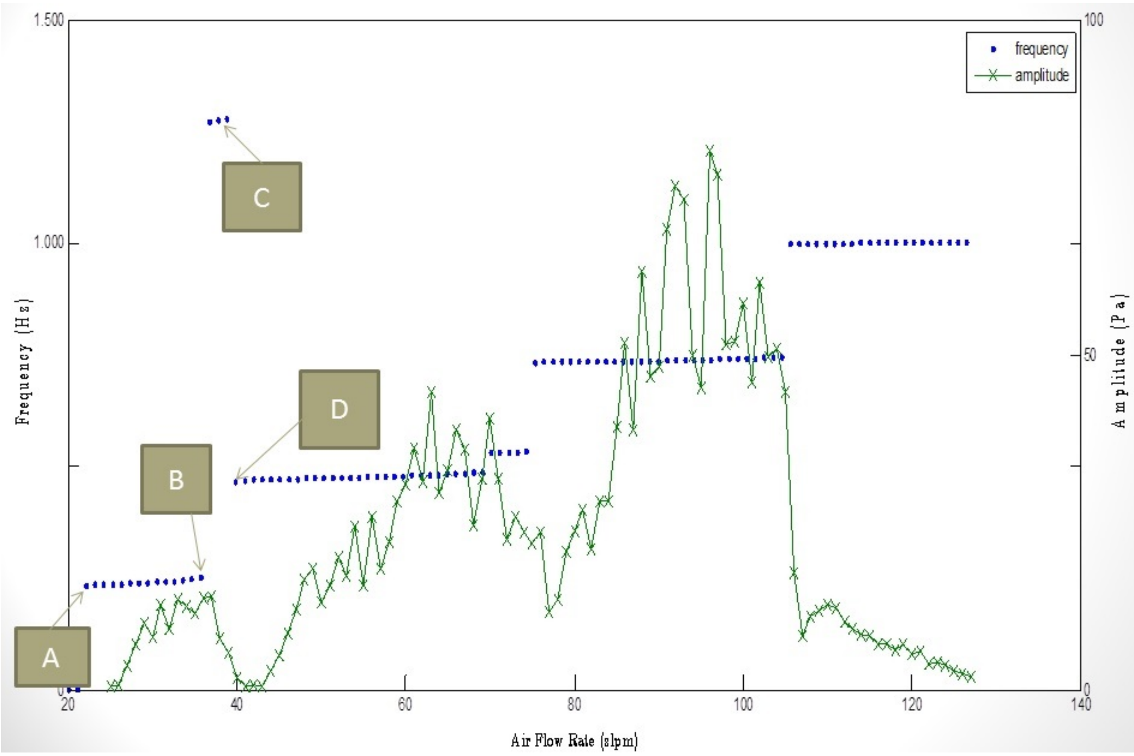


Figure 4.9: Plot Frequency vs Air Flow Rate vs Amplitude

Here (Fig. 4.9), I indicate the points that compared in Fig. 4.7: case A correspond at first, B at second, C at third and D at fourth.

## 4.3 Hurst Exponent

Like already explained in the section (2.4.2),in the description of non-stationary time signals, classical measures such as mean or variance are not very useful since they vary with time. Instead, they are characterized by examining how the moments depend on the time interval over which they are evaluated. For instance, the dependency of the standard deviation of the time signal on time interval is encapsulated in a parameter called the Hurst exponent H (H. E. Hurst, 1951). In our experiments, we have calculated the Hurst Exponent for every measure at the various flow rates and obtained this evaluation (Fig. 4.10).

During the experiments, we took data with increase in the air flow rates followed by decrease of air flow rates from the maximum reached. Comparing the curves evaluation, I found this result (Fig. 4.11) with:

Like we expected, the curves overlap. After 100 slpm, we see a gap between them. But, this gap could be due to different scales used in the calculation of the Hurst exponent. During the data processing to obtain the Hurst Exponent, we

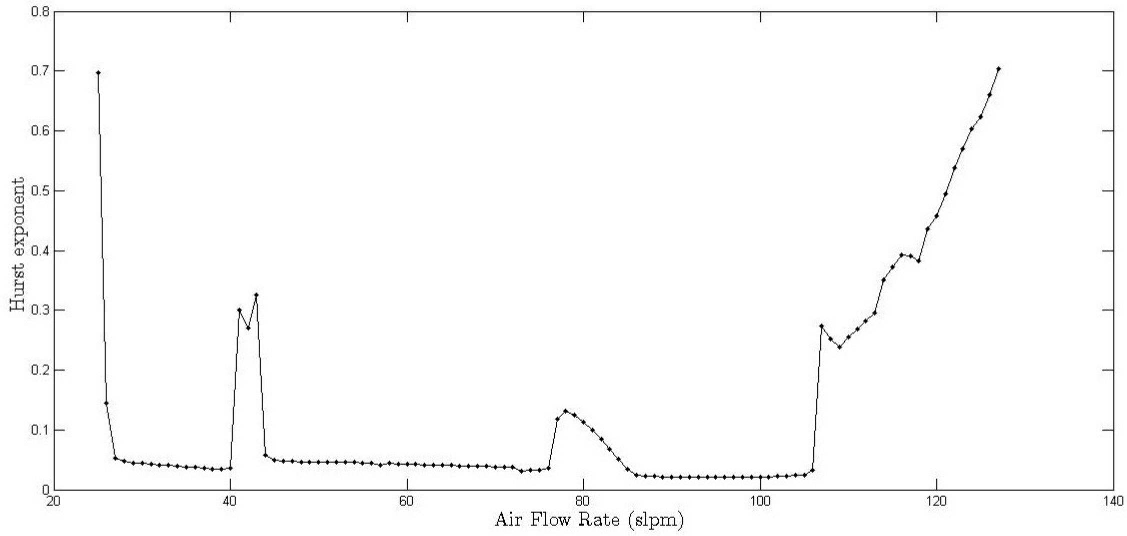


Figure 4.10: Evaluation of Hurst Exponent

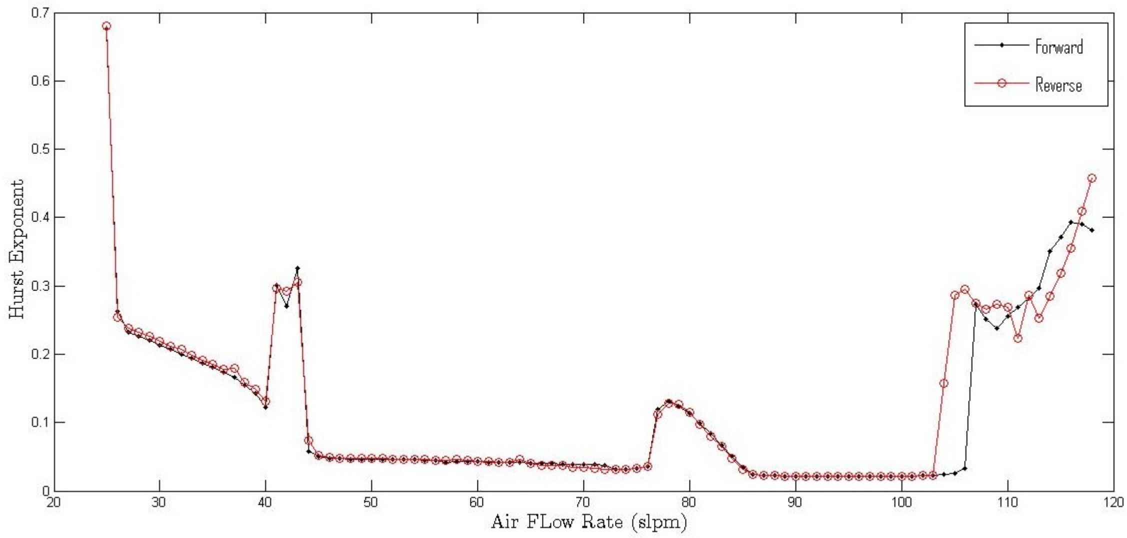


Figure 4.11: Evaluation of Hurst Exponent

needed to change the multifractal scale on varying the air flow rate, but after the third transition, we faced some problem in the determining the correct scales.

## 4.4 Multifractal Spectrum

Many time signals exhibit a complex scaling behavior that cannot be accounted for by a single fractal dimension. A full description of the scaling in such signals involves multiple generalized Hurst exponents, resulting in interwoven subsets of varying fractal dimension (varying Hurst exponents) producing what is termed a "multifractal" behavior (Frisch and Parisi, 1985). In other words, fluctuations in a time signal that have different amplitudes follow different scaling rules. The method of DFA can be expanded to explore multifractality in a time signal and the technique is called multifractal detrended fluctuation analysis (Kantelhardt et al., 2001, 2002). This method can be, also, an alternative to Hurst Exponent to investigate the character of the signal and therefore find the intermittency phenomena, which is the main purpose of the thesis work.

Here, I show the Multifractal Spectrum for some values of air flow rate. In the first plot (Fig. 4.12), I show the spectrum during the first transition and in Fig. 4.13), the spectrum during the second transition:

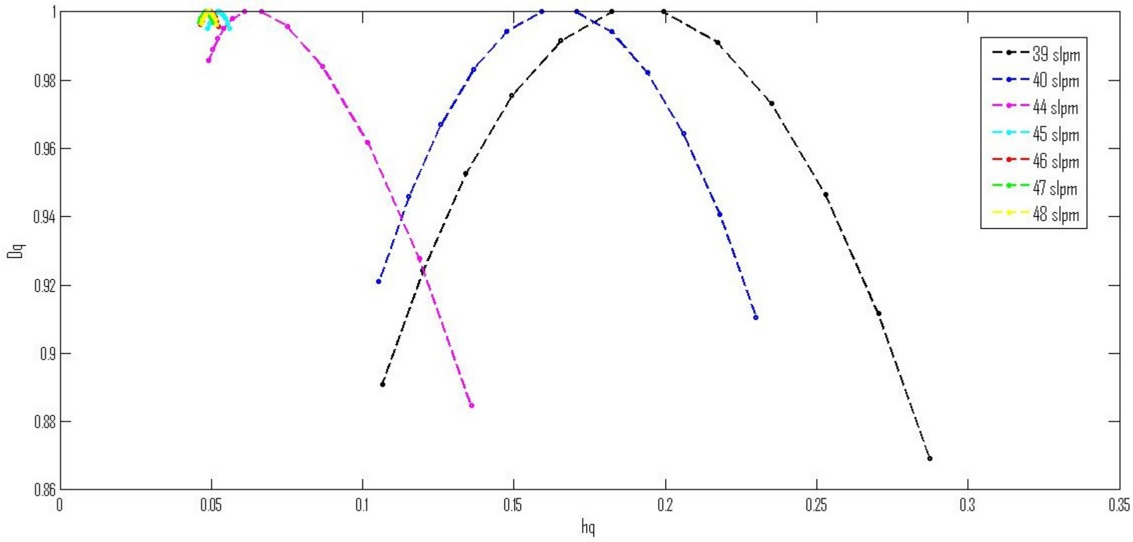


Figure 4.12: Multifractal Spectrum of some point during the first transition

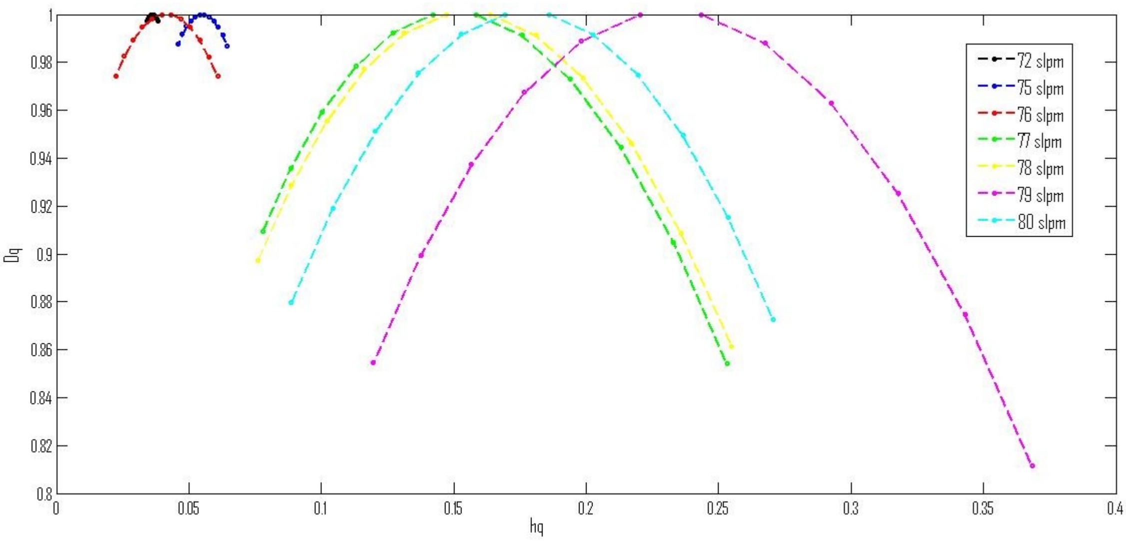


Figure 4.13: Multifractal Spectrum of some point during the second transition

## 4.5 Investigation and identification Intermittency Type

One of the common routes to chaos is intermittency. In such a state, the dynamical system switches between two different kinds of behavior called "phases". The residence time in each of them is different and varies with time. So it is impossible to foresee the moment for the next switching. There exists several types of intermittency, of which three types of intermittencies were investigated by Pomeau and Manneville: type X, V, and a group of chaos-chaos intermittencies among them the on-off and the in-out intermittencies. Each type of the phenomenon is related to a different kind of bifurcation. For example, type I intermittency occurs when the system is close to a saddle-node bifurcation, type II is due to the Hopf bifurcation, and type III - the reverse period doubling bifurcation. One kind of chaos-chaos intermittency is due to crisis phenomena occurring in the system. Thus, the recognition of the type of the intermittency observed in the dynamical system is equivalent to determining the type of the bifurcation characteristic for the dynamics of that system in the particular part of parameter space investigated. The identification of the intermittency type is usually based on the probability distribution of the length l of the laminar phases and the properties of the average length of the laminar phases. Both properties have a statistical character. Thus, to obtain them a long time series has to be examined. In practice, often, the length of the time series is limited, so it is important to find a method capable to recognize the type of the intermittency using short time series.

### 4.5.1 Phase Space

The dynamics of the system at different operating conditions can be visualized by reconstructing the phase space of evolution of the time signal acquired at those conditions. In such a reconstruction, also known as delay-embedding, the measured time series is converted into a set of delay vectors that have one-to-one correspondence with one of the dynamic variables involved in the system dynamics. For example, with our data, I can show the different phases during the second transition (Fig. 4.14). Inside itself the phase change but however include some periodic portions, not all with the same phase.

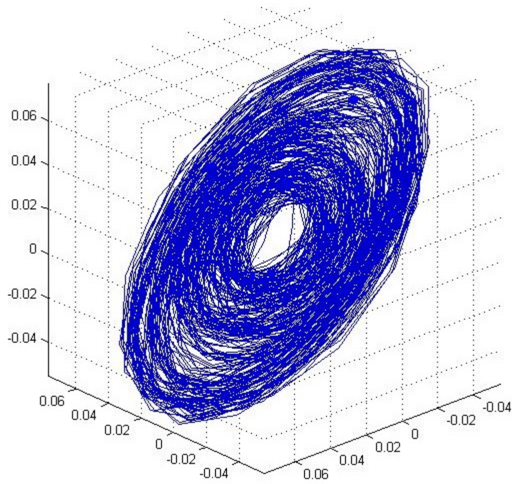


Figure 4.14: Example of phase space during the second transition. We can see the variation of the signal and more of a periodic behavior

We wanted to look at the phase space, to find the periodic portions of the signal, because like already explained earlier, during intermittency this phenomenon is recurring.

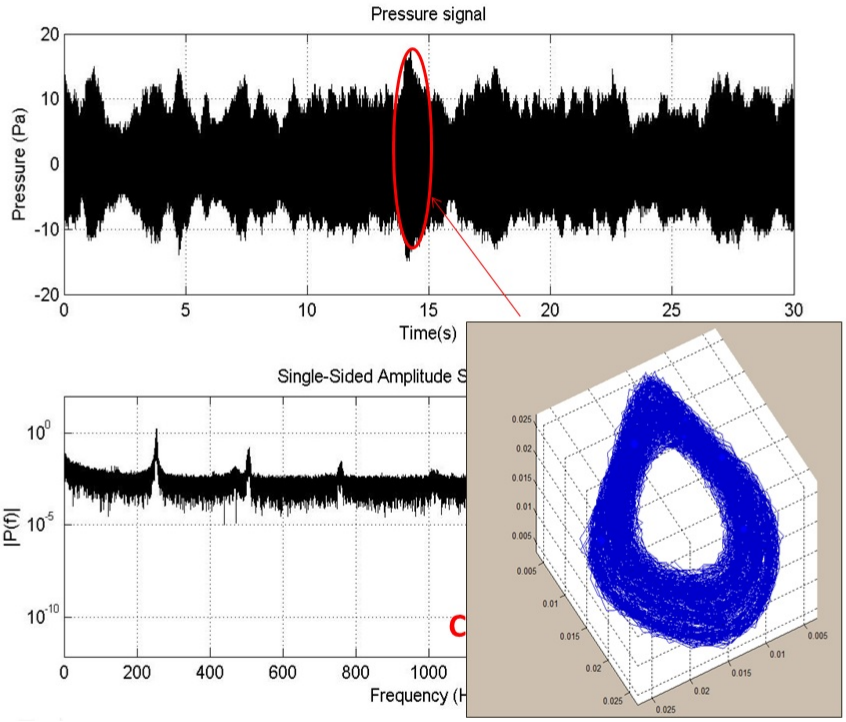


Figure 4.15: Intermittent signal (40 slpm) during the first transition focusing on a portion of a signal which is periodic

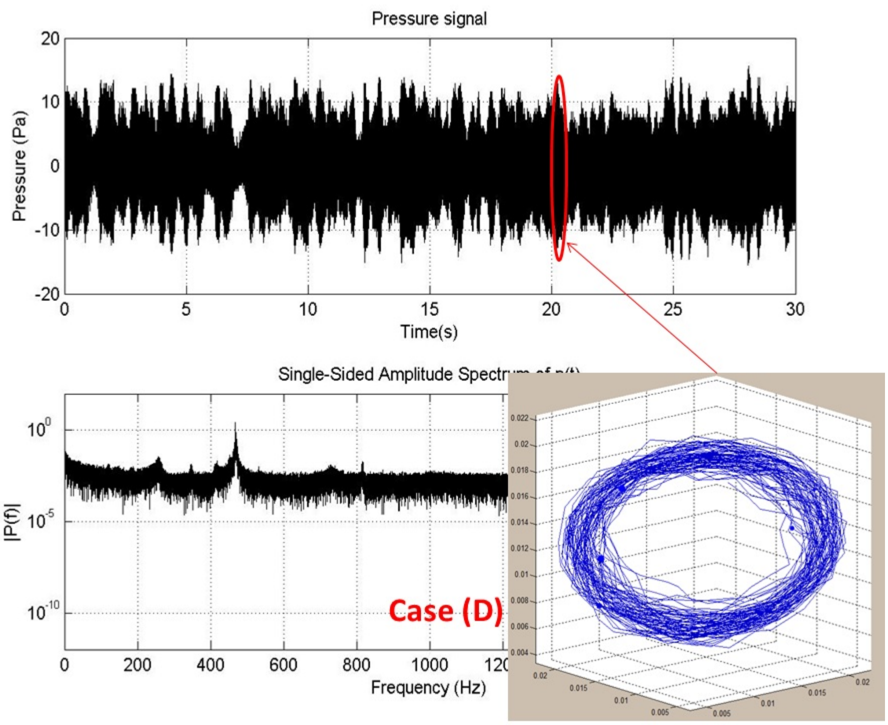


Figure 4.16: Intermittent signal (44 slpm), again during the first transition with focus on a periodic portion, in this case the portion is more little

### 4.5.2 Homoclinic Orbits

The interaction of flow with sound can often lead to unsteady pressure fluctuations that display intermittent bursts, i.e., low amplitude, aperiodic oscillations embedded amongst higher amplitude periodic oscillations in a near-random manner. We show that these intermittent states give rise to homoclinic orbits in the phase space. These homoclinic orbits, which are often difficult to identify visually through phase space reconstruction, can be discerned by quantifying the recurrence properties of the system dynamics. We show that an exponential fall-off of the time spent by the dynamics in the aperiodic states provides an easy way of identifying homoclinic orbits in the underlying phase space. One purpose of the thesis work is to identify the intermittency type in our setup. In literature there are some papers that investigate the intermittency type through the homoclinic orbits for example V. Nair and Sujith et al. 2013. For this reason we have tried to find them in our data:

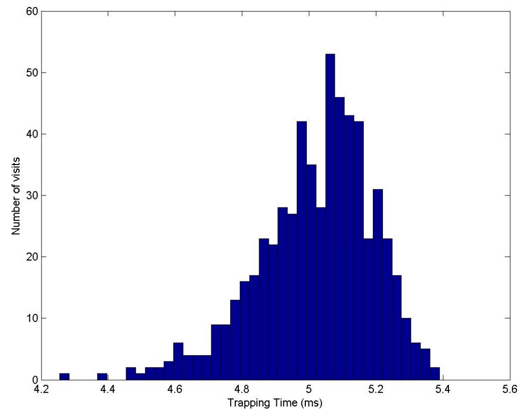


(a) *When the sound start*

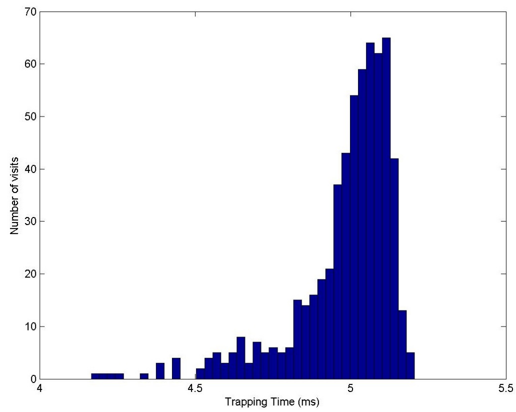


(b) *I transition*

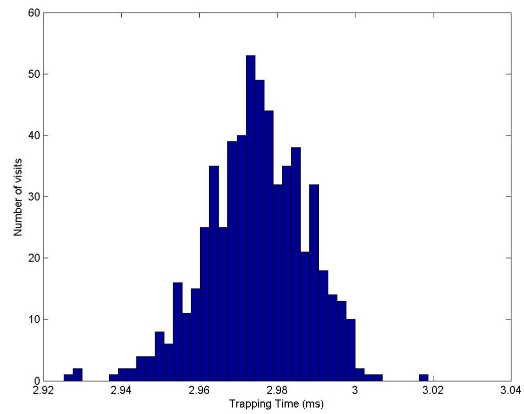


(c) *Start of the II transition*

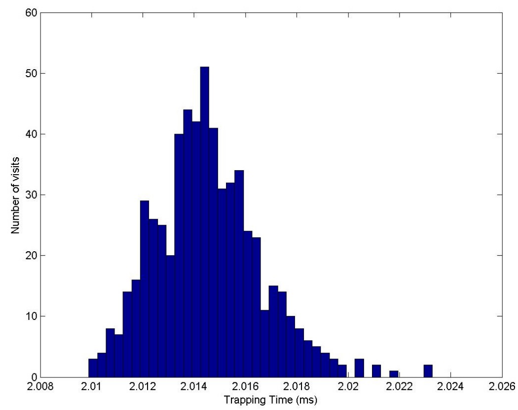


(d) *End of the II transition*

Figure 4.17: Histograms of the frequency of visits as a function of the duration of time spent trapped in the low amplitude aperiodic regimes

From Fig. 4.17, it can be assumed that we have found the homoclinic orbits. They are characteristic of the types II and III, therefore is reasonable think that in our case, we have an intermittency of the II or III type. However we cannot say with certainty with this analysis.

## 4.6 Recurrence Quantification Analysis

Recurrence quantification analysis (RQA) is a method of nonlinear data analysis (cf. chaos theory) for the investigation of dynamical systems. It quantifies the number and duration of recurrences of a dynamical system presented by its phase space trajectory. We have used this method to investigate one more time the evaluation of the signal, in particular, like earlier, its periodicity.

### 4.6.1 Recurrence Plot

In 2002 Marwan et al. showed that it is possible to distinguish between time series with intermittency and with other kinds of chaos using recurrence plots RP and recurrence quantification analysis RQA. They showed that the laminar phases of intermittency correspond to horizontal and vertical lines on the RP and that such lines form squares and rectangles. Occurrences of such patterns on the RP are a sign that intermittency is present in the data. However, Marwan et al. did not define which kind of intermittency they had observed. During the data processing, through use of the "Cross Recurrence Plot Toolbox for Matlab" by Marwan, I obtained the necessary parameters (Dimension, Delay and Threshold) and plotted the Recurrence Plot for all the time series. In this way it has been possible identify the Intermittency. Now, I show the three different Recurrence Plots: Fig. 4.18 during the first transition, Fig. 4.19 during the second and Fig. 4.20 during the third. From them, we can clearly see the intermittency only in the first transition. In the second and third we see an intermittent signal but not as pronounced as earlier. Furthermore, K. Klimaszewska and J. J. Zebrowski et. al. 2009 used this method to detect the Intermittency Type, but in our case, no RP respects completely the characteristics described in the paper. However in our results, like already explained earlier, are very interesting:

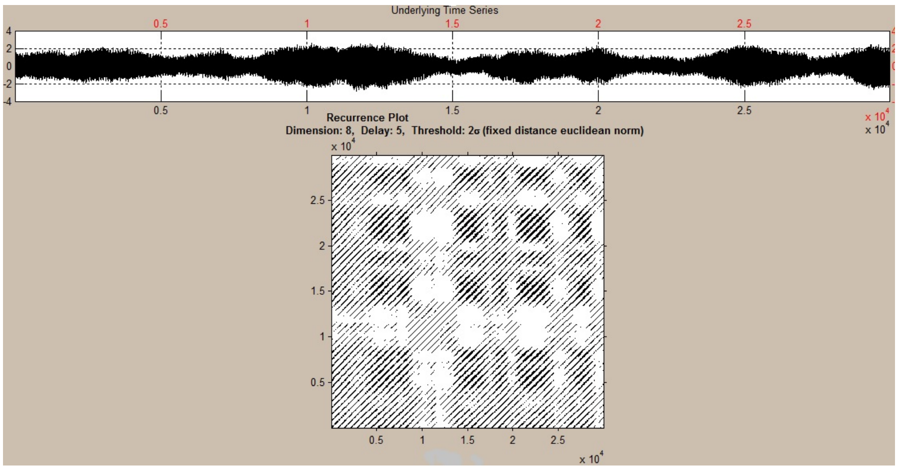


Figure 4.18: Recurrence Plot during the I transition (44 slpm)

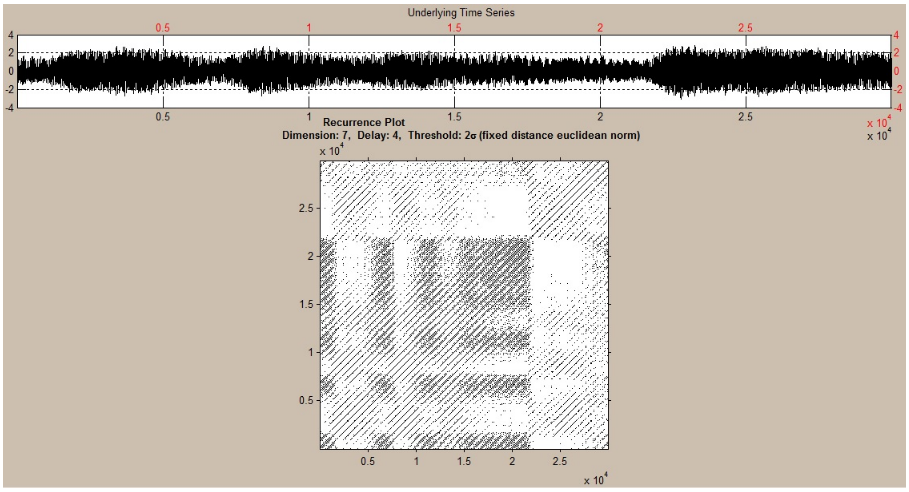


Figure 4.19: Recurrence Plot during the II transition (77 slpm)

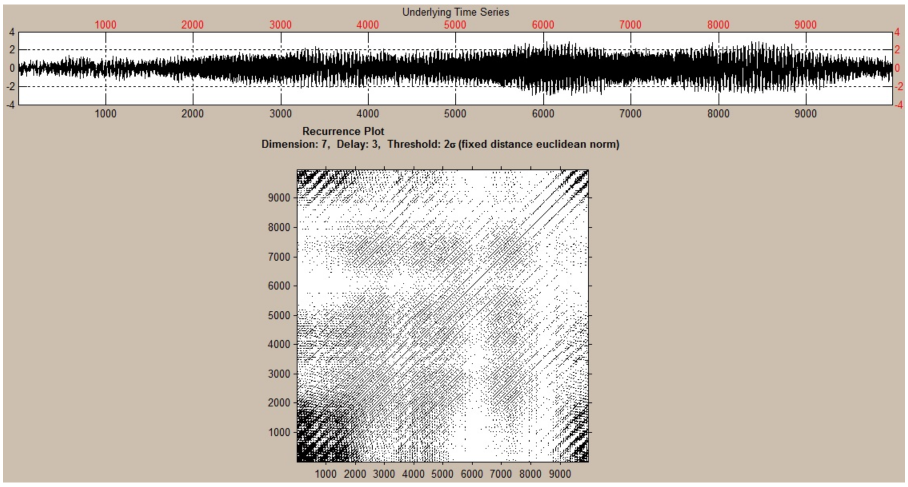


Figure 4.20: Recurrence Plot during the III transition (107 slpm)

### 4.6.2 RQA Parameters

In order to go beyond the visual impression yielded by RPs, several measures of complexity which quantify the small scale structures in RPs, have been proposed and are known as recurrence quantification analysis (RQA). These measures are based on the recurrence point density and the diagonal and vertical line structures of the RP. A computation of these measures in small windows (sub-matrices) of the RP moving along the LOI yields the time dependent behavior of these variables. Some studies based on RQA measures show that they are able to identify bifurcation points, especially chaos–order transitions. The vertical structures in the RP are related to intermittency and laminar states. Those measures quantifying the vertical structures enable also to detect chaos–chaos transitions (N. Marwan, M. C. Romano, M. Thiel, J. Kurths, 2006). During the data processing: I calculated each parameter for all the air flow rates used and made the plot: the RQA parameter on the y-axis and the flow rates on the x-axis. Looking at the evaluation of these parameters, we can understand the trend of the signal and see the periodicity or less of it.

### Recurrence Rate (RR)

The simplest measure of the RQA is the recurrence rate (RR) or per cent recurrences which is a measure of the density of recurrence points in the RP. In our case (Fig. 4.22), it is very clear. We can watch at the generation of the sound and the two different transitions where the RR becomes smaller and there are two low peaks. Furthermore, we can see that with the third transition: the RR has a low value and the signal does not come back periodic as we have seen earlier.

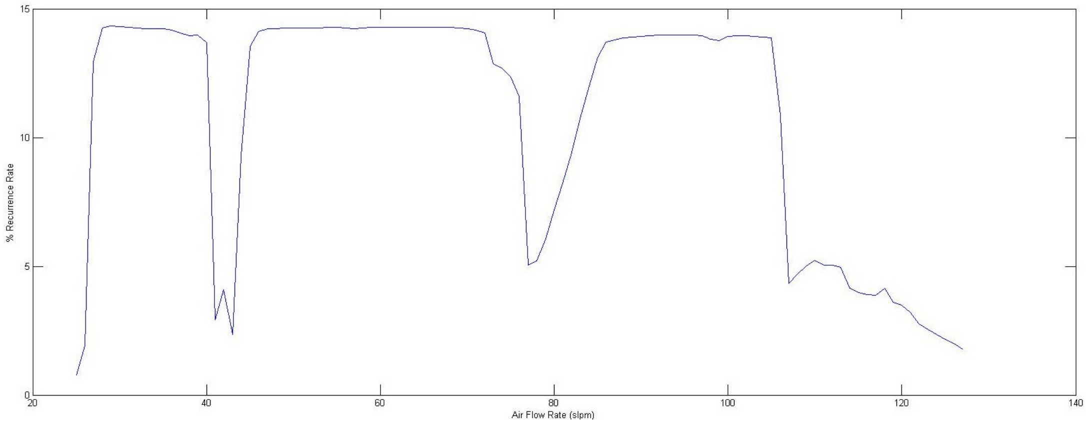


Figure 4.21: Recurrence Rate (RR)

### Determinism (DET)

The ratio of recurrence points that form diagonal structures (of at least length $l_{min}$) to all recurrence points is introduced as a measure for determinism (or predictability) of the system. Also in this case, from our plot (Fig: 4.22)it is possible to distinguish clearly the transition, in particular the first, while for the second it is less clear.

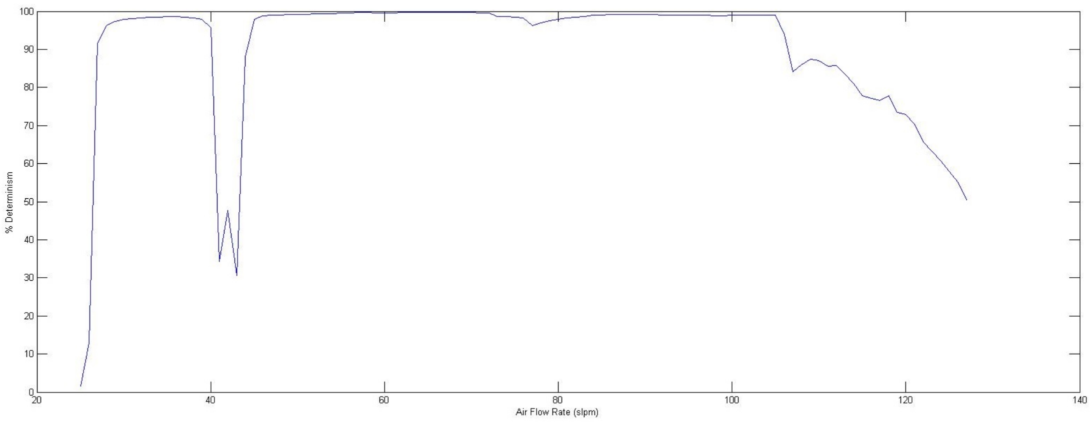


Figure 4.22: Determinism (DET)

### Lmax ($L_{max}$)

Another RQA measure considers the length Lmax of the longest diagonal line found in the RP. Like for the RR, the transitions are very clear, indeed the measure of the longest diagonal ($L_{max}$) decrease very much in correspondence of them (Fig: 4.23).

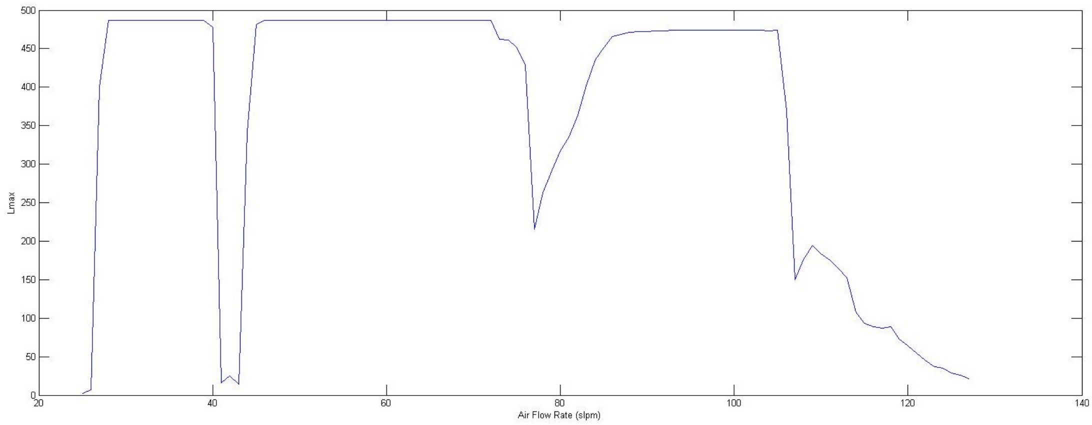


Figure 4.23: Lmax ($L_{max}$)

### Laminarity (LAM)

Analogous to the definition of the determinism (4.6.2) the ratio between the recurrence points forming the vertical structures and the entire set of recurrence points can be computed like Laminarity (LAM). Like in case of the RR and Lmax, The two different transitions are very easy to locate (Fig: 4.24).

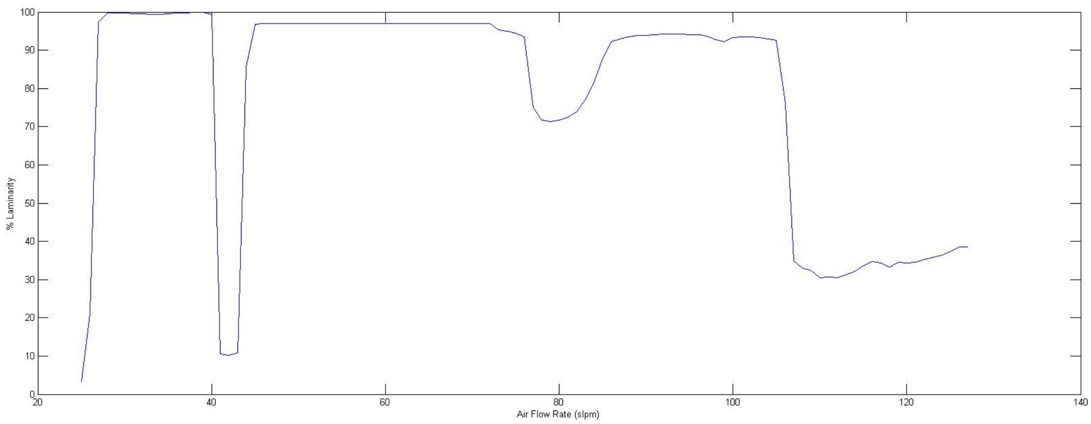


Figure 4.24: Laminarity (LAM)

### Entropy (ENT)

The measure entropy refers to the Shannon entropy of the probability to find a diagonal line of exactly length l in the RP. This parameter, in the our case ((Fig: 4.25), has an evaluation less rigorous respect to the others, but however, we can see clearly the first transition.

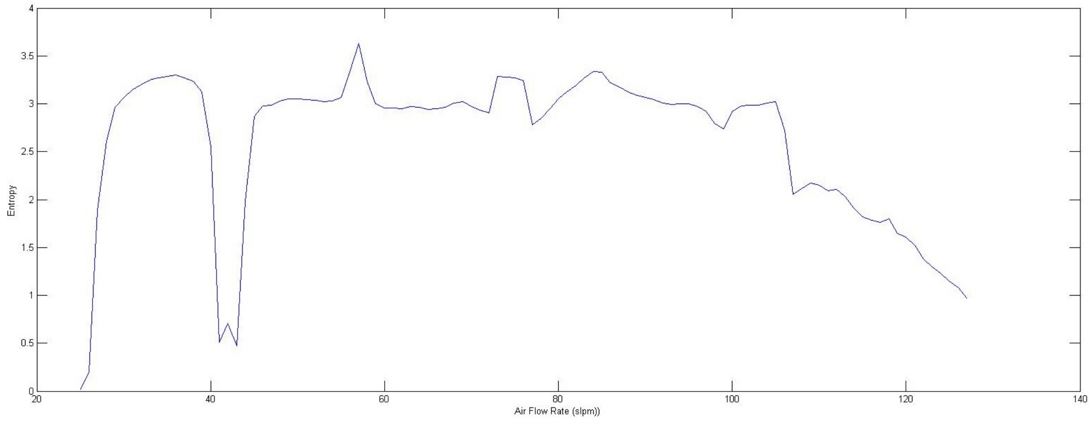


Figure 4.25: Entropy (ENT)

# 5. Conclusions

The present experimental thesis work, is a part of TANGO project (Thermoacoustic and Aero-acoustic Nonlinearities in Green combustors with Orifice structures). This project analyzes and studies instabilities of Thermoacoustic and Aeroacoustic types. Effectively, the combustion instabilities represent a serious problem for combustion-driven devices, such as gas turbine engines and domestic burners. These instabilities can cause intense pressure oscillations, which in turn causes excessive structural oscillations, fatigue and even catastrophic damage to combustor hardware. In recent years, the development of clean combustion systems with reduced pollution of the environment has become a priority; however, such systems are particularly prone to combustion instabilities. There is an urgent need to understand the physical processes that are responsible so that methods to predict and prevent these instabilities can be developed. The research in the TANGO network is intended to address these issues.

In particular, my thesis work is on aeroacoustic intermittency, explaining the low frequency acoustic pulsations in pipe networks which have been observed in many technical applications. These pulsations are undesirable, not only because of the noise produced, but also because of the possibility of mechanical failures in the pipe network (and other parts of the application systems). During the experiments, I performed experiments on a pipe with an orifice. The control parameter was the air-flow rate. I measured the pressure time signals for various air-flow rates. Later I processed these time signals to identify and locate the intermittency and if it was possible to detect the type. With this thesis we show that intermittent burst oscillations are a typical feature of turbulent flow-sound interaction, even in the absence of combustion. The onset of self-sustained oscillations in a turbulent pipe flow across an orifice is investigated in this whistling apparatus. Analysis of measured pressure fluctuations reveals that this emergence of order from turbulence happens through an intermediate intermittent regime characterized by bursts of periodic oscillations that appear in a near-random fashion amidst the background chaotic fluctuations. The interesting feature is that these intermittent bursts correspond to a frequency distinct from the final oscillatory state as the boundary condition at the orifice exit undergoes a transition at the onset of whistling.

The experimental work has permitted us to recreate the intermittency phenomena in our setup in a simple manner. Like already explained, the layout has been selected to simulate a real combustor. Obviously, the main purpose of this work is recreate the intermittency to investigate and understand it in the real systems (combustors, pipe network, valves etc...). The data captured is very interesting, because they show clearly the phenomena that we look for. All methods used, produced the results that expected. Indeed, I have found the flow rate where the sound starts, the changing of the sound tones and the three transitions.

In future it will be necessary to verify the intermittency type using the methods discussed in this work or through alternative solutions. Further, if it will be possible to improve the setup such as refining the internal surface of the pipe. This is because we have seen that minimal roughness or imperfections can change the sound tone and influence the data capture inserting errors of measure. Another possible factor to verify is the position of the microphone. In our experiments, we tried to change the position of it: at the exit of the orifice (5 cm far away from it), at the end of the second pipe (always 5 cm far away from the open end) and also from outside the setup (about 5 cm far away from the open end). The position of the microphone is fundamental, because we needed to make attention if the pressure fluctuations are of acoustic or hydrodynamic nature. To obtain correct measures of pressure by microphone, we required of be in the *Far Field* where the acoustic velocity is predominant on the hydrodynamic velocity and the reactive acoustic power have to be null. With the position of the sensor very close at the orifice, there is the risk that it does not happen.

# Bibliography


[1] Pantieri, Lorenzo e Tommaso Gordini (2012), *L'arte di scrivere con LaTeX*, `http://www.lorenzopantieri.net/LaTeX_files/ArteLaTeX.pdf`.

[2] A. Hirschberg. and S.W. Rienstra.(2004), *An introduction to aeroacoustics*, Eindhoven University of Technology, Dept. of App. Physics and Dept. of Mathematics and Comp. Science, P.O. Box 513, 5600 MB Eindhoven, The Netherlands.

[3] Devis Tonon, Avraham Hirschberg, Joachim Golliard and Samir Ziada, (2010), *Aeroacoustics of pipe systems with closed branches*, Eindhoven University of Technology, Fluid Dynamics Laboratory, Faculty of Applied Physics, P.O. Box 513, 5600 MB, Eindhoven, The Netherlands TNO, P.O. Box 155, 2600 AD, Delft, The Netherlands McMaster University, Department of Mechanical Engineering, Hamilton, Ontario, Canada L8S 4L7.

[4] Yves Pomeau and Paul Manneville (1980), *Intermittent Transition to Turbulence in Dissipative Dynamical Systems*, Commissariat à l'Energie Atomique, Division de la Physique, Service de Physique Théorique, F-91190 Gif-sur-Yvette, France.

[5] Lisa Holden and Thomas Erneux (1993), *Understanding bursting oscillations as periodic slow passages through bifurcation and limit points*, Department of Engineering Sciences and Applied Mathematics, Northwestern University, Evanston, IL 60208, USA.

[6] O. Batiste, M. Net, I. Mercader, and E. Knobloch (2001), *Oscillatory Binary Fluid Convection in Large Aspect-Ratio Containers*, Departament de Física Aplicada, Universitat Politécnica de Catalunya, Barcelona, Spain.

[7] R. Straube, D. Flockerzi and M. J. B. Hauser (2006), *Sub-Hopf / fold-cycle bursting and its relation to (quasi-) periodic oscillations*, Abteilung Theoretische Physik, Hahn-Meitner-Institut Berlin, Glienicker Str. 100, D-14109 Berlin, Germany Max-Planck-Institut für Dynamik komplexer technischer Systeme, Sandtorstr. 1, D-39106 Magdeburg, Germany Abteilung Biophysik, Institut für Experimentelle Physik, Otto-von-Guericke Universität, Universitätsplatz 2, D-39106 Magdeburg, Germany.

[8] Seung Kee Han, D. E. Postnov, (2003), *Chaotic bursting as chaotic itinerancy in coupled neural oscillators* , CHAOS, VOLUME 13, No. 3, p.1105-1109 (2003).

[9] Hiroshi Okamoto, Naoki Tanaka , and Masayoshi Naito, (1998), *Intermittencies and Related Phenomena in the Oxidation of Formaldehyde at a Constant Current*, Advanced Research Laboratory, Hitachi, Ltd., Hatoyama, Saitama 350-03, Japan.

[10] Bergè, P., Dubois, M., Manneville, P. & Pomeau, Y, (1980), *Intermittency in Rayleigh-Bénard convection*, DPh-G/PSRM, CEN-Saclay, Boîte Postale 2, 91190 Gif-s/Yvette, France.

[11] Gollub J.P. and Benson S.V., (1980), *Many Routes to Turbulent Convection*, Physics Department, Haverford College, Haverford, Pa 19041, U.S.A.

[12] King, G. P. and H. L. Swinney (1983), *Limits of stability and irregular flow patterns in wavy vortex flow*, Department of Physics, University of Texas, Austin, Texas 78712, U.S.A.

[13] B. Karthik, S. R. Chakravarthy, and R. I. Sujith, (2003) *Jet forking driven by pipe tone*, Department of Aerospace Engineering, Indian Institute of Technology Madras, Chennai 600 036, India.

[14] B. Karthik, S. R. Chakravarthy, R. I. Sujith and E.G. Tulapurkara, (2000) *Vortex-Resonant sound interaction in a duct containing an orifice*, Department of Aerospace Engineering, Indian Institute of Technology Madras, Chennai 600 036, India.

[15] A. D. Pierce (1989), *An Introduction to Its Physical Principles and Applications*, Massachusetts Institute of Technology, 110 Cummington Mall, ENG 401, U.S.A.

[16] Lighthill, M. J. (1952a) *On sound generated aerodynamically. I. General theory*, Cambridge Monographs on Mechanics. Cambridge, UK: Cambridge University Press U.K..

[17] Lighthill, M. J., (1952b), *On Sound Generated Aerodynamically. II. Turbulence as a Source of Sound*, Cambridge Monographs on Mechanics. Cambridge, UK: Cambridge University Press U.K.

[18] Powell, A. (1964), *Theory of Vortex Sound*, Aerosonics Laboratory, Department of Engineering, University of California, Los Angeles, California 90024, U.S.A.

[19] Howe M.S. (1975), *Contributions to the theory of Aerodynamic sound, with applications to Excess Jet Noise and the theory of the flute*, Engineering Department, University of Cambridge, U.K.

[20] Howe M.S. (1998), *Acoustics of Fluide Structure Interactions*, Engineering Department, University of Cambridge, U.K.

[21] Agarwal N.K. (1994a) *The Sound Field in Fully Developed Turbulent Pipe Flow Due to Internal Flow Separation, Part I: Wall Pressure Fluctuations*, Analytical Services and Materials, Inc., 107 Research Drive, Hampton, Virginia 23666, U.S.A.

[22] Agarwal N.K. (1994b) *The Sound Field in Fully Developed Turbulent Pipe Flow Due to Internal Flow Separation, Part I: Modal Amplitude and Cut-Off Frequencies*, Analytical Services and Materials, Inc., 107 Research Drive, Hampton, Virginia 23666, U.S.A.

[23] Blake W.K. (1986) *Mechanics of Flow Induced Sound and Vibration*, Applied Mathematics and Mechanics, Vol. 17, Orlando: Academic Press, U.S.A.

[24] Chanaud, R.C. and Powell, A. (1965), *Some Experiments Concerning the Hole and Ring Tones*, Aerosonics Laboratory, Department of Engineering, University of California, Los Angeles, California 90024, U.S.A.

[25] Powell, A. (1961), *On the Bulge Tone*, Aerosonics Laboratory, Department of Engineering, University of California, Los Angeles, California 90024, U.S.A.

[26] Rossiter J.E. (1966), *Wind Tunnel experiments in the flow over rectangular cavities at Subsonic and Transonic Speeds*,Communicated by the Deputy Controller Aircraft (Research and Development) Ministry of Aviation, London, U.K.

[27] Bruggeman, J. C., A. Hirschberg, M. E. H. Dongen, and A. P. J. Wijnands (1991), *Selfsustained aero-acoustic pulsations in gas transport systems: experimental study of the influence of closed side branches*, Department of Physics, Eindhoven University of Technology, PO. Box 513, 5600 MB Eindhoven, The Netherlands.

[28] A. Hirschberg, Bruggeman J.C., P. J. Wijnands and N. Smits, (1989), *The "Whistler Nozzle" and Horn as Aero-Acoustics Sound Sources in Pipe Systems*, Department of Physics, Eindhoven University of Technology, PO. Box 513, 5600 MB Eindhoven, The Netherlands.

[29] Hussain A. K. M. F. and M. A. Z. Hasan (1983) *The "Whistler Nozzle" phenomenon*, Department of Mechanical Engineering, University of Houston, Texas 77004, U.S.A.

[30] Selamet A., D. Kurnlawan and R.D. Knotts, (2002), *Whistles with a Generic Sidebranch: Production and Suppresion*, E 509 Scott Laboratory 201 W. 19th Avenue Columbus, OH 43210-1142, Michigan, U.S.A.

[31] A. Hirschberg, Bruggeman J.C., P. J. Wijnands and N. Smits, (1989), *Experiments on the Fluid Mechanics of Whistling*, Department of Physics, Eindhoven University of Technology, PO. Box 513, 5600 MB Eindhoven, The Netherlands.

[32] T. A. Wilson, G. S. Beavers, M. A. DeCoster, D. K. Holger and M. D. Regenfuss, (1971), *The "Whistler Nozzle" and Horn as Aero-Acoustics Sound Sources in Pipe Systems*, Department of Aerospace Engineering and Mechanics, University of Minnesota, Minneapolis, Minnesota 55455, U.S.A.

[33] Durrieu P., Hofmans G., Ajello G., Boot R., Aurégan Y., Hirschberg A., Peters M.C., (2001), *Quasisteady aero-acoustic response of orifices*, Laboratoire d'Acoustique Université du Maine, URA CNRS 1101, Le Mans, France.

[34] Flandro G. A. and Jacobs H. R., (1975), *Vortex Generated Sound in Cavities*, Utah, University, Salt Lake City, Utah; H. JACOBS, Utah, University, Salt Lake City, U.S.A.

[35] Kourta A. (1996a), *Vortex Shedding in Segmented Solid Rocket Motors*, Institut de Mécanique des Fluides de Toulouse, F-31400 Toulouse, France.

[36] Kourta A. (1996b), *Acoustic Mean Flow Interaction and Vortex Shedding in Solid Rockets Motors*, Institut de Mécanique des Fluides de Toulouse, F-31400 Toulouse, France.

[37] Kourta A. (1997), *Shear Layer Instability and acoustic Interaction in Solid Propellant Rockets Motors*, Institut de Mécanique des Fluides de Toulouse, F-31400 Toulouse, France.

[38] Dunlap R., R.S. Brown, S.W. Young and R.C. Waugh, (1981), *Exploratory Experiments on Acoustic Oscillations Driven by Periodic Vortex Shedding*, United Technologies Corp., Sunnyvale, California, U.S.A.

[39] R.S. Brown, Dunlap R. S.W. Young and R.C. Waugh (1985), *Vortex Shedding Studies in a Simulated Coaxial Dump Combustor*, United Technologies Corp., Sunnyvale, California, U.S.A.

[40] Anthoine J., (2000) *Experimental and Numerical Study of Aeroacoustics Phenomena in Large Solid Propellant Boosters*, PhD Thesis, Universite Libre de Bruxelles & Von Karman Institute for Fluid Dynamics.

[41] M. Frigo and S. G. Johnson, (2005), *The Design and Implementation of FFTW3*, IBM Austin Res. Lab., TX, U.S.A.

[42] M.l T. Heideman, D. H. Johnson and C.S.Burrus *Gauss and the History of the Fast Fourier Transform*, Lockheed Engineering and Management Services Company, Houston, TX, U.S.A.

[43] Danielson G.C. and Lanczos C., (1942), *Some improvements in practical Fourier analysis and their application to x-ray scattering from liquids*, Purdue University, Lafayette, Indiana, U.S.A.

[44] Cooley, James W.; Lewis, Peter A.W.; Welch, Peter D. (June 1967), *Historical notes on the fast Fourier transform*, Institute of Electrical and Electronics Engineers.; Signal Processing Society, New York, U.S.A.

[45] Danielson G.C. and Lanczos C., (1942), *Some improvements in practical Fourier analysis and their application to x-ray scattering from liquids*, Purdue University, Lafayette, Indiana, U.S.A.

[46] P. Duhamel and M. Vetterli, (1990) *Fast Fourier transforms: a tutorial review and a state of the art*, Dept of EE and CTR, S.W. Mudd Building, Columbia University, 500 W 20th Street, New York, NY 10027, U.S.A.

[47] A. Edelman, P. McCorquodale, and S. Toledo (1999), *The Future Fast Fourier Transform?*, SIAM Journal on Scientific Computing, 1998, Vol. 20, No. 3 : pp. 1094-1114.

[48] H. Guo and C. S. Burrus, (1996), *Fast approximate Fourier transform via wavelets transform*, Rice Univ. (USA)

[49] Gentleman, W. M.; Sande, G. (1966), *Fast Fourier transforms-for fun and profit*, Bell Telephone Laboratories, Murray Hill, New Jersey, and Princeton University, Princeton, New Jerse, U.S.A.

[50] Welch Peter D. (1969), *A fixed-point fast Fourier transform error analysis*, IBM Watson Research Center, Yorktown Heights, N.Y., U.S.A.

[51] Funda Ergün (1995), , *Testing multivariate linear functions: overcoming the generator bottleneck*,Cornell University, New York, U.S.A.

[52] Edward R. Scheinerman, (1996), *Invitation to Dynamical Systems*, Department of Mathematical Sciences The Johns Hopkins University, 100 Whitehead Hall 3400 North Charles Street Baltimore, MD 21218, U.S.A.

[53] S. H. Strogatz (1994), *Nonlinear dynamics and chaos with Applications to physics, biology, chemistry and engineering*, Addinson-Wesley Publishing Company.

[54] V. Nair V. (2014), *Role of Intermittency in the onset of combustion instability*, Ph.D. Thesis, Department of Aerospace Engineering, Indian Institute of Technology Madras, Chennai 600 036, India.

[55] B.B. Maldebrot (1982), *The Fractal Geometry of Naturey*, W. H. Freeman and Company, San Francisco, U.S.A.

[56] Montroll, E. W. and M. F. Schlesinger (1982), *On 1f noise and other distributions with long tails*, Proc. Natl. Acad. Sci. USA, 79, 3380–3383.

[57] H. E. Hurst, H. E. (1951), *Long-term storage capacity of reservoirs*, Trans. Am. Soc. Civil Eng., 116, 770–799.

[58] Frisch U., (1995), *Turbulence: The legacy of A. N. Kolmogorov*, Cambridge University Press, Cambridge, U.K.

[59] Basingthwaighte, J. B., L. S. Liebovitch, and B. J.West (1994), *Fractal Physiology*, Oxford University Press, Oxford, U.K.

[60] Kolmogorov, A. N. (1941), *Dissipation of energy in the locally isotropic turbulence*, Proceedings: Mathematical and Physical Sciences Vol. 434, No. 1890, Turbulence and Stochastic Process: Kolmogorov's Ideas 50 Years On (Jul. 8, 1991), pp. 15-17.

[61] Karthik, B., S. R. Chakravarthy, and R. I. Sujith (2008), *Mechanism of pipetoneexcitation by flow through an orifice in a duct*, Department of Aerospace Engineering, Indian Institute of Technology Madras, Chennai 600 036, India.

[62] Kantelhardt, J. W. (2011), *Fractal and multifractal time series*, In R. A. Meyers (ed.), Mathematics of Complexity and Dynamical Systems. Springer, New York, U.S.A.

[63] West, B. J., M. Latka, M. Glaubic-Latka, and D. Latka (2003), *Multifractality of cerebral blood flow*, Physica A, 318, 453–460.

[64] Peng, C. K., S. V. Buldyrev, S. Havlin, M. Simons, H. E. Stanley, and A. L. Goldberger (1994), *Mosaic organization of dna nucleotides*, Phys. Rev. E, 49, 1685–1689.

[65] Frisch, U. and G. Parisi, (1985), *On the singularity structure of fully developed turbulence*, Turbulence and Predictability in Geophysical Fluid Dynamics. North-Holland, 1985, 84–88.

[66] Kantelhardt, J. W., E. Koscielny-Bunde, H. H. A. Rego, S. Havlin, and A. Bunde (2001), *Detecting long-range correlations with detrended fluctuation analysis*, Physica A, 295, 441–454.

[67] Kantelhardt, J. W., S. A. Zschiegner, E. Koscielny-Bunde, S. Havlin, A. Bunde, and H. E. Stanley (2002), *Multifractal detrended fluctuation analysis of nonstationary time series*, Physica A, 316, 87–114.

[68] Paladin, G. and A. Vulpiani (1987), *Anomalous scaling laws in multifractal objects*, Phys. Rep., 156, 147–225.

[69] Sreenivasan, K. R. (1991), *Fractals and multifractals in fluid turbulence*, Annu. Rev. Fluid Mech., 23, 539–604.

[70] Taylor, G. I. (1938), *The spectrum of turbulence*, Proc. R. Soc. Lond. A, 164, 476–490.

[71] Richardson, L. F. (1922), *Weather Prediction by Numerical Process*, Cambridge University Press, Cambridge, U.K.

[72] Kraichnan, R. H. (1967), *Inertial ranges in two-dimensional turbulence*, Phys. Fluids, 10, 1417–1423.

[73] Zia, R. K., E. F. Redish, and S. R. McKay (2009), *Making sense of the legendre transform*, Am. J. Phys., 77, 614–622.

[74] Norbert Marwan, M. Carmen Romano, Marco Thiel, Jürgen Kurths, (2006), *Recurrence plots for the analysis of complex systems*, Nonlinear Dynamics Group, Institute of Physics, University of Potsdam, Potsdam 14415, Germany.

[75] Marco Thiel, M. Carmen Romano, Jürgen Kurths, (2004), *How much information is contained in a recurrence plot?*,University of Potsdam, Nonlinear Dynamics, Am Neuen Palais 10, 14469 Potsdam, Germany.

[76] Teresa Aparicio, Eduardo F. Pozo, Dulce Saura (2006), *Detecting determinism using recurrence quantification analysis: Three test procedures*, Departamento de Anàlisis Ecònomico, Universidad de Zaragoza, Gran Vìa 2, 50005 Zaragoza, Spain

[77] Espen A.F.Ihlen, (2012), *Introduction to multifractal detrended fluctuation analysis in Matlab*, Department of Neuroscience, Norwegian University of Science and Technology, Trondheim, Norway.

[78] Richetti, P., F. Argoul, and A. Arneodo (1986), *Type-ii intermittency in a peroidically driven nonlinear oscillator*, Phys. Rev. A, 34, 726–729.

[79] Holmes, P., (1990), *Can dynamical systems approach turbulence?*,In J. Lumley (ed.), Whither Turbulence? Turbulence at the Crossroads, volume 357. Springer, 1990, 195–249.

[80] Zia, R. K., E. F. Redish, and S. R. McKay (2009), *Making sense of the legendre transform*, Am. J. Phys., 77, 614–622.

[81] Klimaszewska, K. and J. J. Zebrowski (2009), *Detection of the type of intermittency using characteristic patterns in recurrence plots*, Phys. Rev. E, 80, 026214.

[82] Jan W. Kantelhardta, Stephan A. Zschiegnera, Eva Koscielny-Bunde, Shlomo Havlin, Armin Bunde, H. Eugene Stanley, (2002) *Multifractal detrended fluctuation analysis of nonstationary time series*, Physica A 316 (2002) 87 – 114.

[83] Anderson, A. B. C. (1952), *Dependence of pfeifenton (pipe tone) frequency on pipe length, orifice diameter, and gas discharge pressure*, J. Acoust. Soc. Am., 24, 675–681.

[84] Anderson, A. B. C. (1955), *Structure and velocity of the periodic vortex-ring flow pattern of a primary pipe tone jet*, J. Acoust. Soc. Am., 27, 1048–1053.

[85] Vineeth Nair and R. I. Sujith (2013), *Identifying homoclinic orbits in the dynamics of intermittent signals through recurrence quantification*, Department of Aerospace Engineering, Indian Institute of Technology Madras, Chennai 600 036, India.

# A. MCR Series - Mass Gas Flow Controllers Alicat Scientific

## Technical Data for Alicat MC and MCR Mass Flow Controllers
### 0 to 0.5 sccm Full Scale through 0 to 3000 slpm Full Scale

**Standard Operating Specifications (Contact Alicat for available options)**

| Performance | MC & MCR Mass Flow Controller |
|---|---|
| Accuracy at calibration conditions after tare | ± (0.8% of Reading + 0.2% of Full Scale) |
| High Accuracy at calibration conditions after tare | ± (0.4% of Reading + 0.2% of Full Scale)<br>High Accuracy option not available for units ranged under 5 sccm or over 500 slpm. |
| Repeatability | ± 0.2% Full Scale |
| Zero Shift and Span Shift | 0.02% Full Scale / ºCelsius / Atm |
| Operating Range / Turndown Ratio | 0.5% to 100% Full Scale / 200:1 Turndown |
| Maximum Controllable Flow Rate | 102.4% Full Scale |
| Typical Response Time | 100 ms (Adjustable) |
| Warm-up Time | < 1 Second |

| Operating Conditions | MC & MCR Mass Flow Controller | |
|---|---|---|
| Mass Reference Conditions (STP) | 25ºC & 14.696 psia (standard — others available on request) | |
| Operating Temperature | −10 to +50 ºCelsius | |
| Humidity Range (Non–Condensing) | 0 to 100% | |
| Max. Internal Pressure (Static) | 145 psig | |
| Proof Pressure | 175 psig | |
| Mounting Attitude Sensitivity | **MC:** None | **MCR:** Mount with valve cylinder vertical & upright |
| Valve Type | Normally Closed | |
| Ingress Protection | IP40 | |
| Wetted Materials | **MC:** 303 & 302 Stainless Steel, Viton®, Silicone RTV (Rubber), Glass Reinforced Nylon, Aluminum, Brass, 430FR Stainless Steel, Silicon, Glass.<br>**MCR:** 303 & 302 Stainless Steel, Viton®, Silicone RTV (Rubber), Glass Reinforced Nylon, Aluminum, 416 Stainless Steel, Nickel, Silicon, Glass.<br>If your application demands a different material, please contact Alicat. | |

| Communications / Power | MC & MCR Mass Flow Controller | |
|---|---|---|
| Monochrome LCD or Color TFT Display with integrated touchpad | Simultaneously displays Mass Flow, Volumetric Flow, Pressure and Temperature | |
| Digital Input/Output Signal[1] Options | RS-232 Serial / RS-485 Serial / Modbus / PROFIBUS[3] | |
| Analog Input/Output Signal[2] Options | 0-5 Vdc / 1-5 Vdc / 0-10 Vdc / 4-20 mA | |
| Optional Secondary Analog Input/Output Signal[2] | 0-5 Vdc / 1-5 Vdc / 0-10 Vdc / 4-20 mA | |
| Electrical Connection Options | 8 Pin Mini-DIN / 9-pin D-sub (DB9) / 15-pin D-sub (DB15) / 6 pin locking | |
| Supply Voltage | **MC:** 12 to 30 Vdc (15-30 Vdc for 4-20 mA outputs) | **MCR:** 24 to 30 Vdc |
| Supply Current | **MC**: 0.250 Amp | **MCR:** 0.750 Amp |

1. The **Digital Output Signal** communicates Mass Flow, Volumetric Flow, Pressure and Temperature
2. The **Analog Output Signal** and **Optional Secondary Analog Output Signal** communicate your choice of Mass Flow, Volumetric Flow, Pressure or Temperature
3. If selecting PROFIBUS, no analog signal is available. See PROFIBUS specifications for supply voltages and currents (***www.alicat.com/profibus***). PROFIBUS and Modbus units do not have the display.

**Range Specific Specifications**

| Full Scale Flow Mass Controller | Pressure Drop[1] at FS Flow (psid) venting to atmosphere | Mechanical Dimensions | Process Connections[2] |
|---|---|---|---|
| **MC** 0.5 sccm to 50 sccm | 1.0 | 3.9"H x 3.4"W x 1.1"D | M-5 (10-32) Female Thread[3] |
| **MC** 100 sccm to 500 sccm | 1.0 | 4.1"H x 3.6"W x 1.1"D | 1/8" NPT Female |
| **MC** 1 slpm | 1.5 | | |
| **MC** 2 slpm | 3.0 | | |
| **MC** 5 slpm | 2.0 | | |
| **MC** 10 slpm | 5.5 | | |
| **MC** 20 slpm | 20.0 | | |
| **MCR** 50 slpm | 2.0 | 5.5"H x 7.7"W x 2.3"D | 1/4" NPT Female |
| **MCR** 100 slpm | 3.2 | | |
| **MCR** 250 slpm | 2.4 | 5.5"H x 7.7"W x 2.3"D | 1/2" NPT Female |
| **MCR** 500 slpm | 6.5 | 5.5"H x 7.4"W x 2.3"D | 3/4" NPT Female (A 1-1/4" NPT Female process connection is available for 2000 slpm controllers.) |
| **MCR** 1000 slpm | 14.0 | | |
| **MCR** 1500 slpm | 17.0 | | |
| **MCR** 2000 slpm | 28.6 | 5.5"H x 8.1" W x 2.9" D | |
| **MCR** 3000 slpm | 16.8 | 5.5"H x 8.9" W x 2.9" D | 1-1/4" NPT Female |

1. Lower Pressure Drops Available, please see our **WHISPER-Series** mass flow controllers at ***www.alicat.com/whisper***.
2. Compatible with Beswick®, Swagelok® tube, Parker®, face seal, push connect and compression adapter fittings. VCR and SAE connections upon request.
3. Shipped with M-5 (10-32) Male Buna-N O-ring face seal to 1/8" Female NPT fittings.

# B. Microphone Preamplifier Power Supply Model 2221 Larson Davis

## Model 2221 Microphone Preamplifier Power Supply

### Technical Specifications

| | | |
|---|---|---|
| **Frequency Response** | (0 to 40 dB gain, 1 Vrms output) | |
| | Flat (Z-weight) | 10 Hz to 100 kHz (± 0.2 dB) |
| | | 2 Hz to 150 kHz (-3 dB) |
| | Z, A and C-weight filters | Conform to IEC 61672-1:2002 "Sound Level Meters" Class 1 |
| | A-weight | 20 Hz to 20 kHz (± 0.2 dB) |
| | C-weight | 10 Hz to 20 kHz (± 0.2 dB) |
| **Microphone bias voltage** | | 0 and 200 Volts; ± 0.25 V |
| **Preamplifier supply** | | ± 18 Volts |
| **Output signal weighting** | | Flat (Z), A and C-weighted |
| **Gain settings** | | 0 to 40 dB in 10 dB steps, plus 0 to 10 dB vernier |
| **Maximum input level** | | 18 Vpeak |
| **Maximum output current** | | 25 mA |
| **Output noise** | input shorted to ground, 20 Hz to 20 kHz | Gain / Flat (Z-wt) / A-wt / C-wt<br>0 / 1.9 µV / 5.9 µV / 4.4 µV<br>20 / 7.8 µV / 20 µV / 6.6 µV |
| **Overload indicators** | Instantaneous | Blinking LED |
| | Latched | Solid LED, reset on keypad |
| **Operating temperature range** | <±0.03 dB @ 1 kHz | -40 to +60 °C (-40 to +140 °F) |
| **Humidity range** | <±0.03 dB @ 1 kHz | 0 to 90% RH, non-condensing at 40 °C (104 °F) |
| **Dimension** | Height | 32.8 mm (1.29 in) |
| | Width | 104 mm (4.10 in) |
| | Depth | 204 mm (8.02 in) |
| **Connectors** | Input | 7-Pin LEMO 1B female |
| | Output | BNC Female |
| **Weight** | | 425 gram (15 oz) |
| **Power requirements** | internal batteries | 6 × AA; 40 hrs with PRM902 preamp |
| | external DC | 10.5 to 30V; 65ma @ 12 V with PRM902 |
| | | connector 2.5 × 5.5 coax, center positive |
| **Power adaptor (provided)** | | Larson Davis PSA017; 115Vac to 9Vdc, 500mA |
| **Cable driving capability: 30 pF/ft cable** | | Length / 14 Vpeak / 4.2Vpeak / 1.4Vpeak<br>250 ft / 38 kHz / 120 kHz / 300 kHz<br>500 ft / 19 kHz / 62 kHz / 180 kHz |
| CE | | CE-mark indicates compliance with the EMC Directive |

*All values are at 20 °C, 50% RH, 12 V supply, <3 m (10 ft) cable, and a direct input from a 50 ohm generator, unless otherwise specified.*

### Accessories and Related Products

| | |
|---|---|
| **PRM902** | ½" Microphone Preamplifier |
| **PRM903** | ½" Microphone Preamplifier with internal heater |
| **CBL097** | 7-Pin LEMO to BNC cable, 6 ft |
| **PSA021** | 230Vac to 9Vdc, 500mA power adaptor |
| **PRA951-2** | 2 mA ICP® current source |
| **PRA951-4** | 4 mA ICP® current source |
| **CAL200** | Class 1 acoustic calibrator 94/114 dB @ 1 kHz |
| **CAL250** | Class 1 acoustic calibrator 114 dB @ 250Hz |

### Input Connector Pinouts

| Pin | Signal |
|---|---|
| 1 | No connection |
| 2 | Signal ground |
| 3 | Microphone polarization voltage 0 or 200 Volts |
| 4 | Signal input |
| 5 | No connection |
| 6 | Power supply positive voltage +18 Volts |
| 7 | Power supply negative voltage -18 Volts |
| Shell | Connected to Case ground |